CODEN:LUTEDX/(TEIE-5490)/1-120/(2023)

Industrial Electrical Engineering and Automation

System impact of micro-production

Photovoltaics and short circuit faults

Annie Haraldsson

Division of Industrial Electrical Engineering and Automation
Faculty of Engineering, Lund University

Master Thesis

System impact of micro-production

Photovoltaics and short circuit faults

by

Annie Haraldsson

Faculty of Engineering LTH at Lund University

Division of Industrial Electrical Engineering and Automation

June 7, 2023

Supervisors: **Olof Samuelsson & Morten Hemmingsson (IEA, LTH)**
Industry supervisor: **Joel Clementson (E.ON)**
Examiner: **Jörgen Svensson (IEA, LTH)**

Printed in Sweden by xxx.
Lund 2023

Preface

This thesis has been conducted at the Division of Industrial Electrical Engineering and Automation (IEA) at LTH in collaboration with the Power System Analytics unit, also called KSA, at E.ON Energy Distribution in Malmö, a unit specialized in power system studies of fault clearing and disturbance analysis.

Additionally, this thesis is based on resources from Göran Runvik a retired power system expert formerly employed at Sydkraft, ABB, Gothia Power and lastly E.ON. He has merits within transmission and distribution networks, power system studies, protection relays and fault analysis. In this thesis work, fault recordings from Göran's residential PV-unit were used.

The intention of this thesis is to provide insights related to large amounts of small scale solar production. Initially, the simulation-work in this thesis was to be carried out on actual network models at E.ON. However, a security law passed by the Swedish government mere weeks before the start of the thesis work obstructed such a close collaboration and a generic network model was constructed as part of the thesis.

Acknowledgement

This thesis concludes my time at the Environmental Engineering program at LTH. I would like to thank E.ON and the whole team at KSA for the opportunity to do this thesis in collaboration with them. Without the provided material, knowledge and insight from them this thesiswork would not have been as fruitful.

I would like to extend my gratitude to Göran Runvik for access to fault-data recorded at his PV-unit, as well as his internal reports with valuable comments. Without his experience, expertise and interest in this subject, the idea of this thesis would not have been formed.

A most sincere thank you to my supervisors Olof Samuelsson at IEA and Joel Clementson at E.ON, and assistant supervisor Morten Hemmingsson at IEA. Their expertise, discussions, suggestions, and above all their unwavering support and patience have been essential for my work and the completion of this thesis.

I would finally like to express my appreciation and gratefulness to Alice Jansson, Martin Lundberg and Imran Maqbool, PhD students at IEA. Their help with simulations and the network modeling has been a great aid. However, for lending me a desk and providing company during tedious and slow simulating-hours I am most grateful.

Thank You!

Abstract

The focus in this thesis has been active power from small scale solar production and what possible impacts an increased proportion of small scale production can have, in a larger context, during short circuit (SC) faults in the grid. The main research question prompting this work was whether active power from small scale solar production can help support voltages during SC faults, and meet LVRT-requirements in the RfG.

The simulation work was performed in the tool DIgSILENT PowerFactory. The work was initially to be carried out using data for an actual network. Instead, part of the thesis work was to construct a power network model, for general validity based on an European benchmark model by CIGRÉ. The model is ranging over all voltage levels from 0.4-380 kV, which is unusual for network models and offer new insights. Static simulations of 3 phase bolted (0 Ω) SC faults were carried out for different study cases, each with varying amounts of PV-production filling up the grid. In addition, analyzes were made of actual disturbance recordings in E.ONs grid, alongside unique PMU-registrations of the same faults made at a residential PV-unit.

The simulation results in this thesis showed that accumulated active power from small scale PV-units can, theoretically, meet the LVRT-requirements in the RfG for generating modules of category B. The most striking result were a low voltage-node registered a voltage increase of 35.5% with PV-production compared to without active power input. Other nodes in the same simulated study case, representing a current PV-production scenario, had an increase of about 20% of the voltage. The case with the largest accumulated active power, representing a future scenario, had a notable impact on voltages across the HV(220 kV)-grid.

Information and analysis of fault registration showed that small scale units seem to have a rather slow up-ramping of power after disconnection due to faults in the grid. This, in the context of increasing amounts of DER in the grid brings up the inquiry if this will cause disturbances in the power balance.

Additionally, registration of a remote 3 phase SC were found to affect a large geographic area and gave such a severe voltage dip that micro-production nearly disconnected. Fault clearing times throughout the grid might need to be further shortened if normal fault clearing could lead to disconnection of micro-production in large areas. Thus, in conclusion, routines of distribution network companies need to start considering impact of extensive micro-production.

Sammanfattning

Arbetets utgångspunkt har varit aktiv effekt från småskalig solcellsproduktion och vad en ökad andel småskalig produktion kan få för inverkan, ur ett bredare perspektiv, under kortslutningar i nätet. Den huvudsakliga frågeställningen huruvida aktiv effekt från småskalig solproduktion kan hjälpa till att upprätthålla spänningen under kortslutningar, och om de kan möta störningstålighets-krav.

Simuleringar genomfördes i verktyget DIgSILENT PowerFactory. Arbetet var först planerat att utföras i en verklig nätmodell. Istället konstuerades en generisk nätmodell, baserat på en modell-standard av CIGRÉ, som en del av examensarbetet. Modellen är övergripande med spänningsnivåer från 0.4 till 380 kV, vilket är unikt för kraftsystem-modeller och möjliggör nya insikter. Statiska simuleringar av stumma (0 Ω) trefas-kortslutningar genomfördes i olika fall med varierande grad av solproduktion som fyller upp kapaciteten i nätet/modellen. Vidare analyserades störningsregistreringar i E.ONs nät, tillsammans med unik PMU-data av samma störningar, inspelade vid en privat solanläggning.

Simuleringsresultaten i detta arbete visade att samlad aktiv effekt från småskalig solproduktion kan, teoretiskt sätt, möta 'störningstålighets'-kraven som gäller för generationsmoduler av typ B i den så kallade RfGn. Det mest framträdande resultatet var i fall 3a, där en lågspännings-nod registrerade en ökning av spänning med 35.5% med solproduktion jämfört med utan input från aktiv sol-effekt. Andra noder i samma simuleringsfall, som representerar dagsläget för solproduktion i vissa nätområden, hade en spännings-ökning på ca 20%. Simuleringsfallet med högst andel samlad solproduktion på 150 MW, som representerar ett framtida scenario, visade sig ha märkbar effekt på spänningen över delar av HV(220 kV)-nätet.

Information om och analys av verkliga felregistreringar visade att småskaliga solanläggningar kan ha långsam upprampning av effekt efter bortkoppling under fel i nätet. Detta, i en kontext av ökande andel småskalig produktion, väcker frågan om varaktiga störningar i effektbalansen kan uppstå.

En avlägsen trefasig kortslutning påverka ett stort geografiskt område och gav ett så kraftigt spänningsfall att mikroproduktion i området nästan kopplades bort. Felbortkopplingstider i elnätet kan således behöva förkortas ytterligare om normal felbortkoppling skulle kunna leda till att mikroproduktion förloras i stora områden under fel.

AVDELNINGEN FÖR INDUSTRIELL ELEKTROTEKNIK OCH AUTOMATION
LUNDS TEKNISKA HÖGSKOLA

EXAMENSARBETE Power system influence of micro-production from photovoltaics
A system wide study on voltage support from PVs during short circuits
STUDENT Annie Haraldsson
HANDLEDARE Olof Samuelsson, Joel Clementson och Morten Hemmingsson
EXAMINATOR Jörgen Svensson (LTH)

Stödtjänster från småskalig solproduktion vid kortslutningar i elnät

POPULÄRVETENSKAPLIG SAMMANFATTNING **Annie Haraldsson**

Ökande andel småskalig solproduktion introduceras i elnäten, detta medför möjligheter och utmaningar för nätägare. I detta arbete har möjligheten undersökts om småskalig solproduktion kan bidra till att upprätthålla spänningen i nätet vid trefasiga kortslutningar.

I dagsläget är det många privatägare som installerar solceller. Denna utveckling har pågått länge, men de senaste åren har intresset skjutit i höjden. Att många väljer att installera och koppla in solceller till elnätet innebär möjligheter men även vissa svårigheter för nätägare (exempelvis E.ON, Vattenfall och Ellevio). Nätägare är generellt sett tvungna att acceptera och koppla in solceller, där det finns en nätanslutning för el-konsumtion sen tidigare. Samtidigt är nätägare ansvariga för den spänning och el som finns i nätet, oavsett om den är producerad av traditionella producenter, eller om bidrag från småskaliga producenter utgör en stor andel.

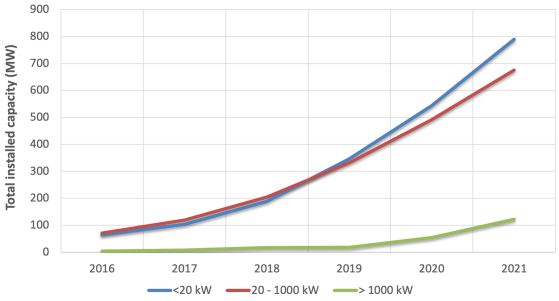

Nätansluten solproduktion i Sverige

Om allvarliga fel, så kallade kortslutningar, uppstår i elnätet kan det ha vidsträckt inverkan. Det kan innebära att spänningen, som behöver vara på en viss nivå för att kunna leverera el, kan bli betydligt nedsatt i stora delar av det berörda elnätet. För att motverka detta och i övrigt säkerställa ett fungerande elnät och en stadig elleverans finns det vissa bestämmelser som elproduktion behöver hålla sig till, dessa kallas nätkoder. I nätkoderna finns det regler som innebär att produktionsanläggningar över en viss effektstorlek måste vara fortsatt anslutna till elnätet även när spänningen sjunker, som den gör om allvarliga fel uppstår i nätet. Detta kallas störningstålighet och gäller i Sverige för all produktion som är över 1.5 MW.

När nu småskalig el-produktion ökar i andel och blir mer betydande i elnätet, vill den här studien undersöka om fel i elnätet kan stödjas på samma sätt av dessa

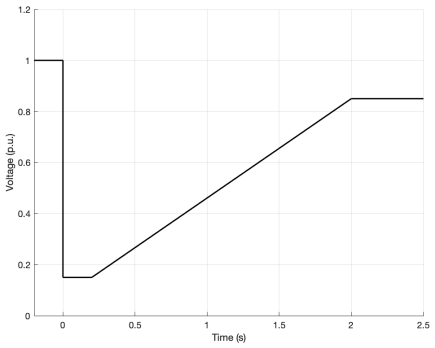

Störningstålighet-krav för anläggningar >1.5 MW

mindre anläggningar, och ifall många samlade småskaliga solcellsanläggningar kan hjälpa att hålla uppe spänningen under olika fel i nätet.

Undersökningen som är utförd i detta arbete består av datorsimuleringar i en egenbyggd elnäts-modell. I simuleringarna undersöks flera olika scenarion med varierande andel solproduktion i elnätet. De olika scenarierna täcker in hur stor andel solproduktion som finns i nätet idag samt förmodade framtida situationer. Simuleringarna kompletteras av analyser av fel-händelser i det verkliga elnätet och av inspelningar på hur dessa störningar upplevts vid och påverkat en privat småskalig solanläggning, strax utanför Malmö.

Undersökningen visade att effekt från småskaliga solceller kan hjälpa till att upprätthålla spänningen i nätet. I ett par fall visade simuleringar att samlad effekt från småskaliga solceller teoretiskt sett kan möta de regler kring störningstålighet som ställs på större anläggningar.

Arbetet upptäckte också att om en stor andel samlad effekt från småskaliga solceller kopplas bort under fel (vilket är praxis) så skulle svårigheter kunna uppstå med att möta de kvarstående el-behov som finns. Detta skulle innebära att allvarligare störningar uppstår, och för att motverka denna risk bör nätägare fokusera mer på småskalig produktion och vara medvetna om dess inverkan i sina egna nät, samt eventuellt se över arbetssätt i nätplanering och felanalys.

Abbreviations

DER - Distributed Energy Resource

ENTSO-E - European Network of Transmission System Operators for Electricity

LVRT - Low voltage ride through

OHL - Overhead line

p.u. - Per unit

PMU - Phasor Measurement Unit, a type of fault recorder

Prosumer - Consumer who is also a producer of electricity

PV - Photovoltaic

RfG - Requirements for Generators, grid code by ENTSO-E

SC - Short circuit

SLD - Single line diagram

TSO - Transmission system operator

Contents

1 Introduction

This opening chapter describes the background and aim of the master thesis, its research questions, limitations as well as the outline of the report.

1.1 Background

The urge for climate action across the world fueled by both climate related catastrophes, climate research and multiple IPCC reports, resulted year 2015 in the Paris agreement, in which countries pledged to decrease global warming and keep the increase of the global average temperature below 1.5 degrees (United Nations, n.d.).This was followed by a race between the large economies to become the first climate neutral in the world with EU, for example, pledging to be climate neutral by the year 2050 (Council of the European Union, 2023).Thus governments and industries have begun to redirect towards a fossil-free future. In turn further accelerating the electrification in society, promoting green shifts in heavy industries and resulting in a large increase in renewable generation in the power system.

The technical development in renewables and specifically photovoltaic panels has been very rapid during the past decades, with significant raise in efficiency and drop in prices (National Renewable Energy Laboratory, n.d.). This led to an increase of installed solar-capacities around the world, and in Sweden, there has been somewhat of a solar-boom the last few years. The interest in solar power still rising according to 'Solcellskollen' (Wallnér, 2022). This is also witnessed by grid owners, at E.ON the connection-requests for PVs have been record-high during 2022 with an increase of around 180% from previous year, much of those being small-scale units/micro-producers, and a slowdown is not expected in 2023 (E.ON Energy Networks, 2023). According to statistics from the Swedish Statistics Authority, SCB, the increase of generation by grid-connected solar units during the 12 month period January-December 2022 increased by 75% compared to the last year, including the estimated self-consumption by prosumers. (Statistiska Central Byrån, 2022)

The Swedish Energy Agency provides various statistics on energy development, among those are statistics on the current status in solar installations and production in the country. In the figure 1.1 below, the total installed solar capacity is shown for the years 2016-2021. The installations are divided up in unit sizes from 20 kW

up to 1 MW, but the data shown are the total cumulative power installed of that unit-size in Sweden.

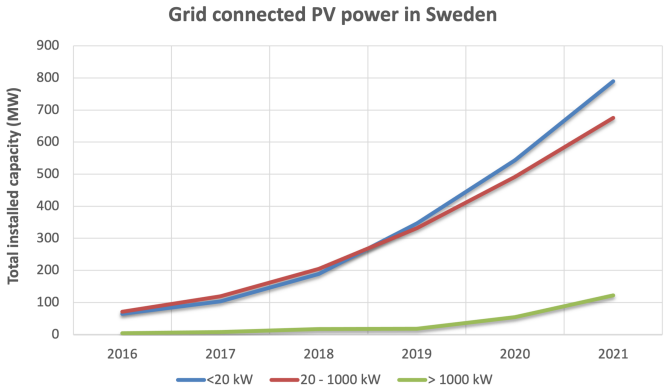

Figure 1.1: Yearly total installed solar capacity, based on unit-size (Energimyndigheten, 2022a)

Even though large scale units have increased the last few years, the total increase in solar capacity is dominated by small scale units. In fact, an update from the Swedish Energy Agency from 2022 stated that the unit-size "<20 kW" stood for 50% of the total installed power at the end of 2021, while the large-scale sizes ">1000 kW" only stood for 8%. (Energimyndigheten, 2022b)

Since the interest in solar has increased this rapidly lately, it is of interest to continue to evaluate the anticipated development of solar power. Predictions like these made on both short and long-term timescales imply that the growth rate of solar power installations will likely continue to increase. (Energimyndigheten, 2022c)

Grid owners have an obligation to connect solar installations to their grid. They cannot refuse the connection of a PV-unit to an already existing fuse-contract (Energimarknadsinspektionen, 2023). Thus, grid owners are obliged to continue to connect distributed generation to their grids and uphold and develop a grid that can sustain a larger hosting capacity of inverter based generation. This while simultaneously sustaining personal safety. This is one of the most essential responsibilities by grid operators and is secured by protection schemes, systems and fault clearing.

At the same time, grid owners are also required to maintain service availability in the power system. This in order to secure a reliable supply of electricity to customers at all times and prevent service interruption or power outages throughout the grid.

The responsibility to achieve a high enough reliability in the power system is divided on all actors in the power system industry. (Svenska Kraftnät, 2021d)

A part of maintaining service availability is to make sure that the grid is robust enough to supply enough power even during faulted conditions. In order to ensure this, there are grid codes that require generators or any production of certain power levels to have so called LVRT or fault ride through capabilities, meaning that it shall remain connected to the network and operate through periods of low voltage at the connection point (European Commission, 2016). Since the quantity of distributed energy resources has increased substantially, how these resources respond to power system disturbances has changed from minimally consequential to potentially critical (Kenyon and Mather, 2020).

Thus, these technology neutral grid-codes by ENTSO-E, enforced across the EU, in combination with an increasing amount of PV-units/systems signify that fault ride through capability of PVs will be of growing interest.

A registration that has been made on a small scale residential PV unit during a fault and the preceding disconnection is shown in figure 1.2 below. (Runvik, 2022a)

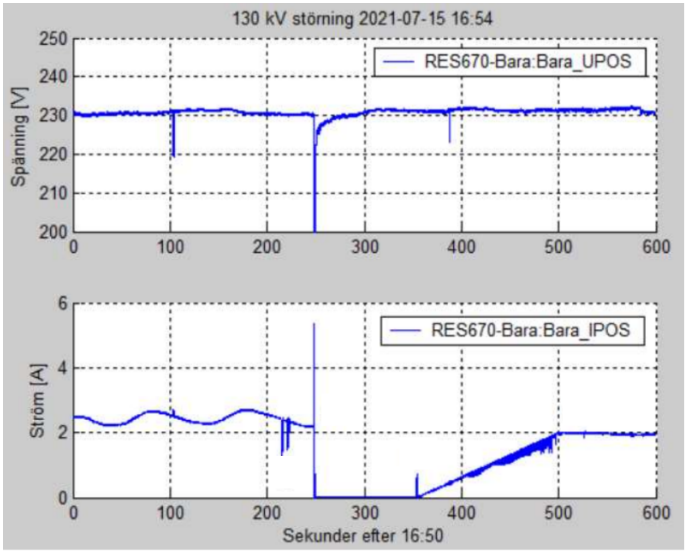

Figure 1.2: Response at small scale PV-unit after 130 kV disturbance (lightning), voltage and current-ramping

The figure shows the network voltage at the connection point to the grid, as well as the current output at the terminals of the PV unit. From that, it can be derived

that the up-ramping of power from a small scale unit may be rather slow after a fault. Which begs the question if this increase in amount of generation from small scale units might cause issues with the power balance and service availability in the power system and thus if these fault ride through criteria mentioned earlier should be implemented even on small scale units.

To get a grip on this, it is of interest to study micro-production with a collective approach and to perform an overall analysis on the impact of microproduction on higher voltage levels in the power system. This requires a conjuncture of the otherwise two-parted sector, that is separated into 'high voltage' and 'low voltage network models' respectively as well as overall work and reasoning. Therefore, this thesis will present and use a simulation model with a combined network from transmission levels down to the lowest distribution voltage.

As is stated in this background, there have been an increase of installed solar capacity in the past few years and future scenarios predict further expansion. An increased penetration of inverter based generation is in general observed which raises new issues for the development and operation of the grids. This master thesis is an attempt to pro-actively assess and investigate some of the problems that the grid and grid owners might face.

1.2 Aim

The aim of this master thesis is to investigate how distributed microproduction affects the power system and the security of supply. More specifically the goal is to study how voltages at PV-units are affected by faults at different locations and voltage levels in the electric grid and how an increased amount of photovoltaics in the power system may mitigate disturbances by the implementation of LVRT.

In addition, this master thesis aims to present a simplified and comprehensive model for the electrical grid as a whole, which is necessary for extensive studies of DERs. This in contrast to the common standard practise with separate models for high-medium voltage systems and low voltage systems.

1.3 Research questions

- Power generation from PVs are traditionally neglected during faults, should this be re-examined?

- Does active power from micro-production of PVs help uphold voltage at connection, and at upstream voltage level during faults?

- How geographically widespread is the impact of SC-faults in different parts of the grid? What impact could disconnection of micro-production have?

- Are there other aspects or concerns regarding micro-production that grid owners and operators should be aware of, study further or act against?

1.4 Limitations

For practical reasons the study will be limited in various aspects.

The scope of this thesis is not to provide extensive or detailed answers to grid owners/operators concerning micro-production but rather to serve as an initial survey to identify points of interest for further work. This study will only take photovoltaic systems into account, and thus will not include any other inverter based renewable technology or storage systems (e.g. Battery Energy Storage Systems), even though they share much of the same functionality. Neither will this thesis consider LVRT in wind power; it will not make any comparisons or draw conclusions based on development, implementation or impact of these criteria in the wind domain.

The simulations carried out in this thesis is so called static simulations which is a natural first step before dynamic simulations that are more complex and time consuming.

Throughout the thesis, the voltage magnitude is the only central system parameter, thus frequency and load-angle/angles for example, are disregarded. Furthermore, the focus is on active power so no consideration of reactive power will be made. Thus the PV-units in simulations are all modeled to only generate active power output. Due to simplicity reasons all simulated PV-components are assumed to produce at its maximum installed capacity, and no respect to regional/local or seasonal variation

in solar production is made.

The main focus of this study is single occurrences of bolted 3 phase short circuit faults. Since these are the most severe fault-cases with lowest voltage dips thus most serious consequences, and also are the simplest to model. This implies that no account will be taken of the zero sequence in the model.

Even-though there are resources from fault registrations at a residential PV-unit used in this thesis, there will not be a direct comparison between these fault registrations and the simulated results. This since the network model is deemed too generalized for comparisons of that sort to give added value or clear interpretations.

The simulation will not take the control response of the PV systems into account. Neither will any synergistic effect from inverters of the neighbouring PV systems be investigated. The work will purely focus on the impact of aggregated active power in study cases with SC faults.

1.5 Outline

This initial chapter gave a short introduction to the thesis and its background. In chapter 2 the relevant theory for the thesis is introduced, chapter 3 presents the method and the study cases that will be studied. In chapter 4 the results from the power system simulations are stated. Chapter 5 gives an extensive overview of the fault registrations made at a residential PV-unit, as well as fault analysis made on the same disturbances recorded in E.ON's grid. Chapter 6 contains discussion of the simulated results and the fault registrations. Lastly, chapter 7 presents conclusions as well as suggested future work based on the work of this thesis, followed by references and appendices.

Throughout the thesis, many figures have details that are too small to read on an printed A4 with the naked eye. This is a conscious choice to keep the readability of the report, as otherwise reading would require extensive flickering of pages to try to keep continuity and consistency of the paper. For a closer look at the details of certain figures, opt to the web based pdf-version uploaded at LUP and at IEA's publications.

2 Theory

In this chapter, theory and essential concepts are presented serving as background for the remaining thesis.

2.1 The electric grid

The Swedish power grid consists of two parts, the transmission grid which transfers electrical power, at very high voltages, long distances across the country and the part called the distribution grid, which distributes the electricity down to the consumers, see figure 2.1. The distribution grid in its turn consists of the regional grid and the local grid. (Svenska Kraftnät, 2022) The regional grid can also be called subtransmission grid and the local grid can also be named Medium Voltage (MV) and Low Voltage (LV) grid, depending on the voltage level in the local grid.

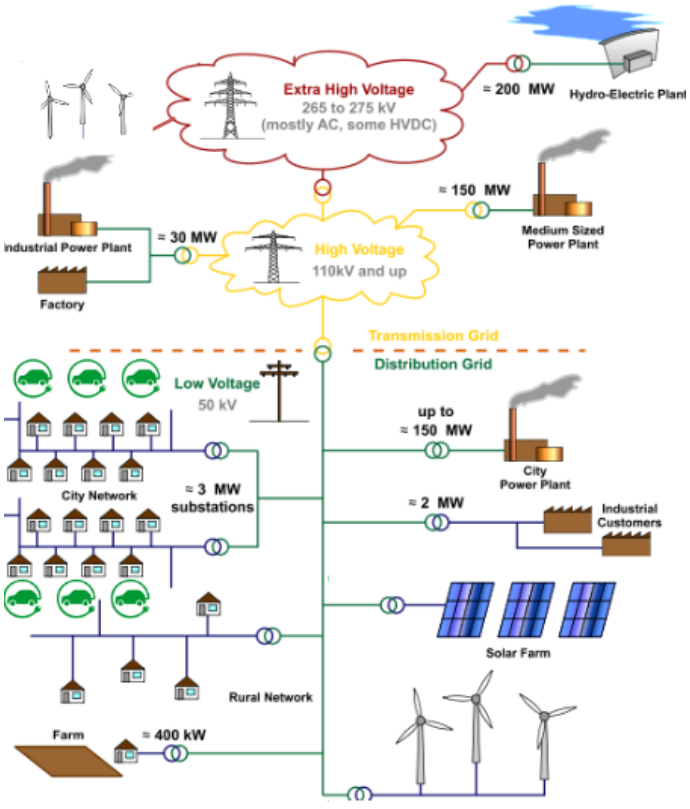

Figure 2.1: Exemplifying figure over the grid (Samuelsson, 2021a)

2.1.1 Voltage levels - and description of grid part

The Swedish transmission grid operates at voltage levels of 220 and 400 kV and transports electricity from the largest electricity producers out to the different regional or sub-transmission grids. Apart from these producers, there are also HVDC-links in the transmission grid to several countries in Europe for power export/import. The transmission grid is owned and operated by the Swedish TSO (Transmission System Operator), Svenska Kraftnät. The regional grids connect to the transmission grid and transport the electricity to the various local grids. Large consumers and some semi-large producers are often connected to the regional grid. This part of the grid normally operates at 130 kV. The regional grids are owned by larger grid operators. The three biggest sub-transmission grid owners in Sweden are E.ON, Vattenfall and Ellevio. The local grids transport the electricity the last part, from the regional grid out to all consumers. Small scaled production, such as residential photovoltaic production, can be connected to the local grids. These grids operates at 20 kV or lower, as the voltage is transformed along the way down to a final 400 V at household consumers. The local grids are owned by many small grid companies. (Svenska Kraftnät, 2022)

As previously mentioned, the naming of the different parts of the electric grid is ambiguous, so in an attempt of clarifying it table 2.1 below was created.

Table 2.1: Nomenclature for the different voltage levels in the power grid in Sweden

	Name/s	Voltage level
	Transmission grid	220 - 400 kV
Distribution grid	Subtransmission/Regional grid	50-130 kV
	Local grid - MV part	10-20 kV
	Local grid - LV part	230*-400 V

* *While all other voltages are line-line voltages, 230 V is a line-ground voltage.*

However, this thesis will have a network model that is based on a benchmark report valid for Europe, so the voltage levels used henceforth will not correspond exactly to the reality in the Swedish system. The nomenclature for the voltage levels in the network model in this thesis will be as stated in table 2.2.

Table 2.2: Nomenclature for the different voltage levels in the model used throughout this thesis

Name	Voltage level
EHV	380 kV
HV	220 kV
SUB	110 kV
MV	20 kV
LV	0.4 kV

2.1.2 Grid structure and network strength

There are different types of grid structures that are commonly used in the power system. Generally, power grids can either be built in so called radial or meshed structures. A radial structure is characterized by that each part only has one direction of the power flow - from feeding point to end-consumers. In a meshed grid however, the network is more intra-connected. The meshed structure gives multiple possible directions for the power flow to reach each outlet-node. If a line or cable in such a structure has to be disconnected due to a fault, the power flow from this can easily be taken over by other lines/cables and no disruptions in the service is noted. (Alaküla, Gertmar, and Samuelsson, 2011)

Figure 2.2 below shows the two different structure types, where the direction of power flow is shown by arrows.

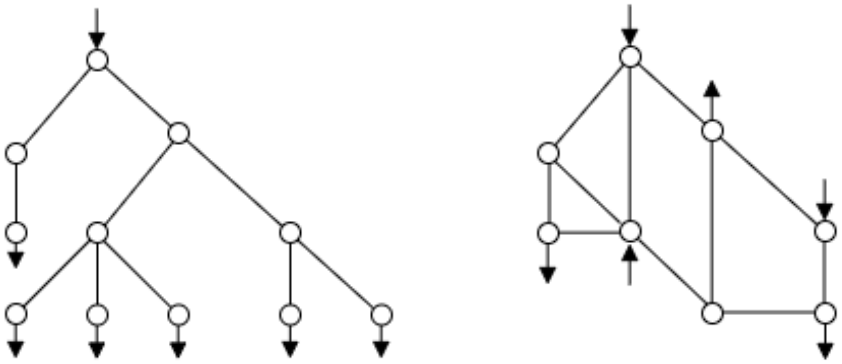

(a) Radial structure **(b)** Meshed structure

Figure 2.2: Grid structures (Alaküla, Gertmar, and Samuelsson, 2011)

In general the low voltage parts of distribution grids are built as purely radial grids, but might in some cases have a connection to another part of the overlying grid, that can be operated manually as a backup. In contrast, the high voltage transmission grids are built meshed, in order to minimize disruptions in underlying grids during fault or maintenance on single OHLs. Regional grids are often built in a meshed structure but have open 'loops' that are operated radially. (Clementson, 2022)

Another important quality of the grid is the network strength. This strength dictates how much the voltage is affected by loading of the grid. On higher voltage levels, in the transmission grid e.g., the grid is strong and can be heavily loaded without any significant change in voltage. At lower voltage levels, the network is commonly much weaker which is mostly experienced in rural grids. The determining factor/parameter of how strong the grid is in a certain point in the grid is essentially the series impedance between this point in question and the generation.(Alaküla, Gertmar, and Samuelsson, 2011) This is illustrated by the figure 2.3 and subsequent equations.

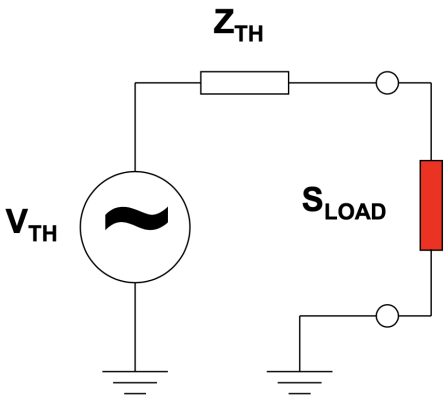

Figure 2.3: Illustration of network strength (Samuelsson, 2021b)

$$Z_{LOAD} >> Z_{TH} \iff S_{LOAD} << S_{SC} \tag{2.1}$$

$$Z_{LOAD} \text{ not } >> Z_{TH} \iff S_{LOAD} \text{ not } << S_{SC}/2 \tag{2.2}$$

The relationship set up in 2.1 is valid for strong networks, there it will be a small voltage drop across Z_{TH} and the load voltage is insensitive of the load. In contrast, the relationship in 2.2 is true for weak grids, and the voltage at the load point is

sensitive to loading. (Samuelsson, 2021b)

The network strength is thus practically meant its short circuit power, which with the help of a Thévenin equivalent can be derived in a certain point of the grid according to equation 2.3.

$$S_{SC} = \sqrt{3} \cdot V_{TH} \cdot I_{SC} = \frac{V_{TH}^2}{Z_{TH}} \tag{2.3}$$

where Vth [V] is the voltage in the point before short-circuit, Isc [A] is the short-circuit current that will run in an zero impedance short circuit, and Zth [Ω] is the impedance that exists up to the point in the grid.(ibid.)

2.2 Power system operations

2.2.1 Power balance

In order for the power system to function and deliver electricity, power balance must at every instant be ensured. Maintaining power balance means, simply put, to make sure that there is equally supplied electricity to the grid that is being consumed each second, hence that there is a balance between production and consumption of power. Many factors affect this balance between injected and consumed power, and disturbances in the power balance risk to damage equipment or could lead to a blackout in the power system. The frequency in a power system is a measure, and direct result of how well the production and consumption of electricity/power is balanced in a system. The Nordic synchronous area has a nominal frequency of 50 Hz. To preserve this balance in the power system is one of the most crucial responsibilities that the TSOs have. (Svenska Kraftnät, 2021a)

2.2.2 Fault types

For this thesis, the main focus is on short circuits, so this fault type will be briefly covered in this section. Single phase earth faults will also be brought up since earth fault is the most common fault in grids.

Phase components that are generally established and used can be resolved into three

sequence components: Positive, Negative and Zero sequence components, which may come in handy while analysing faults. The positive sequence represents balanced 3-phase conditions, and thus zero sequence and negative sequence components are only present during unbalanced faults. The zero sequence is affected by earthing and the negative sequence is mainly associated with harmonics. (Glover, Overbye, and Sarma, 2016)

Three phase bolted short circuit fault (3ph 0Ω SC)

A three phase bolted ($Z_F = 0\Omega$) short circuit, as illustrated in figure 2.4 below, is a critical kind of fault that includes the highest currents. This fault type is also the one used in simulations, due to said reason.

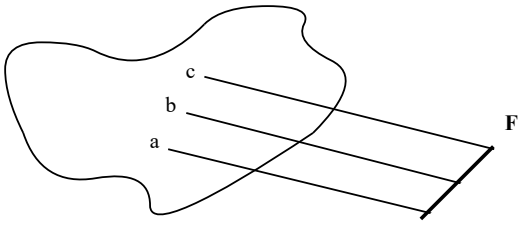

Figure 2.4: SLD of a 3ph bolted short circuit in an arbitrary three phase system

The phase currents during a balanced 3ph SC is symmetrical and equal in magnitude, with exactly 120°phase shift, presuming a balanced symmetrical system, thus the fault current magnitude is balanced equally within the three phases.

The voltages however are all short-circuited to zero, since the conductors are all connected in the fault point and thus the voltages are summarized and according to Kirchhoff's voltage law: the algebraic sum of voltages around any closed path is zero.

During a bolted three-phase fault, the sequence fault currents are:

$$I_0 = I_2 = 0$$
and
$$I_1 = V_F/Z_1$$

The sequence fault voltages are $V_0 = V_1 = V_2 = 0$, since the phase voltages are $V_a = V_b = V_c = 0$. (ibid.)

Phase to earth fault

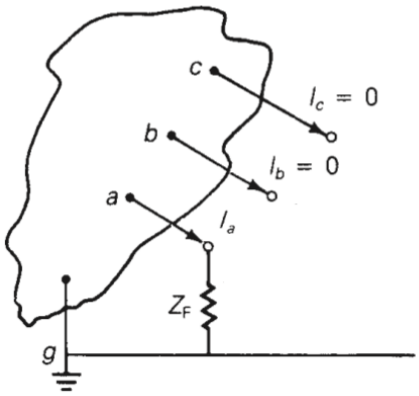

Figure 2.5: Illustration of single line-to-ground fault in an arbitrary grid

Fault conditions during a single line-to-ground (SLG) fault, as shown in figure 2.5 above, are in phase domain:

$$V_a = Z_F I_F$$
$$I_b = I_c = 0$$

and in sequence domain as following:

$$I_0 = I_1 = I_2$$

$$(V_0 + V_1 + V_2) = 3Z_F I_1$$

As can be seen by the equations for the sequence domain during SLG faults, the sequence networks are interconnected in series.(ibid.)

A one-phase to earth short-circuit fault in a high-impedance earthed distribution system will cause a substantial voltage rise on the other healthy phases. Which in turn may result in a flashover and short-circuit fault elsewhere in the system. This is known as a cross-country fault. (Alstom Grid, 2011)

2.2.3 Fault clearing/protection

There are numerous types of fault clearing relays that can detect faults in several ways. In this section the most common ones will be briefly explained. For further interest in this subject, textbooks or technical guides are referred to for more details.

To limit the extent of the power system that is disconnected when a fault occurs, protection is arranged in numbered zones, as shown in fig 2.6a. Ideally, the zones of protection should overlap, so that no part of the power system is left unprotected, which is illustrated in fig 2.6b. (Alstom Grid, 2011)

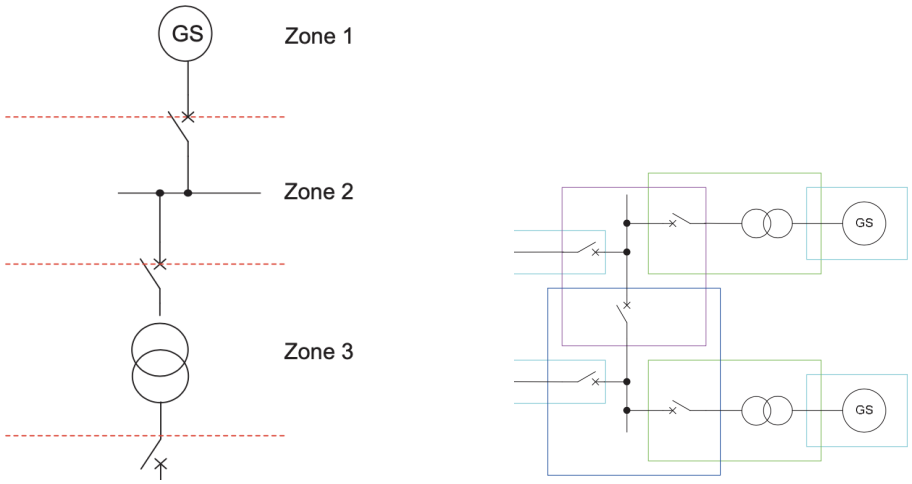

(a) Division of protection zones **(b)** Overlapping zones

Figure 2.6: Zones of protection in power system

A simple relay type is the overcurrent relays, which observe and respond to the magnitude of current and trip the line/object either instantaneously or after a pre-set time delay based on different overcurrent intervals. (Glover, Overbye, and Sarma, 2016)

Adjustable time delays can be selected not only for overcurrent relays but for many different relays/circuit breakers in a protection scheme. This is done so that the breaker closest to the fault opens first, while other upstream breakers with larger time-delays remain closed. In this manner the relays can be coordinated to operate in sequence in order to interrupt minimum load during faults. (ibid.)

Impedance/distance relays operate by comparing the rated/unfaulted voltage-to-

current ratio of the line to the same ratio during operation. If the voltage-to-current ratio, or impedance, is lower than the defined default value, a fault has occurred and the relay trips. (ibid.)

Differential protection is another protection type where the principle is that relays sense the difference in currents between the incoming and outgoing terminals of the unit being protected, see illustration in fig 2.7 and equation of trip criterion below.

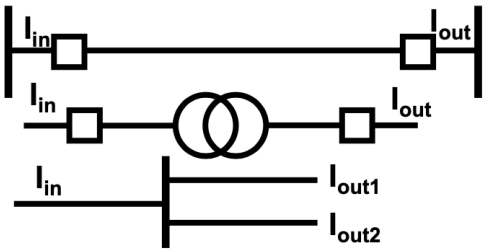

Figure 2.7: Principle of differential protection. (Samuelsson, 2021b)

$$|I_{in} - I_{out}| > 0$$

This protection type involves measurement of fault currents (and possibly voltages) at each end of the protected zone, and communication between the equipment at zone boundaries. By continuously measuring and comparing the values at both ends of an OHL, for example, the relay senses when there is a difference, caused by some type of fault, and trip the line. (Alstom Grid, 2011)

2.2.4 Voltage support and stability

For grid operators the perseverance and stability of the voltage in their grids are central concerns, which both could be affected by production from DERs.

The impedance of grids are generally both resistive and reactive, meaning that $Z_{grid} = R + jX$, which is shown in the general model in fig 2.8 below. Which one of these terms, the resistance or reactance, that are dominant for different grids and lines/conductors is highly relevant. There is a ratio expressing this, called the R/X ratio which tells how resistive a conductor/line/cable or grid is relative to its reactance.

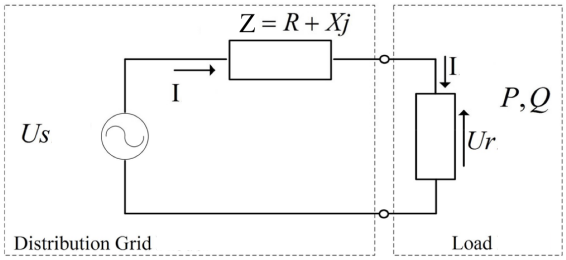

Figure 2.8: SLD of a general grid model - Thévenin equivalent circuit (Patsalides et al., 2013)

Transmission grids are usually dominated by reactances, while in distribution grids the resistive part is dominating resulting in a higher R/X-ratio. Thus, as voltage support in transmission grid is carried out by injection of reactive power Q, feed-in of active power P raises the voltage in distribution grids. (Samuelsson, 2021c)

The relationship between power injection from DERs and voltage at distribution grids is shown by the following equation.

$$\frac{dU}{U_N} = \frac{(P \cdot R) + (\pm Q \cdot X)}{|U_N|^2} \tag{2.4}$$

where dU is the voltage deviation over the grid impedance, U_N is the fixed voltage at an infinite bus representing grid voltage, R and X is the grid impedance (Z=R+jX) and finally P and Q the active and reactive power provided to the grid.

From equation 2.4, it is revealed that the feed-in of active power causes a voltage rise while the reactive power can either be used to reduce the voltage (-Q=inductive consumption) or to increase the voltage (+Q=capacitive consumption). The higher the resistive part of the grid impedance, the more significant the effect of active power feed-in will be on the voltage rise. (Stetz, Marten, and Braun, 2013) As stated above, distribution grids are dominated by resistive impedance, why active power voltage support is possible (and most prominent) in these grids.

Voltage stability is associated with the capability of a power system to maintain stable voltage magnitudes while transporting active and reactive power during both normal and faulted conditions. Key to voltage stability are the system loads and the behaviour of sources during fault conditions, in terms of active and reactive power injections. Voltage instability occurs in the form of progressive voltage rise or fall,

known as voltage collapse. System operators are responsible for controlling voltage so that it remains between specific limits, and they often rely on the assistance of producers in their grid to do so. (Christensen et al., 2020) With regard to voltage stability, there are several concerns identified by ENTSO-e that was brought up in this previously cited report, two of them in line with the scope of this thesis:

- Loss of generation in the context of fault-ride through capability
- Inadequate support to restore system voltage immediately post fault

2.3 Grid codes and regulations for power supply

2.3.1 TSOs and ENTSO-e

Transmission system operators, or TSOs have responsibilities concerning the whole power network, to make sure that it is within operational limits during both normal and faulted conditions. They are responsible for the secure and coordinated operation of the power system, thus they set demands on and monitor system parameters such as power, voltage and frequency. (Svenska Kraftnät, 2019) These demands are stated in grid codes specified by the TSO which all actors in the power system must comply with.

ENTSO-e, the European Network of Transmission System Operators, is the association for cooperation of the European TSOs. The network is representing 39 TSOs across Europe that together are responsible for the secure and coordinated operation of Europe's electricity system. It coordinates TSOs' actions in the fields of transmission system operation, system development, market development and research.

Furthermore, it also has an active and important role in the European rule setting process, in compliance with EU legislation, where ENTSO-e carries out legally mandated tasks as their key responsibility. One of these tasks being: "Developing and implementing standards, network codes, platforms and tools to ensure secure system and market operation as well as integration of renewable energy." The TSO-network also supports its members in the implementation and monitoring of the agreed common rules. (ENTSO-E, 2023a and ENTSO-E, 2023b)

2.3.2 Low Voltage Ride Through in EU grid codes

Fault ride through also known as Low Voltage Ride Through, or LVRT for short, is the capability of generators/generating modules to be able to remain connected to the network and operate through periods of low voltage at the connection point caused by faults. Criteria for this is conveyed in Network codes. (European Commission, 2016)

ENTSO-E was in charge of drafting Network codes upon request of the European Commission and in line with the framework guidelines specified by the European Union Agency for the Cooperation of Energy Regulators (ACER), which were then adopted by and determined as regulation by the Commission (ENTSO-E, 2012). These set of rules called Network codes means to facilitate the harmonisation, integration and efficiency of the European electricity market. Each network code is an integral part of the drive towards completion of the internal energy market, and achieving the European Union's energy objectives. The network codes are essentially the grid codes of EU, since they are ratified and implemented and entered into force in the individual grid codes of TSOs of member-states. (ENTSO-E, n.d.)

The European Commission determined a regulation that establishes a network code for grid connection of generators, for short called RfG, in which criteria for LVRT are stated. (European Commission, 2016) These requirements are independent of technology, and instead based on the voltage level and the maximum production capacity of the power generating module. The grid code thus divide all generators or generating modules into separate categories, which are stated in table 2.3 below. There are different thresholds for these categories in the five different synchronous areas in EU and the categories stated below are those valid for the Nordic synchronous area. (ibid.)

Table 2.3: Grid code generator categories/types for the Nordic synchronous area

Type	**Voltage at connection point**	**Maximum capacity**
A	<110 kV	0.8 kW
B	<110 kV	1.5 MW
C	<110 kV	10 MW
D	≥110 kV*	30 MW

* A generator is considered to be of type D even when its connection point is below 110 kV if its maximum capacity is at or above certain threshold determined by each member state or regulatory authority. The Swedish TSO, Svenska Kraftnät has stated that a generator is to be considered type D even when its connection point is below 110 kV if the maximum capacity is at or above 30 MW threshold. It is also considered a type D generator if the maximum capacity is below the threshold but the connection point is at or above 110 kV. (Svenska Kraftnät, 2021b)

These different categories of generators must comply with different criteria and thresholds for LVRT, which also differs regionally.

2.3.3 Swedish regulations and conditions

EIFS 2018:2

The criteria for LVRT in Sweden is implemented by regulation EIFS 2018:2 by The Swedish Energy Markets Inspectorate. It is based on the criteria and categories in RfG. The LVRT-requirements on power park modules of type B and C are shown in figure 2.9 below.

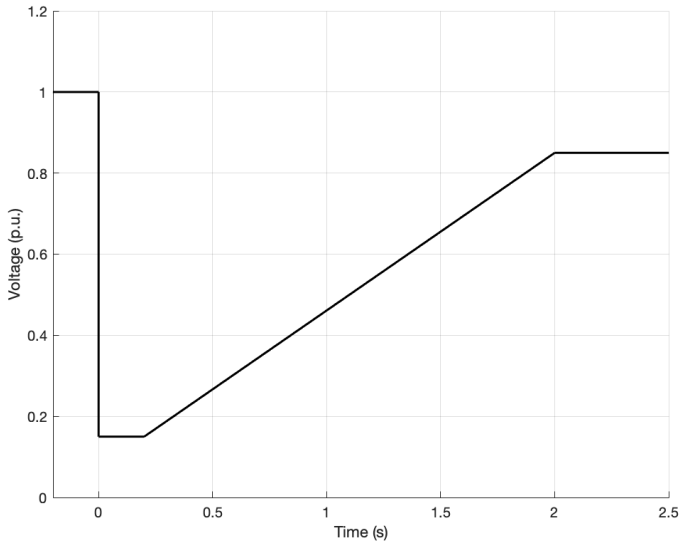

Figure 2.9: LVRT criteria in Sweden for generating power park modules of type B-C. The limits are 0.15 and 0.85 p.u. respectively, and the lowest level lasts for 0.2s.

Generating modules shall be capable of remaining connected to the grid/network as long as the voltage at the point of connection remains above this presented voltage-time curve. The operating point for a power park module of type B and C shall

previous to a fault correspond to its maximum output of active power, and zero reactive power. After ten seconds succeeding the fault, the voltage at the connection point is assumed to be restored to 90 percent. (EIFS, 2018:2)

As of today, there are no regulations regarding LVRT for type A generators/generating modules in the grid codes. However, with increasing numbers of small scale PV-units being connected to the grid, there might be a need for similar requirements on type A categories in low voltage grids as well. This thesis will investigate and compare voltage dips at LV-buses with the grid codes, specifically with the previously stated LVRT requirement of type B and C generating modules.

Regulations on micro-production

The definition of micro-production is "production unit with a maximum capacity of 43.5 kW, connected to a 230/400 V consumption-entity with a main fuse of maximum 63 A" (Energiföretagen, 2018).

Grid operators must uphold the same grid standards regardless if the electricity is being generated in traditional large power-plants or by "prosumers", and they are responsible for the service in their own grids at all times. Which is why there is a praxis for relay settings, a few shown in table 2.4 below, which are recommended for all units connected to low voltage grids.

Table 2.4: Praxis for a few relay settings for micro-production, according to standard SS-EN 50438

Parameter	Function time (s)	Function level
Under voltage	0.2	230 V - 15%
Islanding	0.15	

These relays are intended to protect both the production-unit and the grid. (ibid.)

However, since there is an immense increase of micro production PV-units in Sweden, this old praxis may need to be reconsidered. The SS-EN 50549-1 standard (accessed by Per Hugosson at E.ON), for one, makes the assessment that LVRT requirement also should apply to generating modules classified as type A and smaller,

even though it is not obliged in the RfG (European Committee for Electrotechnical Standardization, 2019).

Tax legislation concerning PV production

Swedish legislation has previously had subsidies on the installation of solar power, this is no longer the case but current tax-legislation is beneficial for solar production up to certain thresholds, which most likely have affected the investment pace in PVs.

Micro-producers (with a unit of $\leq$ 43.5kW) are exempted from paying energy tax. They can also get tax-deduction on the electricity that is fed into the grid, with 0.6 SEK deduction per kWh. However this deduction is only valid up to the kWh-limit that is the highest actual consumption at the connection point. (Skatteverket, n.d.(b)) The power-limit for tax exemptions from energy tax for producers were raised during 2021, from 250 to 500 kW. Additionally, since the 1st July 2021 there is a tax-exception on electricity produced by units with less than 500 kW installed solar capacity. (Skatteverket, n.d.(a) and Skatteverket, n.d.(c))

Even though the legislation is beneficial for micro-producers, PV-plants of record sizes are also constructed around Sweden, especially in the southern parts where two plants of 18MW each are in operation (Svensk Solenergi, 2023).

2.4 Photovoltaics

Photovoltaics or photovoltaic systems, also called PVs for short, are composed by a number of components. The key component converting solar irradiance to energy is the PV-array, but there are additional units needed in order to connect a PV-unit to the grid and maximize power output. A general overview is shown in figure 2.10 below. However, since this thesis mainly has a grid-perspective, the grid-interface and inverters are of most interest.

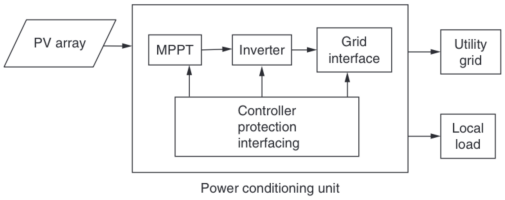

Figure 2.10: General topology of grid-connected PV-unit (El Chaar, 2011)

2.4.1 PV inverters and control

A power converter is the technology that enables efficient and flexible interconnection of DC link and AC grid. An article by Blaabjerg et al.(2015) summarized the configurations of grid connected PVs as is shown in figure 2.11 below.

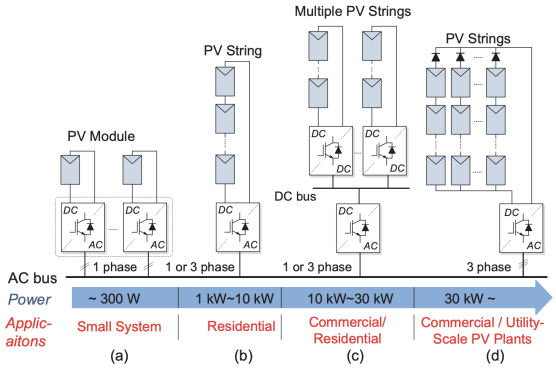

Figure 2.11: Grid-connected PV configurations based on: (a) module inverter, (b) string inverter, (c) multi-string inverter, and (d) central inverter (Blaabjerg et al., 2015)

The inverters can also be further classified on various premises; per way of input source, per wave state of output voltage or per association. Arranged by information source, the inverter types are: voltage source inverters (VSIs) and current source inverters (CSIs). Ordered by their output voltage wave structure, there are square-wave inverters, quasi-square-wave inverters and pulse width modulation (PWM) inverters. Per association of thyristor and commutating parts, inverters can be organized into:

- Arrangement inverters
- Parallel inverters
- Span inverters: Half-bridge or Full-bridge inverter

These classifications were introduced in the context of single stage string-converters. Of these, voltage source inverters (VSI) topologies are widely used for interfacing PV, and these are dominated by two-level VSI with PMW technique. (Kumar, Albert Alexander, and Rajendran, 2020)

To add more flexibility to the string inverter and improve the performance of the PV system, the multi-string concept was developed. The strings are divided into smaller pieces (fewer modules in series) and connected through independent converters to the

grid-tied inverter.(Sood and Abdelgawad, 2019) The multi-level and multi-modular topologies are for short called MLIs. There are three main types of MLIs: diode-clamped, capacitor-clamped and cascaded H-bridge inverters. These inverters have capabilities to operate at high voltages, have low switching losses and high efficiency. (Kumar, Albert Alexander, and Rajendran, 2020)

Power converters are fundamental components in PV systems since they carry out control actions.

The control of a grid-connected PV system can be divided into two important parts:
1. A MPPT (maximum power point tracker) controller to extract the maximum power from the PV modules, and
2. An inverter controller, which ensures the control of active/reactive power fed to the grid; the control of DC-link voltage; ensures high quality of the injected power and grid synchronization. (Sood and Abdelgawad, 2019)

Besides synchronization and power quality control, there are additional functions such as anti-islanding protection, energy storage regulation, and grid support that are required by concepts of quality, continuity, and reliability. These functions are essential in following grid codes. The objective is that grid-connected PV systems can enhance the power system dynamics by contributing to fault mitigation and ensuring stability. (Dhaker, 2023)

As the penetration level of renewable energy resources continues to grow, ancillary services like LVRT, reactive power control and frequency control through active power control are becoming more crucial in order to achieve a reliable and efficient power conversion from renewables. The power electronics technology will also be more active into the grid in the future with interactions among inverter-based sources becoming more apparent. This will consequently bring more challenges for the stability and power quality of future power grids. As a result, beyond the basic power extracting control, the renewable energy resources also have to perform advanced control functions and strategies. (Blaabjerg et al., 2015)

2.4.2 Predictions of future solar installations

The Swedish Energy Agency have made predictions on future development of the energy sector and whole energy system , both short-term and long-term forecasts. The current short-term prediction contains predictions to the year 2025. By then it is believed that the solar electricity production would be increased from 1.1 TWh 2021 up to 5.4 TWh in 2025. (Energimyndigheten, 2023a)

In their long-term forecast, multiple scenarios are investigated. However, they all have in common that wind- and solar power increase. The contribution from solar power is predicted to be between 9 and 32 TWh in the different scenarios by the year of 2050.(Energimyndigheten, 2023b) If an increase in solar power to 10 TWh would exclusively be made by rooftop-installations it would require a total area of 80 square-km. This corresponds to only around 6% of the total roof-area in the country and this roof-demand is estimated to be well below the roof-area available and suitable for PV-units.(ibid.) According to IEA it has been estimated that the potential for electricity produced by roof-mounted solar cells in Sweden amounts to over 40 TWh per year.(International Energy Agency, 2021)

The Swedish TSO also makes predictions on the development in the energy-market and the power system. These predictions are not forecasts but instead long-term scenarios with the aim to investigate possible future needs and challenges for the Swedish power system, in order for the TSO to work proactively toward future goals. The scenarios in this report reach to the year 2050 and show four different pathways for the power system and their associated needs. All scenarios assume that the need for electricity will increase, but how much depends on factors as energy efficiency, hydrogen production, digitalization etc. Although, with regard to the rapid development of the past year, e.g. in the electrification of the industry, the need for electricity might well be higher than assumed in the scenarios, according to the authors. The production capacity for solar power ranges from 9.7 to 31.8 GW in the scenarios, from an initial point of 840 MW in 2020. The report also simulate a yearly mean generation for 2045. In these simulations the generation from solar power range from 8-28 TWh, with a mean value of total electricity need for 2045 at between 180-225 TWh for the different scenarios. (Svenska Kraftnät, 2021c)

At E.ON, no such forecasts are made or worked after but after discussion with em-

ployees at the Grid planning unit and at Power system analytics it can be said that customer requests from solar installations fills up the capacity of the grid at different parts of their grid-areas in the south of Sweden. (Johansson, 2022 and Clementson, 2022) However, the grid planning unit did have a rough template for micro-production; 3% of the customers where PV-installment is relevant/suitable, will be assumed to install micro-production. The current situation during the autumn of 2022 in a selected grid area in Skåne there were 5% of all suitable/relevant consumers that was micro-producers. The same area had an expected increase of over 5 times the installed capacity for the 3-5 years ahead, which could be thought or assumed to be the case for all their LV-grids (Johansson, 2022).

3 Method and study cases

This thesis will be based on fault simulations on a simplified and composite model over all the voltage levels of the electrical grid, based on a benchmark report. This chapter describes said modelling and simulation method as well as the study cases considered. The resulting simulations are complemented with real fault-data recorded at a personal PV system on a resident rooftop, in addition to fault recordings from the overlying 130 kV station, which all will be presented in chapter 5.

3.1 Fabrication of network model in Power Factory

The network model is simulated as a 50 Hz, symmetric balanced three phase network visualized by single line diagrams, SLDs, in the simulation tool digSilent PowerFactory. Since bolted three phase short circuits are the only fault that will be considered, the negative and zero sequence are neglected. Two separate network models are constructed, one with a rural network structure in the 20 kV MV-grid, hereon after called "Rural model", the other simulation model constructed with a more city-like structure in the MV-grid, called "City model". An overview of both these network models are seen in figure 3.1 below, where the colour boxes indicates the different voltage-levels of the network.

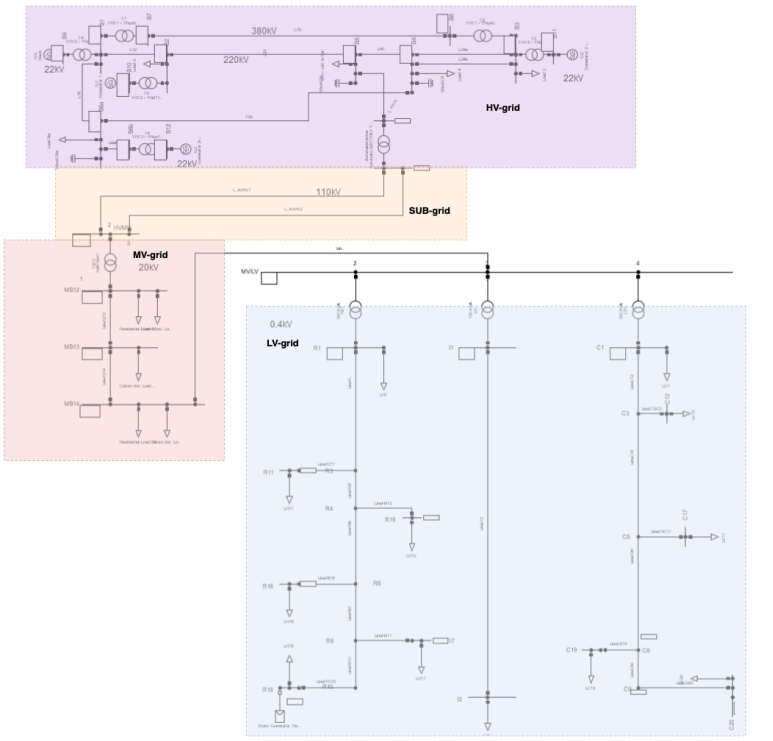

(a) Rural model

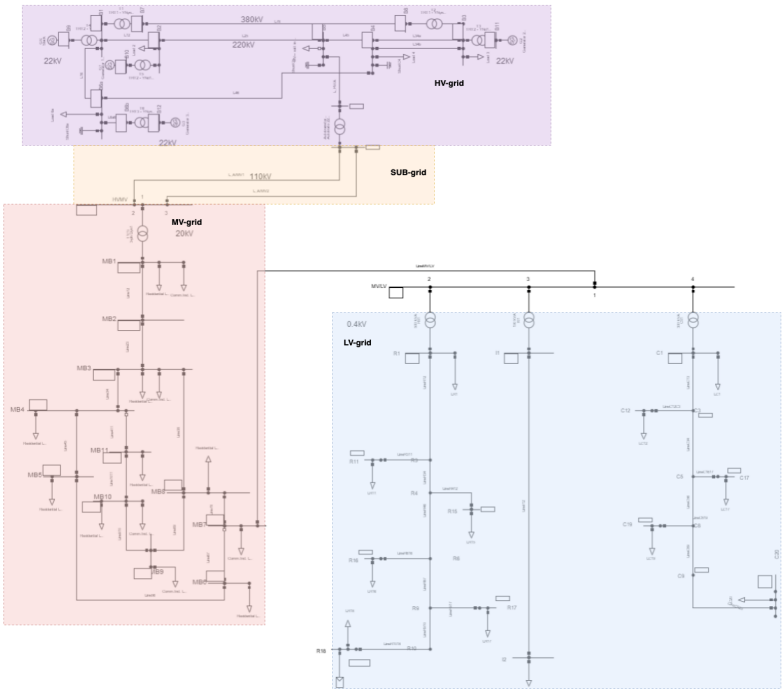

(b) City model

Figure 3.1: Overview of composite network from top to bottom: models with HV-grid (380 & 220 kV), SUB-grid (110 kV), MV-grid (20 kV) and LV-grid (0.4 kV)

Further detail of respective grid-parts and the incorporated components are found in the following sub-chapters.

3.1.1 Network model segments

There was an ambition to ensure that the simulations carried out in this thesis would be as authentic and credible as possible. Thus the first step of this thesis work was to carefully model a network model for the simulations. In order for this to be broadly representative, a benchmark report by CIGRÉ, was chosen as basis and part of the network model could be reused from previous work done by Martin Lundberg at the IEA-division at LTH.

The network model constructed for this thesis is based on the European configuration of the CIGRÉ Benchmark models for High Voltage-, Subtransmission-, Medium Voltage- and Low Voltage networks (CIGRÉ, 2014). This configuration is thus valid for networks all over Europe, but it allows for adaptations to regional and national requirements. In this thesis however, no such adaptations were made, which is why the voltages of the network model does not correspond to voltage levels in the Swedish power system..

High voltage part of model

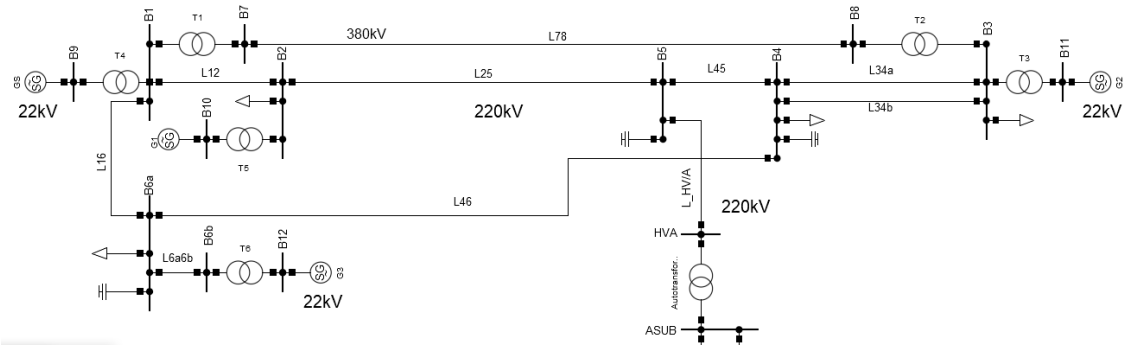

Figure 3.2: SLD of the HV-part of the network model used in simulations

The network transmission voltages used in this HV-part of the model, seen in detail in figure 3.2 above, are 220 kV and 380 kV(one OHL from B7 to B8), which are typical in European transmission systems. Generation voltages are 22 kV. The generators are of ratings S_{rated} 700, 500 and 500 MVA respectively, with corresponding P_{out} of 500, 200 and 300 MW. The fourth generator, called GS in fig 3.2 above, is a so called "slack" or "swing" generator, with the only parameters being a voltage in

magnitude and angle (1.03 p.u. and 0 deg).

The transformers are all of a size 1000 MVA except the transformer at B6b which has S_{rated} of 500 MVA.

Subtransmission part of model

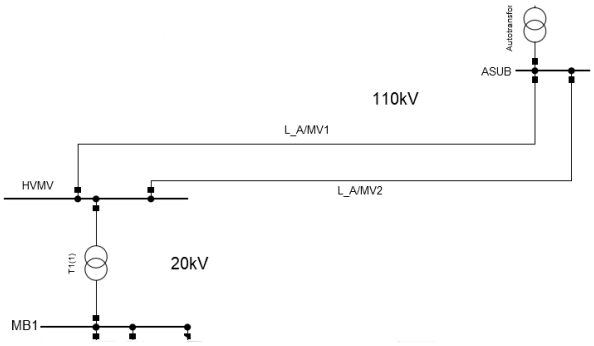

Figure 3.3: SLD of the subtransmission-part of the network model used in simulations

The subtransmission network, shown in detail in figure 3.3, consists of only two parallel lines and transformers between the grid parts. Note that the two parallel lines are identical. The top-most line called "L_AMV1" is of interest as it is used as a fault location in the simulations, further explained below in this chapter.

Medium voltage part of model

The CIGRÉ benchmark model for the Medium Voltage network consisted of two areas, one representing a rural area with radial structure and the other a more city-like area with a meshed structure. This was split up into two different simulation network models, one with Rural MV-part ('Rural model') and one with City MV-part ('City model'), shown in figure 3.4 below. This since it was of interest to investigate differences between the two network structures, and since there was a constraint in the PowerFactory licence to 50 nodes, in which both MV-parts did not fit.

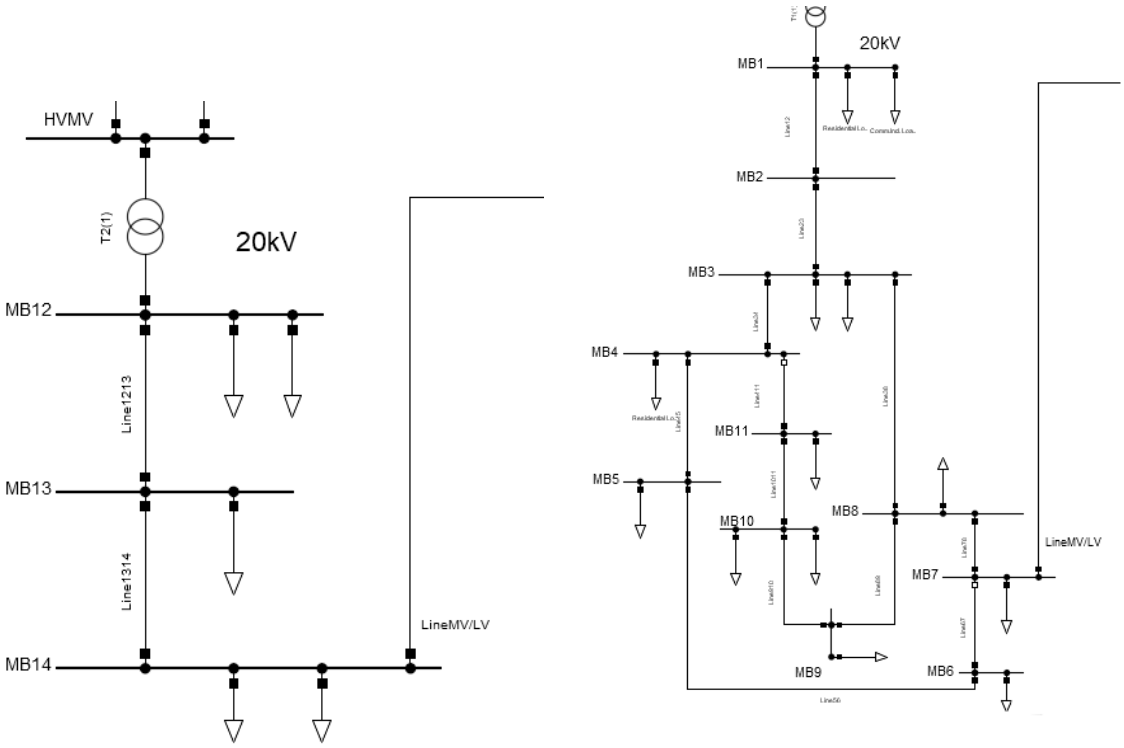

(a) Rural MV-grid **(b)** City MV-grid

Figure 3.4: SLD of the MV-part of the network model used in simulations

Eventhough the City model is constructed as a meshed network, the two loops are opened in the simulations (marked by non-filled squares) and it is *operated* as radials. This is in line with the reality where much of the networks are built meshed but where loops are manually switched on and off, and thus only act as reserves.

Low voltage part of model

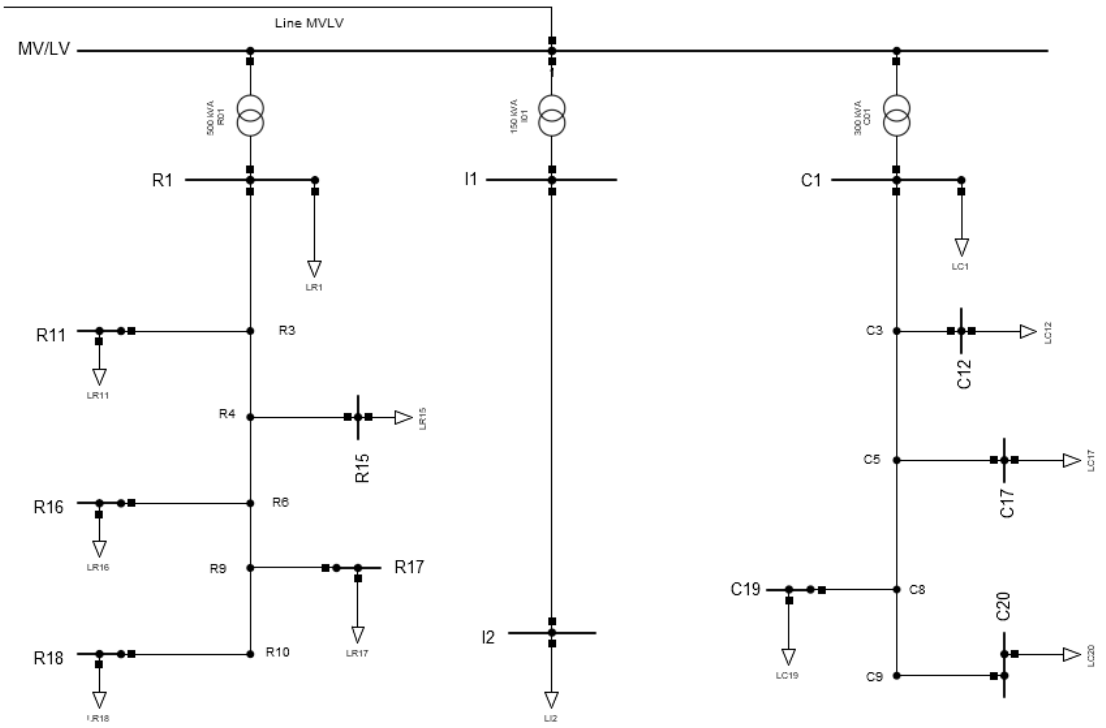

Figure 3.5: SLD of the LV-part of the network model used in simulations

This low voltage network, seen in figure 3.5, is made up by three radial feeders, each representing different types of areas and consumers, where the loads are the main difference. The leftmost feeder correspond to a residential area, the rightmost a commercial area and the middle feeder an industrial area.

In this thesis, different sized PV-units will be connected to all three feeders, but the initial focal point is the busbar called R18.

3.1.2 Re-calculation of network parameters

The Benchmark report (CIGRÉ, 2014) provided data of line parameters, topology, tower geometry, conductor data, load values, shunt capacitor values, transformer and generator parameters. Of these, nearly all data were used, with exception of geometries of cables and lines which were dismissed.

All parameters necessary to build the network model were provided by the CIGRÉ

report as mentioned above. Entering the models into PowerFactory required some conversions, which are described below. For a detailed list of parameters used see appendix B.

Since this is a component network model, the whole network model has to be based on the same S_{base}, in this case 100 MVA. Thus the parameters for the generators in the HV-part of the network, which initially were given on a component base of S_{base} =25 MVA, were corrected with a factor 4.

In contrast, the HV-transformer parameters in CIGRÉ were given in p.u. on system base, but PowerFactory treated input impedances as component-based, which is why they needed to be re-calculated aswell. This using the following relationship:

$$Z_{trafo,comp} = Z_{trafo,system} \cdot \frac{S_{comp}}{S_{system}} \tag{3.1}$$

The line parameters for the HV network were given in p.u. in the benchmark report, and the simulation tool PowerFactory required physical units as component input. Thus a conversion was made where Zbase and then Z(ohm) were calculated as following:

$$Z_{base} = \frac{V_{base}^2}{S_{base}} \tag{3.2}$$

$$Z(ohm) = Z(p.u.) \cdot Z_{base} \tag{3.3}$$

In the same manner, the line parameters of the subtransmission grid were converted from p.u. to physical units, using the same equation as above, but with a V_{base} of 110 kV instead.

Line parameters of the MV-network were given in physical units, so these were easily transferred into the PowerFactory model.

The transformer parameters of the MV-network were also given in actual physical units, but PF requires the input to be in per unit, based on the transformers own rated power S_{rated}. Thus the parameters were re-calculated from actual units to per-unit values based on the rated power and voltage of the transformer; same procedure as in eq 3.2 and 3.3 above, but with Z(p.u.) as final product.

In order to simplify the model (to fit into the licence constraints in PowerFactory), load-aggregations were made in the LV-part. This by calculating equivalent impedances of multiple load points and connecting cables in the commercial feeder. I.e. multiple "consumers" were conversed into collected loads.

3.1.3 PV model: parameters and component model

The initial modelling of the PV-unit is based on ratings and settings from a residential PV installation in Bara outside of Lund, see figure 3.6 .

Figure 3.6: Residential PV system in Bara (photo: Annie Haraldsson, 2022)

The topology of the overlying grid where the residential PV-unit is connected is shown in figure 3.7 below. The resident that has this PV-unit in question also has a Phase Measurement Unit (PMU) that records disturbances experienced at this low-voltage connection point, which will be studied in this thesis. Registrations from an additional PMU unit located at LTH are also considered, this is fed from a station which is not depicted, underlying the station called "STW-".

This thesis will also incorporate observations and analyses of disturbances recorded by E.ON at the overlying station for the PV-unit called Station M or "STM-". These

faults are presented in section 5.

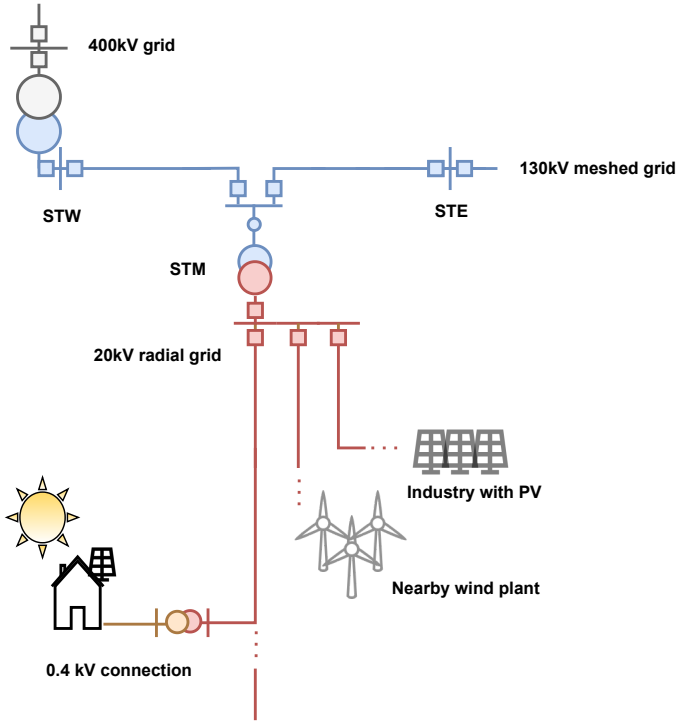

Figure 3.7: Topology of overlying grid for the residential PV-unit

Input parameters from the residential PV-unit are used in simulations, the data used stated in table 3.1 below (Runvik and Juntti, 2022).

Table 3.1: Input parameters to the simulated PV-unit in the the initial case

Rated active power	6 kW
Normal operational power	3 kW
Cos (ϕ)/ power factor	0.85-1 (adjustable)
S_{rated}	7.06 kVA

During simulations cos ϕ is assumed to be equal to 1 at all times as operating point for the PV unit, this because the scope of the thesis is to investigate active power of solar installations and thus disregards any contribution of reactive power. Although, when calculating the rated apparent power, S_{rated}, of the PV unit, a power factor of 0.85 was used, since this gives the highest apparent power and thus the PV and its auxiliary systems must have been dimensioned thereafter. The rated apparent power were calculated as follows:

$$S_{rated} = \frac{P_{rated}}{cos(\phi)_{min}}$$

The PV unit is modelled with a local controller to keep constant cos ϕ, for the same reason as mentioned above. During simulations it is also assumed that there is a constant output of the maximum installed capacity.

Component model in Power Factory

When it comes to the simulation model of photovoltaics, Power Factory (PF) has two options of component-models. A model called "PV system" or a "Static Generator".

The "PV system" model in Power Factory, is either based on constant power injection or on solar calculations with input parameters as solar irradiance etc, which is outside of the scope. Firstly this model was applied with a constant active power injection, but it seemed to be disconnected automatically when simulating SC faults. Thus the objective to investigate how active power affect LV-buses *during* fault, would be impossible. Thus, the possibility to model a PV as a "Static Generator" in PF was instead reviewed. The static generator model in Power Factory can be configured as many different devices. Here the option to model the PV unit as a full size converter was chosen, since the model configured in this manner represents generation connected to the network via power electronics. (DigSILENT Power Factory, 2021)

In the static generator configured as a full size converter contributions are modelled as constant current injections in the short circuit calculations. The fact that the PV-unit is modelled as a constant current injection means that a fixed positive sequence current is injected to the grid from the terminals of the PV-unit during short circuit faults. The magnitude of the current depends on the voltage dip after the short circuit calculation has been performed with only rotating machines (i.e. with only generators contributing). In practise this current injection may affect the voltage at the point of connection to the grid, i.e. at the LV bus where the PV unit is placed.

This component model implies some constrains on the simulations. It was first intended to simulate short circuit faults and let the whole installed capacity of active power from the PV unit stay connected and uphold the voltage at the nearest busbar.

However, since Power Factory's component model has the aforementioned current (and thus power) calculation during faults, it is not possible to "keep" all of the installed active power during faults, since the current and thus power input depends on the voltage dip at the connection point. Thus the results of these simulations will be on a more conceptual basis, than based on exact kW of power corresponding to an exact impact of x p.u. reduction of the voltage dip at the LV busbar. Yet, since these component models are realistic and authentic the simulations are regarded as reliable.

3.2 Fault simulation and analysis

The simulations in this thesis are made on the previously described grid-model in the simulation tool digSilent PowerFactory. No dynamics are introduced so entirely static simulations are performed.

The fault type simulated is a 3 phase (3ph) short circuit (SC). This was chosen since it is the most severe fault type, that renders the highest fault currents and thus renders the largest impact on the voltages. This fault type is also the simplest in a simulating-perspective since only positive sequence impedances in every component are utilized, thus only positive sequence was modelled.

With the chosen simulation method it is possible to simulate multiple faults at different locations in the network, due to time constraints this is left to future work.

3.2.1 Short circuit model in PowerFactory

The simulation tool, digSilent PowerFactory, has a number of short circuit methods for calculating short circuits in different manners. The decision on which calculation model that was most appropriate to use was based on the Power Factory User Manual.

The following documentation was found in the user manual for Power Factory:

> The IEC 60909/VDE 0102 Part 0/DIN EN 60909-0 Method is a simplified short-circuit calculation method which doesn't require accurate system loading information to be present in the network model in order to produce useful results. Unlike the complete method, a preceding load-flow calculation is not required. Instead, the system nominal voltage at

> the point of fault is increased or decreased by a specific safety factor (the so called c-factor) with the intention of producing either conservatively high or conservatively low results according to the user's specific requirement. (p.476, DigSILENT Power Pactory, 2021)

Thus this IEC short circuit model would not result in sufficiently realistic voltage-data, since the pre-fault voltages depend on a c-factor; a constant altered in the simulation by the user. Since this thesis has an emphasis on voltage, this method was not deemed sufficient. Another short circuit calculation model called 'the complete method' was instead considered and its documentation canvassed:

> Using the Complete Method it is possible to calculate results which take account of the procedures outlined in Issue 1 and further developed in Issue 2 of the ENA Engineering Recommendation G74. The Issue 2 update introduced two additional short-circuit models for converter driven plant, specifically a doubly fed induction generator model and a full size converter mode. In PowerFactory the configuration of these models is carried out in either static generator models or in a doubly fed induction machine models. (p.483, ibid.)

I.e. using the complete method it is possible to get results which take into account the short circuit models of converter based generation, such as a PV unit with a full size converter. In addition, the pre-fault voltages are calculated from load flow calculation. Thus the complete model was found to be the most appropriate for the simulations to be carried out in this thesis.

The complete model is a superposition method of SC-calculation. The results are determined by superimposing healthy load-flow results for the network model at the moment before short circuit (see a) fig 3.8) with a set of results that represent the faulted system (see b) fig 3.8). All voltage sources are shorted in the faulted state, and an additional voltage source is connected at the fault location injecting an equal and opposite voltage than the prefault voltage at that location, as determined from the preedeceeding loadflow calculation. (ibid.)

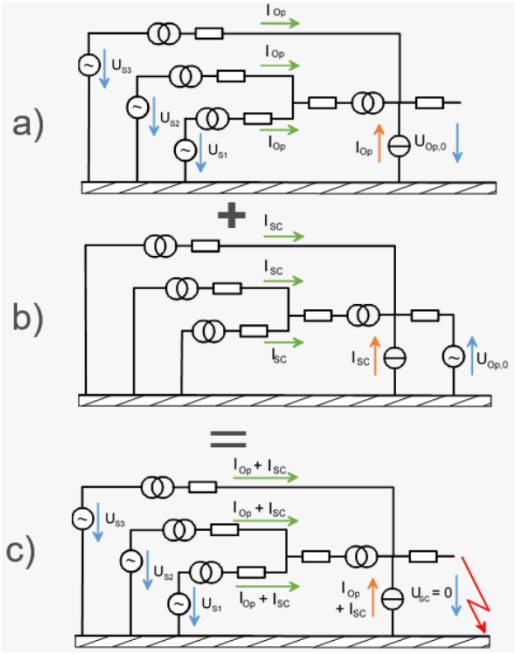

Figure 3.8: Illustration of the superposition used in the Complete method, where the prefault situation in a) and the fault contribution b) together yield the fault situation.

None of the supervisors recognized any of the short circuit model, which is why a brief comparison and analysis was carried out as stated above. Multiple models were based on one or more standards (IEE/ANSI, IEC, ENA G74), although these standards are not widely accessible for free. Thus if any future work were to replicate this method with short circuit simulations it is optimal to have access to these standards in order to make a more informed choice.

3.2.2 Fault locations during case simulations

The scope of this thesis is to investigate SC-faults and the impact of active power from PV-units during faults. Since grid owners/operators have to plan for or at least be aware of worst possible outcome, this thesis focus on the severity of the faults rather than likelyhood of an actual fault occurring at a certain spot. Thus the placement of the SC-fault in the grid model will be chosen to be as severe as possible while still maintaining power supply, in order to correspond to a worst case scenario.

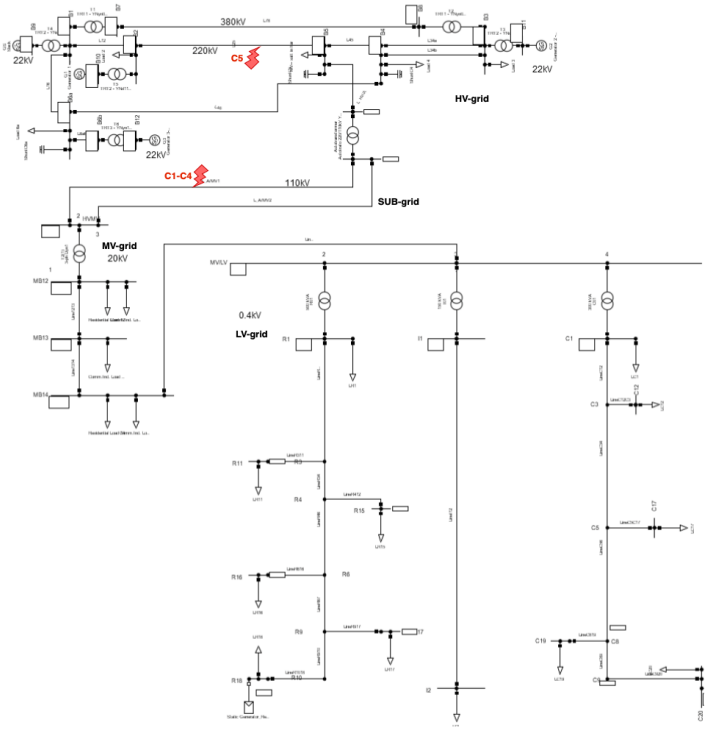

Figure 3.9: Fault location for the different study cases C1-5

The fault location used in Case 1 to 4 is placed at 50 % of the length of an OHL line in the SUB-grid, as shown in the figure above. This line is one of two parallel lines in the SUB-part of the network model and is thus a critical point in the network model.

In Case 5 multiple fault locations are used in order to study the effect on the HV-grid. Although, in the first part of Case 5 the LV-nodes are of interest and the fault location is placed on one OHL in the HV grid, seen as a red lightning-bolt in figure 3.9.

3.2.3 Fault analysis of distrubances recorded at E.ON

Disturbances recorded at E.ON in the 130 kV-station, STM in figure 3.7 above, overlying the residential PV-unit in Bara were retained for a few months in the winter of 2021-2022. Selected faults were analysed in order to determine the most probable fault-sequence. These faults will be presented in chapter 4, as a supplement to the simulated results. A description on the central signals used and analysed in these recordings are presented in table 3.2 below.

Table 3.2: Signals in fault recorder at "STM" (Clementson, 2022)

Signal	Description
iLx	phase current of phase x
uLx	phase voltage of phase x
iE	earth fault current, calculated sum from iL1-3
uEn	residual voltage
iEs	earth fault current, recorded

The signal called uE_N is the measured neutral point potential. This potential is normally zero, or close to zero, since it is connected to ground, but during earth faults there is a so called neutral point displacement. (Samuelsson, 2021b)

3.2.4 PMU setup and method

In addition to the fault recordings from E.ON, there were also data recorded from a PMU placed at the residential PV unit in Bara. This allows for comparison and discussion on how faults are perceived both at grid owners ordinary fault recorders, but also how those faults "look like" at a LV-connection point. Thus giving a unique opportunity to a "bottom-up" approach, and see how disturbances are observed both at lowest part of grid (LV-connection point) as well at higher voltage levels in the grid.

Access were also obtained to data from a PMU placed in one of the laboratories in LTH, which in this thesis served as a way to determine if faults recorded at Bara were of 'local' or 'regional' nature.

The PMU installed at the resident is of type RES670, manufactured by ABB. It records phasor/vector-data of currents, voltages and frequecy-data which are continuously sent to a central server for comparison with data recorded by other units. The recorded data are mainly suitable for observing system-wide processes/patterns (timescale of a minute and up), but since there is a 50 Hz sampling with precise time-stamps, quick events can also be caught. (Runvik, 2022b)

Since PMUs like these renders an extensive amount of data, only the events that were recorded by the disturbance recorder at the overlying station were analysed.

3.3 Simulation: Grid-model assessment

Proceeding the main simulations with focus on PVs, some initial simulations will be carried out as a model assessment, together with some simulations that will serve as a baseline for comparisons.

3.3.1 Network model pre-fault

Firstly, the pre-fault voltages at different locations in the network model will be computed. Pre-fault voltages will be shown for busbars in each voltage part of the network model, and for both simulation models, i.e. both for "Rural" and "City" model.

3.3.2 Impacts of SC faults at different voltage levels

The second part of the grid assessment is to simulate the impact of SC-faults at different voltage levels in the network model. This in order to showcase the relation between fault location-voltage level and range of impact of a short circuit fault. A short circuit fault was placed at each of the different voltage level parts of the network models, one at a time, and the voltages of selected nodes were stored after each simulation. These busbar-voltages were plotted in one graph to show that short circuit faults are more severe and impact more nodes the "higher up" in the network (and thus higher up in voltage) it is located. In figure 3.10 below, the fault locations in the different grid-parts are marked by a red flash-symbol and the busbars from which the results are gathered are marked by a green circle.

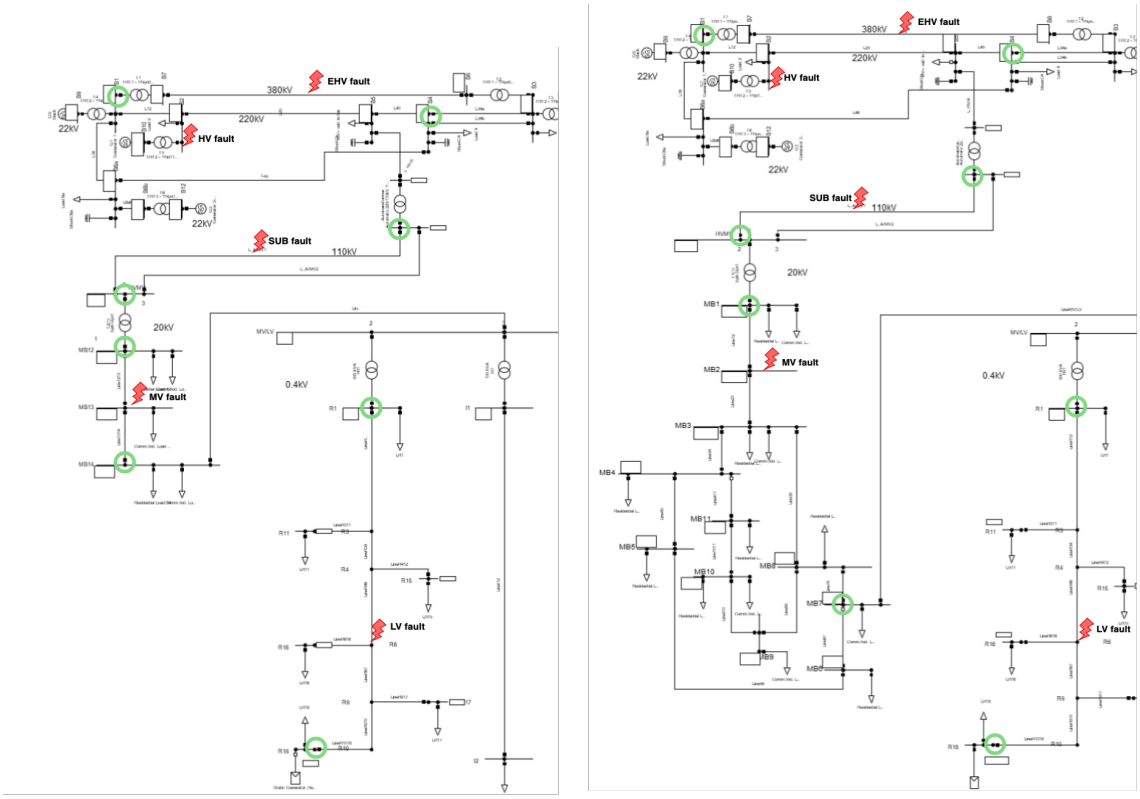

(a) Rural model **(b)** City model

Figure 3.10: Fault placements (red flash) at different voltage levels in the network for 'grid-model assessment'-simulation. Result-nodes marked with a green circle.

3.3.3 Geographic impact of faults at high voltage

Lastly, the impact of SC-faults in the HV-part of the grid was of interest. More specifically, to show the geographical spread of the voltage impact by SC faults at different busbars. In order to do this, the SLD of the HV-grid part had to be re-arranged visually to represent the distances between the busbars. This was done by letting the lengths of the OH-lines and create a 'map' of the area, somewhat to scale. The different parts of the HV-grid were also named with quarters ("West"/"East" etc). The geographic figure serves as a basis for a 3D matlab-plot, where the respective busbar voltages were placed at the corresponding busbar-position.

3.4 Study Cases

The main simulation focus in this thesis is on a set of study cases presented in this section. The initial study case will represent the production from the PV-unit in

Bara that is studied in this thesis. Case 2 to 3 portray two scenarios with more up-scaled production that is represented in present day to some extent. Case 4 and 5 represent future scenarios with PV-production that fill up the capacity of the grid up to MV- and SUB-voltage levels respectively.

3.4.1 Case 1: Base case

A base case that will be examined is modelled with a residential PV unit based on input data from a PV installation on a roof located in Bara, south of Lund. The relevant parameters that are used from this PV-unit are stated in table 3.1.

3.4.2 Case 2: Expanded Residential PV units

This second case will investigate the effects of short circuits if every consumer in a residential area would have solar panels on their roof. These PV units are modelled as the same size as in Case 1.

3.4.3 Case 3: Maximum PV at LV-level

In this case, the PV units are not only increased in number but also in magnitude of installed and operational power. This case was formed with an intention to include the current situation in some regions of the grid in Skåne where micro-production is prominent. This case correlates solar production to the load-consumption. The grid model used in this thesis has no information on the area it feeds, i.e. if the load-points are single households or other construction types (apartment complex, skyscraper, etc), more than that the three feeders in LV-grid is of "residential", "industrial" and "commercial" type. As a way around this, the case will consist of two sub-cases. One sub-case were all nodes in LV-grid is assumed to be a single house/construction, and a second were the nodes are assumed to be multiple consumers of variable quantity. In both sub-cases all loads are applied, unchanged from the CIGRÉ-benchmark data.

Case 3a - Each loadpoint is a single prosumer

In this sub-case, all load-points at the three feeders in the LV-network, residential, industrial and commercial (R-,I-,C-), are equipped with PV-units of different sizes. Each load-point in the residential feeder in the LV-part of the network is considered to be a single household that produces a maximum output of active power of 43.5

kW. The same reasoning is made for the load-points at the commercial feeder. See the input parameters for this PV-unit type in table 3.3.

Table 3.3: Input parameters to the simulated PV-units at R- and C-nodes in case 3a

Rated active power	43.5 kW
Output power	43.5 kW
Cos (ϕ)	1

At the industrial loadpoint the PV-unit is instead modelled as a larger unit of 500 kW. This is based on a reasoning that industries generally have much larger areas available for PV installation, and that they might have a higher incentive to produce electricity. Especially since tax-legislation in Sweden is favourable for PV installations up to 500 kW installed top capacity.

Case 3b - Each loadpoint has x prosumers with total production that equals the consumption

In this sub-case, all loadpoints in the LV grid are considered a variable amount of households, that each has a microproduction of 43.5 kW. The number of houses are not explicitly determined but instead the total active power from each load-point is set to equal the maximum consumption at that node (amount of kVA load = amount of kW production). The simulation is run with full loads and equal amounts of production, which theoretically could cancel out. However this is not the outcome of the simulation in PowerFactory, suggesting that the loads might only be used in the load flow calculation and not taken into account during the short circuit calculation.

However, the loads in the CIGRÉ-benchmark are given in apparent power, S, with power factors (cos phi) ranging from 0.85-1. Thus the consumption is not merely active power but also some reactive power. Since the scope of the thesis being active power, a simplification was made in this case, where all drawn apparent power S were assumed to be active power and thus the dimensioning of PV-units based on the load will result in equal magnitude of active power. Thus an amount of x kVA is equated to x amount of kW. The size of the PV-unit at each node was determined by the load connected to the same node. See table 3.4 below for PV-parameters.

Table 3.4: Active power of PV units (P_{PV}) in Case 3b, based on loads at each node

Loads at LV nodes	S (kVA)	PV-units in Case 3b	P_{PV} (kW)
LR18	47	PV_C4(R18)	47
LR17	35	PV_C4(R17)	35
LR16	55	PV_C4(R16)	55
LR15	52	PV_C4(R15)	52
LR11	15	PV_C4(R11)	15
LR1	200	PV_C4(R1)	200
LI2	100	PV_C4(I2)	100
LC20	8	PV_C4(C20)	8
LC19	16	PV_C4(C19)	16
LC17	33	PV_C4(C17)	33
LC12	65	PV_C4(C12)	65
LC1	120	PV_C4(C1)	120

This sub-case is the corresponding case as if all prosumers were to produce the same amount of power they usually draw from the power system. The worst case of this scenario, in reality, would be if all prosumers produced their maximum and simultaneously not consumed anything, then the direction of power would be reversed in overlying stations.

3.4.4 Case 4: Maximum PV MV-level

The aim was that this report would be a worst-case and include even larger magnitudes of solar power than forecasted, described in section 2.4.2. Although, during the course of the simulation work, it became clear that the current simulation model was restricted in capacity, and thus that would be the restriction of the future scenario. A future "worst case scenario" would be that multiple PV-units (of either micro-size or larger plants) take up all the available capacity in the grid. This corresponds to some customer request in Skåne today already, according to E.ON, where customers looking to install solar power are seeking to build as big as possible and thus use up all the available capacity at that grid area. These "future cases" presented in Case

4 and 5 are then to some extent already corresponding to the reality at some parts of the grids.

These future max PV cases (case 4 and 5) will be based on the transformer size in the current model. Size of transformers are generally determining or restricting what is allowed to connect in grids during grid-planning. The transformer in the simulation model in the MV-grid has a rating of 25 MVA.

Due to time restrictions these cases are simulated with all active power input from future PV-units aggregated and placed at one location in the simulation model. Since this is a rather simplified version of a future case, especially considering that the location of the PV-block will be crucial, two sub-cases are created with different location of this PV-block. Case 4a with the PV-block placed as far from the LV-part of the grid as possible at busbar "MB12" in Rural, and "MB1" in City model. Case 4b with the PV-block placed as close to the LV-grid as possible at busbar "MVLV". See the busbars in question in figure 3.4.

3.4.5 Case 5: Maximum PV at SUB-level

Equivalently to Case 4, this case will also simulate a scenario where solar installations (independent of size) have taken up all the available capacity in the grid. In this scenario, solar power has taken up all the capacity up to the SUB-level. The capacity of grids are determined by the transformer sizes, a functional limit set by grid-owners and operators. The network grid utilized in this thesis has a transformer size of 150 MVA at the interface between the HV and sub-transmission level of the grid. Thus this case is simulated with a 150 MW block of active power, placed as close as possible to the HV grid.

Since the location of the PV-block is above the standard fault location, the location was changed in this case to an OHL in the HV grid called L25 (see section 3.2.2 for details).

This case will be evaluated in two procedures. Firstly it will be presented and evaluated like the other cases, where nodes of all underlying grid-levels will be viewed with regards to voltage dip and difference. Furthermore, with installed solar capacity of this amplitude, it was also of interest in this thesis to investigate any geographic

extent the impact of accumulated PV-power may have. This to evaluate the possible mitigating effect that active power input may have on the voltage during faults at this "future up-scaled" size, or conversely, the effect of disconnecting PV-units of a total sum of 150 MW during fault. The method used for this second evaluation is as follows: The simulation is repeated with the fault location changed each time to a different OHL or busbar in the HV-grid. These results were then presented in a 3D graph in Matlab, on top of a figure of the HV-network as shown in section 3.3.3. Not all results are presented, but only a selection of the most interesting. The results are also compared to the results of section 3.3.3, to get a direct measure of the impact of 150 MW solar power during SC-faults.

4 Results

This chapter presents the results from simulations carried out on the network model presented, and with method described in chapter 3.

4.1 Network model pre-fault

Initially, simulations were made with only loads and conventional generation, in order to observe pre fault values of the modelled network. For a selection of busbars, the prefaulted voltages are shown in table 4.1 below.

Table 4.1: Voltage in unfaulted network model, busbars from all different voltage levels

Node	Voltage level	Unfaulted voltage (p.u.)	
Sim.model		*Rural*	*City*
B1	220 kV	1.035	1.035
B4	220 kV	0.963	0.963
HVMV	110 kV	1.093	1.088
MB12/1	20 kV	1.064	1.051
MB14/7	20 kV	1.048	0.975
MVLV	20 kV	1.036	0.962
R1	0.4 kV	1.018	0.942
R18	0.4 kV	0.964	0.883

As is seen in these results, this model does not have a strict limit of a normed 1 p.u. of the voltages, instead it allows a more realistic representation of voltage that is based on load flow calculations of generation as well as loads and line/cable impedances. The generators of this model has a target voltage of 1.03 p.u. as per the benchmark report CIGRÉ, 2014, thus a voltage slightly higher than 1 p.u. is as expected.

4.2 Individual impact of SC-faults in grid

4.2.1 Impact of faults at different voltage levels

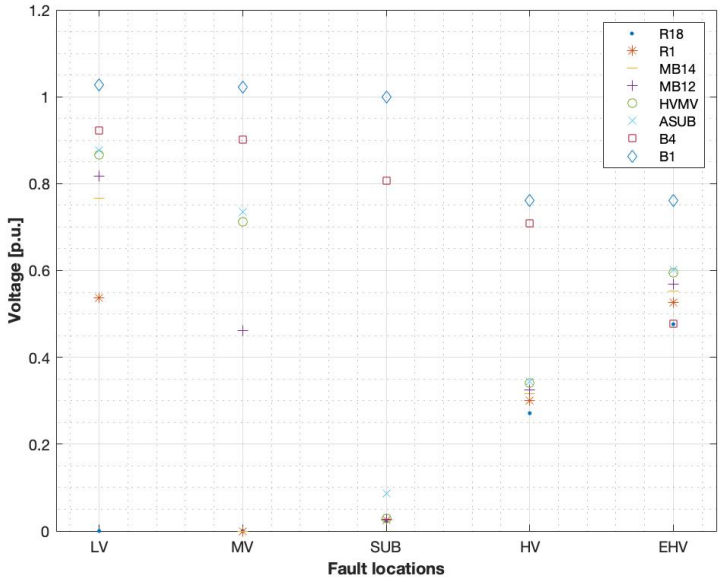

(a) Rural model

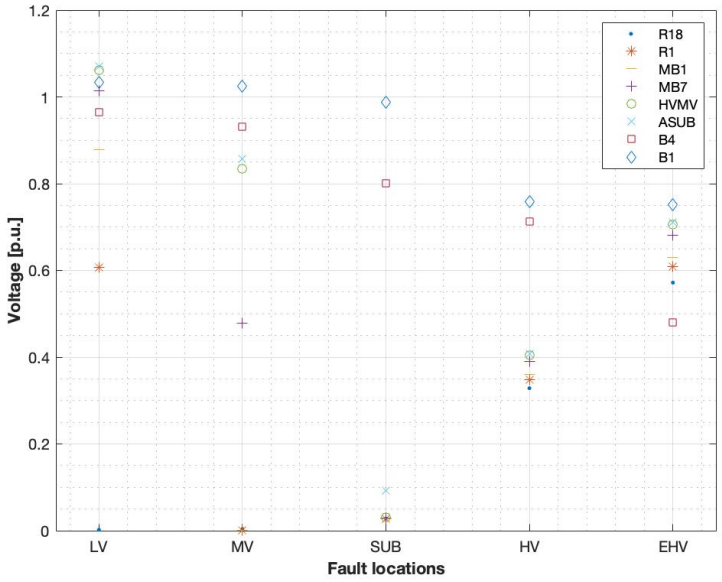

(b) City model

Figure 4.1: Voltage at selected buses during faults placed at different voltage levels. Buses R18 & R1 are in LV, MB1 & MB7 are in MV, HVMV & ASUB are in SUB and B4 & B1 are in HV-grid.

The graphs in figure 4.1 show voltages at selected busbars from all grid-parts when a short circuit fault is placed at LV, MV, SUB and HV-grid part respectively, simulated

in both the 'rural' and 'city' network model. Thus, an increase in x-axis means a short circuit fault placed at a higher voltage level. The results depict a general trend of decrease in busbar-voltages with increasing voltage level of the fault location, which is as expected. Nonetheless, there is some details worth pointing out.

For professionals used to working with normed voltages and strict limits of 1 p.u. the voltages of some nodes/busbars ("B1" for example) might seem wrong since it is initially above 1 p.u. in both graphs. However, this is simply the pre-fault voltage at that busbar. The prefault conditions are impacted by both generation and loads as the simulations in this thesis are not made on a "flat" network but actually based on inital load flow simulation and these models are without upper voltage restraints on 1 p.u. In this sense, this model is different from grid owners praxis, since this is load flow plus a short-circuit "on top" of it.

There is also a deviation from the general trend in both 4.1a and4.1b at the fault location "SUB" where the voltages at all busbars but B1 and B4 are severely decreased, more so than with the fault in the HV-part. This is due to the network structure in the SUB-grid, there is a bottle-neck with only two parallel OHL lines, which results in this vulnerability. Thus, the grid structure and planning is also crucial, not only voltage level at fault.

The fact that the fault placed at EHV does not have considerably larger effect on the voltages than the fault at HV-level is also explained by the network structure. The EHV level only consists of one single OHL that connect the eastern and western part of the grid model, thus there is not an overlying grid that feeds the HV-part. Each point of connection of the EHV-OHL is between generator busbars, which further limit the impact of the voltage dip.

The careful reader might also have noted that the individual voltages of most busbars/nodes during nearly all but most prominent in the LV, MV and EHV faults were lower in the Rural network model than in the City model. This suggest that the city model constitutes a stronger network that is more insensitive to voltage changes.

However, subsequent calculation of network strength and validation in PowerFactory showed that the MV part of the city model had a lower short circuit power/capacity than that the rural network (about 20 MVA and 30 MVA respectively). And since

the MV network is the only aspect that is different in the two models, a logic conclusion would be that this holds true for the entire network. Hence the slightly lower voltages in the rural model most likely depend on something else than network strength, such as line/cable distance and impedance between fault and result-node for example.

Consequently, the general results were as expected, with a more severe decrease in voltage affecting more voltage levels the higher up in voltage level the fault was placed. Some details were however not as expected but these will not be further investigated since it is outside the scope of the thesis, and do not affect the overall results.

4.2.2 Geographic impact of faults at high voltage

The geographic impact of faults placed close to the key busbar B5 is shown in this section. The simplified HV-grid model which was used in the construction of the matlab-plots is shown in figure 4.2 below. The red lines serve as a base in the geographic plot. The generator sizes are 500 MW at B2, 300 MW at B6b and 200 MW at B3 respectively, and B1 is a slack-bus. The busbars B4 and B6a do not have any generation connected to them directly.

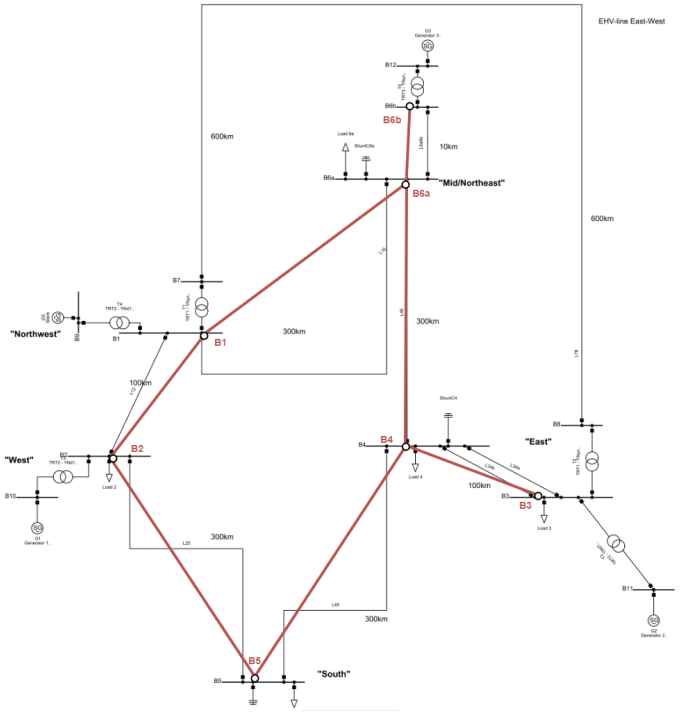

Figure 4.2: Simplification of Topography of HV-network. Vertical red line from B4 to B6a conceal a black SLD-line.

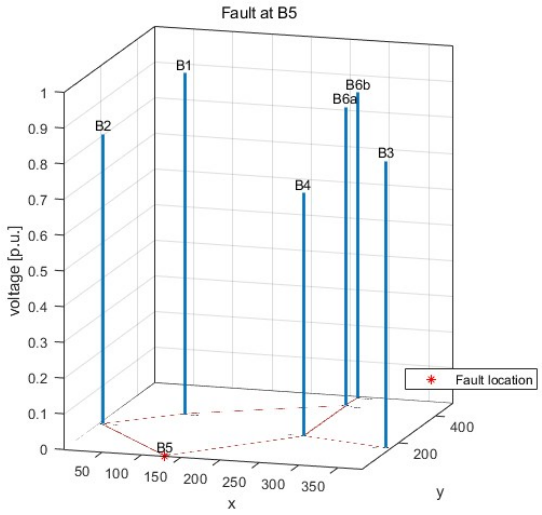

Figure 4.3: Fault at B5

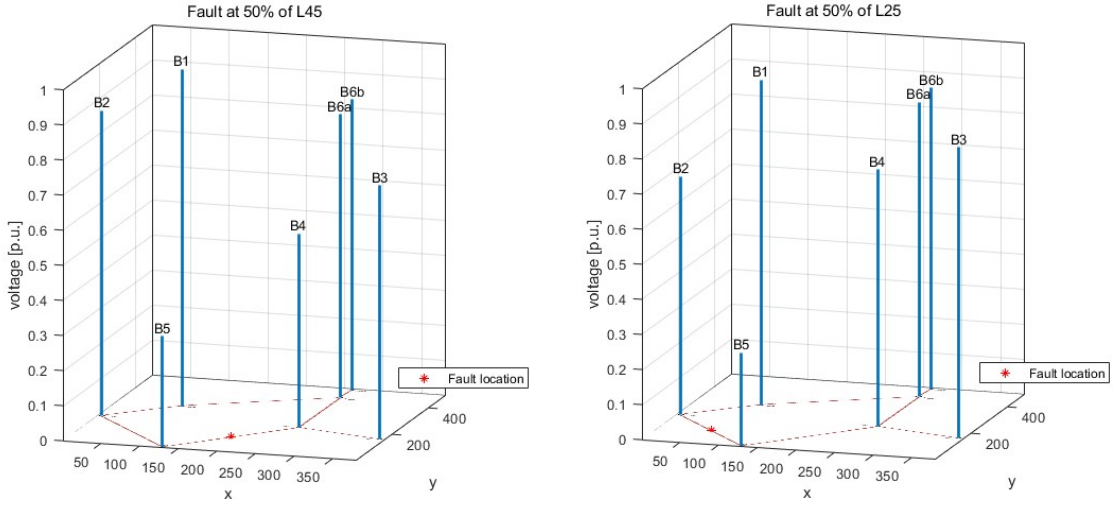

(a) Fault at L45 **(b)** Fault at L25

Figure 4.4: Fault at overlying OHL-lines in each direction from B5 or "South"

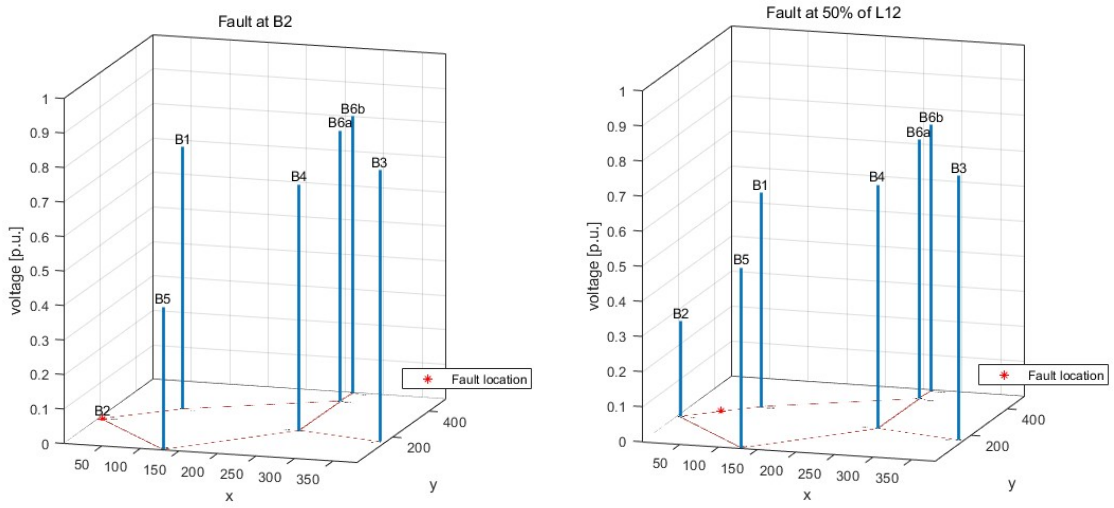

(a) Fault at B2 **(b)** Fault at L12

Figure 4.5: Fault two "steps" further away from B5/"South", in westerly direction

The focal busbar is B5 (also called "south" in figure) since this is the location of the underlying distribution networks in the simulation model. The faults are placed with increasing distance from B5, in both easterly and westerly direction. When the fault was placed at B5, most of the voltages at the other busbars were rather unaffected, see fig 4.3. When the fault was placed a step further away, at L45 and L25, the voltage at B5 was severely affected, seen in figures 4.4a-b. The fault at L25 had larger impact on B5-voltage than the fault at L45, which can be explained by

that there are no generation at B4 while at B2 the largest generator in the grid is connected.

The faults were then placed two steps further away from B5 in this westerly direction, as seen in figures 4.5a-b. Faults at B2 and L12 affected the busbar voltages across the grid in a higher sense, especially the fault at L12. However, the voltage at B5 was higher than during previous faults, which is as expected since the fault locations is further away from B5.

From all these results with different fault placements, it is seen that apart from B5, B4 is also highly affected even when the fault is placed more remote in westerly direction. Thus, a three-point busbar like this, with generation 100 and 300 km away is sensible to faults.

4.3 Case 1: Base case

The results from the first case are as follows:

Table 4.2: Voltage in p.u. at selected busbars for worst possible fault, Case 1

Node	w/o PV	with PV	Δ
MVLV	0.0288	0.0290	$1.8{\cdot}10^{-4}$
R1	0.0283	0.0287	$4.19{\cdot}10^{-4}$
R18	0.0267	0.0305	$3.81{\cdot}10^{-3}$
I1	0.0282	0.0284	$1.77{\cdot}10^{-4}$
I2	0.0273	0.0274	$1.71{\cdot}10^{-4}$
C1	0.0282	0.0284	$1.77{\cdot}10^{-4}$
C20	0.0266	0.0268	$1.67{\cdot}10^{-4}$

(a) Rural model

Node	w/o PV	with PV	Δ
MVLV	0.0267	0.0269	$1.9{\cdot}10^{-4}$
R1	0.0262	0.0265	$3.4{\cdot}10^{-4}$
R18	0.0244	0.028	$3.6{\cdot}10^{-3}$
I1	0.0261	0.0263	$1.86{\cdot}10^{-4}$
I2	0.025	0.0252	$1.78{\cdot}10^{-4}$
C1	0.026	0.0262	$1.85{\cdot}10^{-4}$
C20	0.0243	0.0245	$1.74{\cdot}10^{-4}$

(b) City model

In table 4.2 above the results shows that a single PV-unit of $6kW_{peak}$ and 3 kW nominal operating power has minimal effect of the voltage in its surroundings. Highest impact on voltage is, as expected, on the busbar to which it is connected (R18) and the head of the R-feeder, busbar R1.

One can also note that all voltages are slightly lower in the simulation with City model than in that with the Rural model. This is probably explained by the higher impedance of the rural model, which according to equation 2.4 gives a higher increase of voltage with injection of active power $(P \cdot R)$.

Although the impact on the voltage is minimal, the fact that one can note a difference with this low amount of installed solar capacity, indicate that up-scaled scenarios with multiple units is of interest.

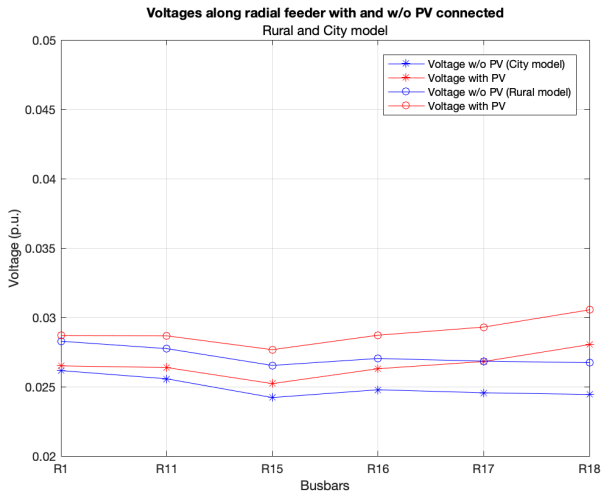

Figure 4.6: Voltage at all busbars along residential feeder in Case 1, data from Rural and City model

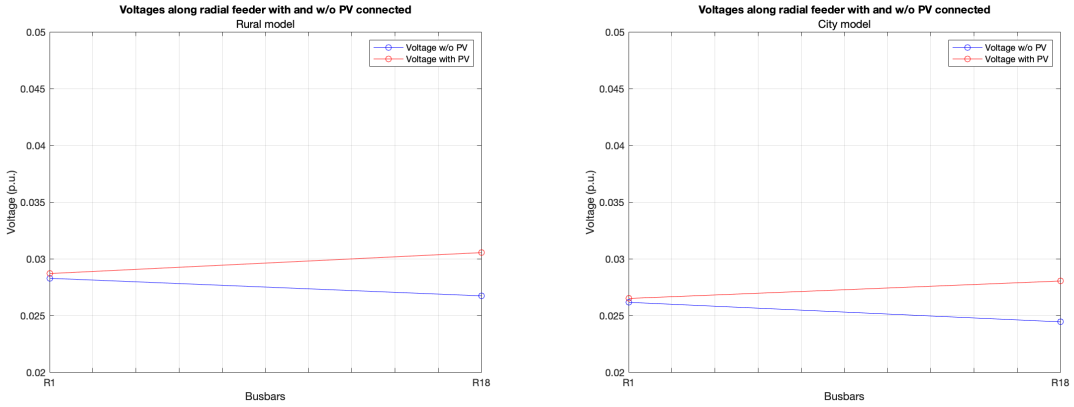

(a) Rural model **(b)** City model

Figure 4.7: Voltage at the 'remote busbars' of the feeder. R1 is the busbar at the top and R18 at the bottom of the feeder, PV unit connected at R18

Due to space-conservation and to maintain readability in the Results-chapter, these

plots with visual representation of the result-tables will only be shown for one of the simulation models, for the "City" model. The general results seen in these graphs are in all cases the same for both simulation models and it only differs by a few decimals, which can be seen in the tables.

Furthermore, only the graphs that show the feeder-head and feeder-bottom (in figure text called "remote busbars") will be shown, since the scope of this thesis is not as detailed as to investigate the behaviour of single busbars along a feeder, but more the general impact of PV at "highest" and "lowest" part of voltage-levels.

4.4 Case 2: Expanded Residential PV system

The result of case 2, with PV-units of 3 kW connected at 5 nodes along the R-feeder, is shown below.

Table 4.3: Voltage in p.u. at selected busbars for worst possible fault, Case 2

Node	w/o PV	with PV	Δ
MVLV	0.0288	0.0299	$1.11{\cdot}10^{-3}$
R1	0.0283	0.0310	$2.73{\cdot}10^{-3}$
R18	0.0267	0.0375	$1.07{\cdot}10^{-2}$
I1	0.0282	0.0293	$1.09{\cdot}10^{-3}$
I2	0.0273	0.0283	$1.05{\cdot}10^{-3}$
C1	0.0282	0.0293	$1.08{\cdot}10^{-3}$
C20	0.0266	0.0277	$1.03{\cdot}10^{-3}$

(a) Rural model

Node	w/o PV	with PV	Δ
MVLV	0.0267	0.0279	$1.2{\cdot}10^{-3}$
R1	0.0262	0.0286	$2.39{\cdot}10^{-3}$
R18	0.0244	0.0346	$1.02{\cdot}10^{-2}$
I1	0.0261	0.0273	$1.17{\cdot}10^{-3}$
I2	0.0250	0.0262	$1.12{\cdot}10^{-3}$
C1	0.0260	0.0272	$1.17{\cdot}10^{-3}$
C20	0.0243	0.0254	$1.09{\cdot}10^{-3}$

(b) City model

Table 4.3 shows a similar result as in Case 1, the voltage is slightly more affected but it is still a rather small difference of a magnitude 10^{-2} at most. Figure 4.8a shows the impact of the five 3 kW PV-units in the Residential feeder. Figure 4.8b in contrast shows the impact on a parallel feeder where no PV-unit is connected, which is as expected; a small but unison increase of voltage at the whole feeder. The (b) figure in this case shows the C-feeder, but the same general result is seen in the I-feeder.

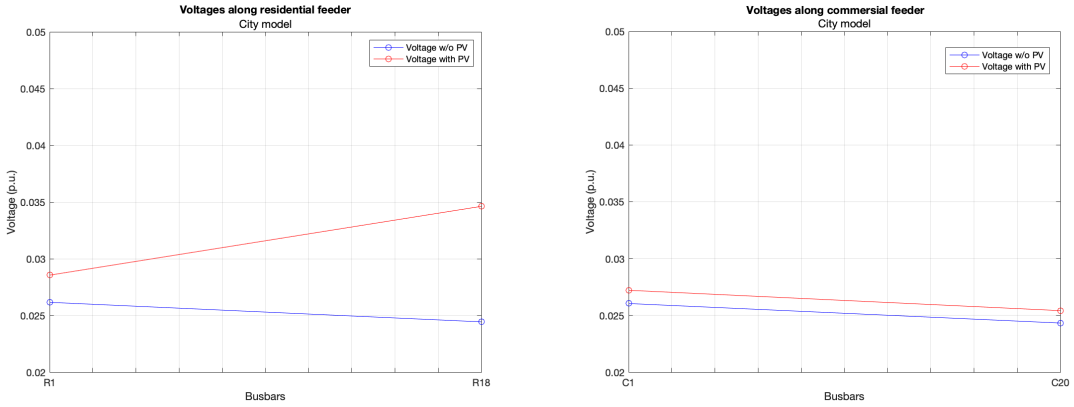

(a) Residential feeder **(b)** Parallel feeder

Figure 4.8: Voltage at remote busbars at LV-feeders for Case 2

4.5 Case 3: Maximum PV at LV-level

In this case all consumers are also producers. All nodes assumed to have one single prosumer in case 3a. In case 3b each node is x amount of micro producers that equals the maximum load at that node, so that total production equals load at each node.

4.5.1 Case 3a - Each loadpoint is a single prosumer with 43.5 kW

In this case, each loadpoint at the residential and commercial feeder in the LV-part of the model is considered to be a single household, with a PV-unit producing exactly 43.5 kW. The industrial feeder equipped with a larger unit to represent an industrial PV-site.

Table 4.4: Voltage in p.u. at selected busbars for worst possible fault, Case 3a

Node	w/o PV	with PV	Δ
MVLV	0.0290	0.0605	0.0315
R1	0.0283	0.0755	0.0472
R18	0.0267	0.1255	0.0987
I1	0.0282	0.2020	0.1738
I2	0.0273	0.3647	0.3375
C1	0.0282	0.0830	0.0548
C20	0.0266	0.2109	0.1843

(a) Rural model

Node	w/o PV	with PV	Δ
MVLV	0.0267	0.0700	0.0433
R1	0.0262	0.0869	0.0608
R18	0.0244	0.1352	0.1108
I1	0.0261	0.2181	0.1919
I2	0.0250	0.3803	0.3553
C1	0.0260	0.0949	0.0689
C20	0.0243	0.2222	0.1979

(b) City model

The results of case 3a in table 4.4 show that the voltages at these LV-busbars are more affected in this scenario with significantly more solar capacity installed. The busbar/node with highest impact is I2, the bottom node of the industrial feeder, where a larger "industrial unit" of 500 kW was connected. Here the power from the PV units affected the voltage with as much as 35.5% (see I2 in table 4.4b).

In figures 4.9 a) - c) the impact of this up-scaled solar production is shown for the residential, industrial and commercial feeder respectively. The voltage is highly affected in all cases, with the I-feeder showing the highest difference.

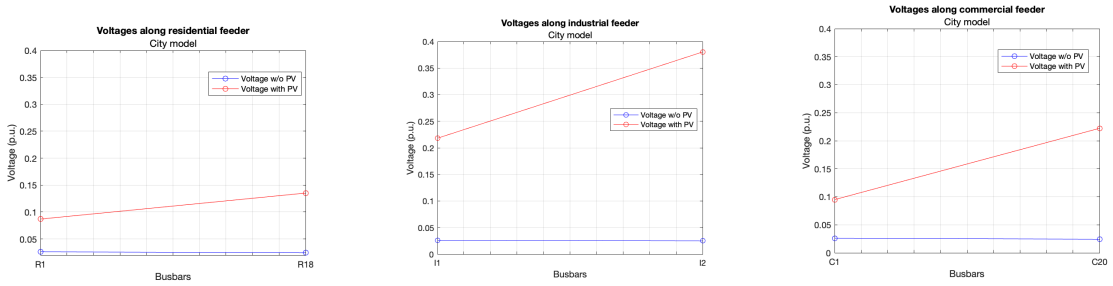

(a) R-feeder **(b)** I-feeder **(c)** C-feeder

Figure 4.9: Voltage at outmost busbars at LV-feeders for Case 3a

4.5.2 Case 3b - Each loadpoint is x prosumers with 43.5 kW

In this sub-case, each node is considered a variable amount of households, which each has a PV unit of 43.5 kW. The number of houses are not explicitly determined but instead the total active power from each node is set to equal the maximum of consumption at that node (amount of kVA load).

Table 4.5: Voltage in p.u. at selected busbars for worst possible fault, Case 3b

Node	w/o PV	with PV	Δ
MVLV	0.0290	0.0509	0.0220
R1	0.0283	0.0763	0.0480
R18	0.0267	0.1252	0.0984
I1	0.0282	0.0712	0.0430
I2	0.0273	0.1026	0.0753
C1	0.0282	0.0760	0.0478
C20	0.0266	0.1250	0.0984

(a) Rural model

Node	w/o PV	with PV	Δ
MVLV	0.0267	0.0564	0.0296
R1	0.0262	0.0834	0.0573
R18	0.0244	0.1310	0.1066
I1	0.0273	0.0781	0.0508
I2	0.0262	0.1083	0.0821
C1	0.0272	0.0830	0.0558
C20	0.0254	0.1310	0.1055

(b) City model

In this case with solar power that corresponds to/equal the load at each node, the voltage is clearly affected by the PV-units, although to a slightly smaller extent than the previous case. Compared to case 3a, the voltage differences is here lower at all nodes. Particularly the industrial (I-)feeder has lower voltages, which is due to that the installed PV-unit at the remote node I2 in this case is only at 100 kW instead of 500 kW in the previous case.

The results of this case shows a larger impact of the PV-units in the R and C-feeder, as seen in figure 4.10. This is explained by the fact that there are more loads in the residential and commercial feeder than in the industrial, both in number and in total kVA (see table 3.4).

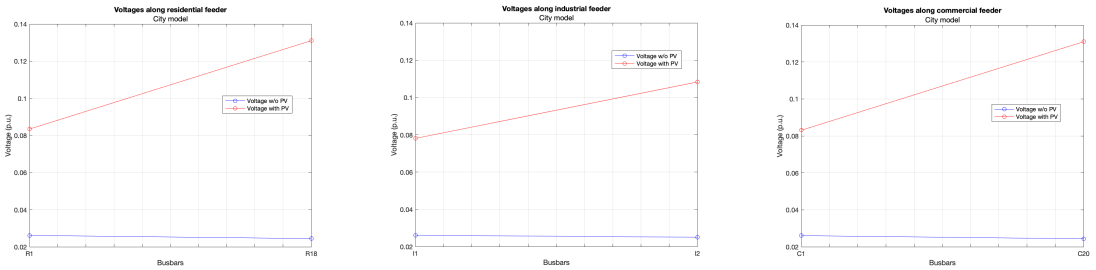

(a) R-feeder **(b)** I-feeder **(c)** C-feeder

Figure 4.10: Voltage at outmost busbars at LV-feeders for Case 3b

4.6 Case 4: Maximum PV MV-level

This case was one of two "future scenarios", with an up-scaling of solar power to the capacity limit of the grid. In case 4 the limit of the network model was 25 MVA, and thus 25 MW solar power was simulated. Due to time restrictions and simplicity these future cases are simulated with all active power input from future PV-units aggregated and placed at one location in the simulation model. Since this is a rather simplified version of any future case, two sub-cases were created with different location of this PV-block. Case 4a with the PV-block placed as far from the LV-part of the grid as possible, and Case 4b with the PV-block placed as close to the LV-grid as possible.

4.6.1 Case 4a: PV-block far from LV-grid

Table 4.6: Voltage in p.u. at selected busbars for worst possible fault, Case 4a (Bold type indicates placement of PV-block)

Node	w/o PV	with PV	Δ
HVMV	0.03044	0.0372	0.0068
MB12	0.0296	0.1372	0.1077
MB14	0.0291	0.1352	0.1061
MVLV	0.0288	0.1315	0.1027
R1	0.0283	0.1292	0.1010
R18	0.0267	0.1248	0.0981
I1	0.0282	0.1313	0.1031
I2	0.0273	0.1271	0.0999
C1	0.0282	0.1311	0.1029
C20	0.0266	0.1244	0.0978

(a) Rural model

Node	w/o PV	with PV	Δ
HVMV	0.0304	0.0372	0.0067
MB1	0.0294	0.1361	0.1068
MB7	0.0271	0.1268	0.0997
MVLV	0.0267	0.1251	0.0984
R1	0.0262	0.1227	0.0965
R18	0.0244	0.1154	0.0910
I1	0.0261	0.1224	0.0963
I2	0.0250	0.1179	0.0929
C1	0.0260	0.1222	0.0961
C20	0.0243	0.1150	0.0906

(b) City model

With the placement of the PV-block furthest from the LV-nodes one can observe that the results in table 4.6 above are of roughly the same magnitude as in the previous cases (3a and 3b). Which is rather suprising considering the vast increase of installed PV-capacity in this future scenario. The PV-block gave a slightly higher impact on the voltages in the Rural model 4.6a than on the City model 4.6b.

4.6.2 Case 4b: PV-block close to LV-grid

Table 4.7: Voltage in p.u. at selected busbars for worst possible fault, Case 4b (Bold type indicates placement of PV-block)

Node	w/o PV	with PV	Δ
HVMV	0.0304	0.0392	0.0088
MB12	0.0296	0.1720	0.1424
MB14	0.0291	0.5589	0.5298
MVLV	0.0288	1.0800	1.0512
R1	0.02828	1.0696	1.0413
R18	0.0267	1.0392	1.0125
I1	0.0282	1.0686	1.0403
I2	0.0273	1.0494	1.0222
C1	0.0282	1.0676	1.0394
C20	0.0266	1.0374	1.0108

(a) Rural model

Node	w/o PV	with PV	Δ
HVMV	0.0304	0.0364	0.0060
MB1	0.0294	0.1206	0.0913
MB7	0.0271	0.6310	0.6038
MVLV	0.0267	1.1687	1.1420
R1	0.0262	1.1501	1.1239
R18	0.0244	1.0952	1.0708
I1	0.0261	1.1483	1.1222
I2	0.0250	1.1139	1.0889
C1	0.0260	1.1464	1.1204
C20	0.0243	1.0918	1.0675

(b) City model*

*note: Only 21 MW input simulated here, due to capacity restriction in 'City' model.

In this sub-case, with the PV-block of 25 MW instead placed as close to the LV-nodes as possible, the resulting impact on the voltage is immense. In table 4.7 above, differences in voltage above 1 p.u. is recorded. This may seem unrealistic, and caution should be used in drawing conclusions from these results, as the simulation most likely resembles a park-module of 25 MW rather than the impact of scattered micro-production units with a total power of 25 MW, so the truth may lie in-between the result from case 4a and 4b. In order to get a better understanding/insight in what impact micro-production of this size would result in, future studies are required on a larger network model and with units connected only at LV-nodes.

4.7 Case 5: Maximum PV at SUB-level

4.7.1 Effect on LV-nodes

In this case, the fault location is moved, since the PV-block is placed above the fault location used in previous study cases. The fault location in this study case is set to at 50 % of the lenght of one OHL in the HV-grid, called L25, that is feeding B5, which is the connection point to the underlying grids.

Table 4.8: Voltage in p.u. at selected busbars for worst possible fault, Case 5

Node	w/o PV	with PV	Δ
HVA	0.2663	0.4070	0.1407
ASUB	0.2640	0.5830	0.3190
HVMV	0.2622	0.5790	0.3169
MB12	0.2549	0.5635	0.3086
MB14	0.2509	0.5549	0.3040
MVLV	0.2481	0.5488	0.3007
R1	0.2436	0.5391	0.2955
R18	0.2302	0.5105	0.2802
I1	0.2431	0.5203	0.2771
I2	0.2348	0.5381	0.3033
C1	0.2427	0.5372	0.2945
C20	0.2294	0.5087	0.2793

(a) Rural model

Node	w/o PV	with PV	Δ
HVA	0.2657	0.4062	0.1404
ASUB	0.2628	0.5809	0.3181
HVMV	0.2605	0.5761	0.3156
MB1	0.2514	0.5567	0.3054
MB7	0.2324	0.5166	0.2841
MVLV	0.2290	0.5093	0.2803
R1	0.2240	0.4987	0.2747
R18	0.2093	0.4675	0.2582
I1	0.2235	0.4977	0.2742
I2	0.2144	0.4782	0.2639
C1	0.2230	0.4966	0.2736
C20	0.2083	0.4655	0.2572

(b) City model

With a PV-input that fills up the capacity in even the SUB-transmission level, the node-voltages are affected in almost an equal amount over the different voltage-levels. Both LV nodes, MV nodes and the bottom-node at the SUB-grid show results of approximately 0.3 p.u. in voltage difference with or without overlying PVs connected during fault. However, these results should also be interpreted with some caution since the aggregated power, filling up capacity in all voltage levels, is simulated as one PV-block. Thus only general conclusions should be drawn based on this and no detailed specifics should be considered .

4.7.2 Effect on HV-grid

This future scenario may also impact the grid on HV-level, which is why the result-range is widened in this last case. Firstly, the voltage at the key busbar 'B5' is shown for faults at all locations in the HV-grid. Secondly, the voltages at all central busbars are visualised geographically for a few selected faults.

Table 4.9: Voltage at B5 for SC-faults at different parts of the HV-grid, while PV-park of 150 MW is connected at SUB(110 kV)-grid

Fault location	Voltage at B5 (p.u.)
Unfaulted	1.1051
Line 12	0.7766
Line 16	1.0343
Line 25	0.4058
Line 45	0.4463
Line 46	0.9898
Line 34 a/b	0.8631
Line 6a6b	1.0252
Line 78	0.9401
Busbar 1 (B1)	0.7483
Busbar 2	0.6364
Busbar 3	0.8325
Busbar 4	0.7266
Busbar 5	0
Busbar 6a	1.0227
Busbar 6b	1.0274

(a) Rural model

Fault location	Voltage at B5 (p.u.)
Unfaulted	1.1030
Line 12	0.7744
Line 16	1.0317
Line 25	0.4050
Line 45	0.5509
Line 46	0.9873
Line 34 a/b	0.8605
Line 6a6b	1.0225
Line 78	0.9371
Busbar 1 (B1)	0.7463
Busbar 2	0.6343
Busbar 3	0.8311
Busbar 4	0.7256
Busbar 5	0
Busbar 6a	1.0201
Busbar 6b	1.0248

(b) City model

In this case, the PV-park with 150 MW active power is placed at the busbar called ASUB. The voltage is almost unaffected when the fault is placed far from the busbar of interest, as is seen in table 4.9 for fault location at Busbar 6a and 6b, as well as at the line connecting them; Line 6a6b. Highest impact on the voltage level at

connection point to the underlying grid is, non-suprisingly with the SC-fault located at B5. The busbar from which the underlying grid is fed. Apart from that, faults at the lines to/from this busbar, L45 and L25, have the highest impact on the voltage in B5. Which is in line with what was shown earlier in section 4.2.2 as well.

4.7.3 Geographic visualisation of selected faults in HV-grid

In this section, the results are compared to those from section 4.2.2. This in order to see if PV-installations up to this magnitude have a larger 'geographic impact'. The graphs below show the results of SC-faults placed at different parts of the HV-grid with 150 MW active power input at the SUB-grid, directly underlying B5. This in an attempt to visualize the possible mitigating effect active power input may have on the voltage during faults at this "future up-scaled" size, or conversely, the effect of disconnecting PV-units of an accumulated power of 150 MW during fault.

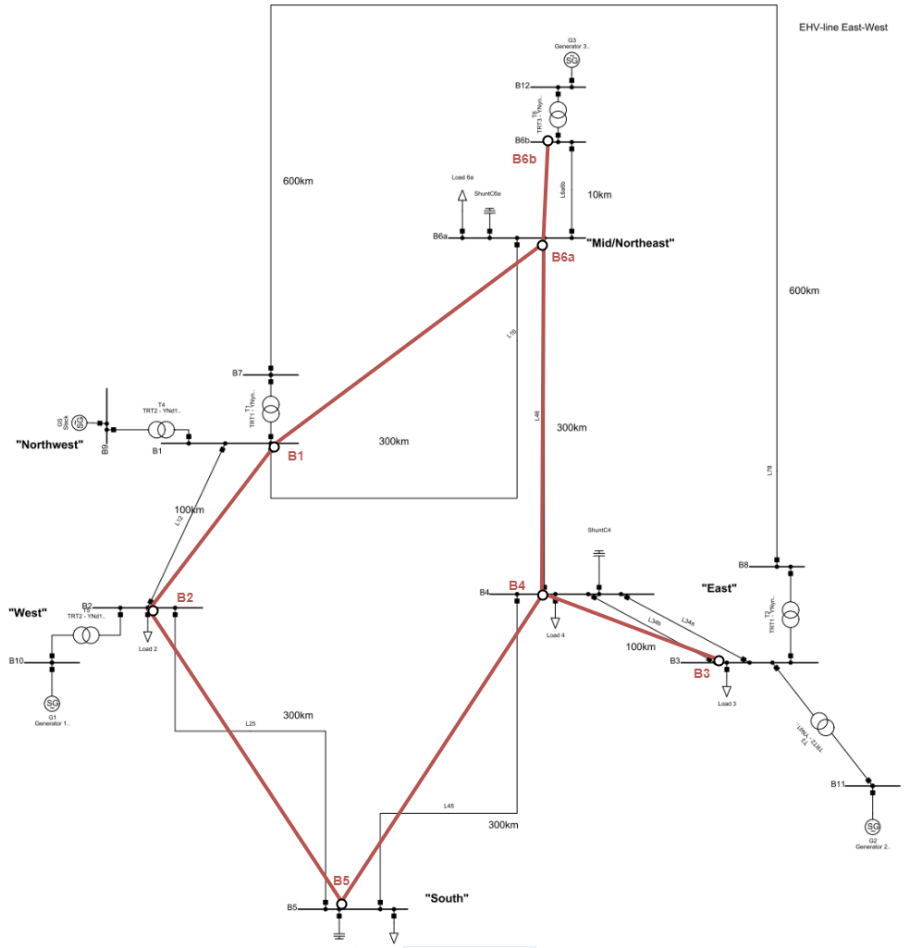

Figure 4.11: Topology of HV-network, simplification used in plots are shown in red

The figure 4.12 and 4.13 show the same fault-locations as in section 4.2.2, but now with the difference that 150 MW active power is placed in the from B5 underlying SUB-grid, as described for Case 5. In each graph, the results from section 4.2.2 is shown as a purple cross in respective busbar-staple.

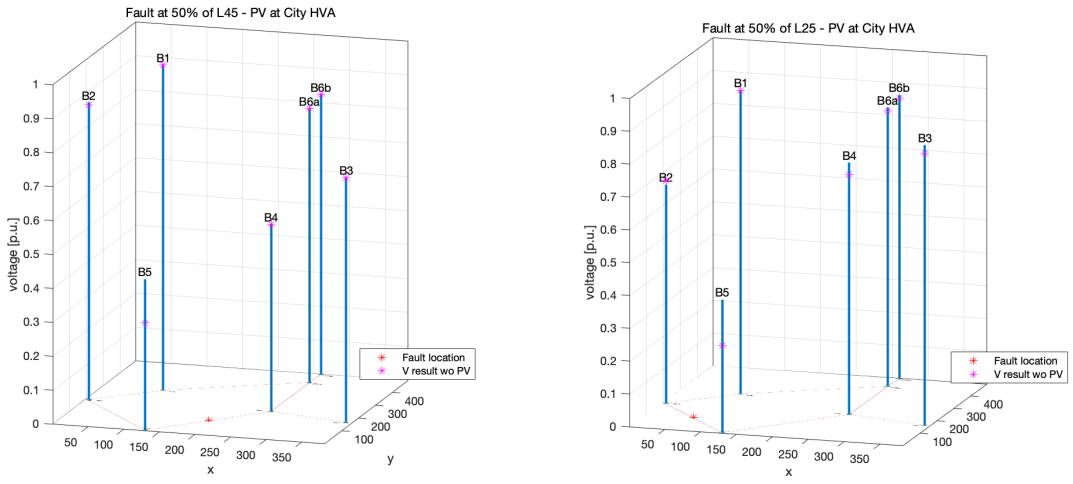

(a) Fault at L45 **(b)** Fault at L25

Figure 4.12: Fault at overlying OHL-lines in each direction from B5/"South" with 150 MW PV connected in underlying SUB-grid (110 kV)

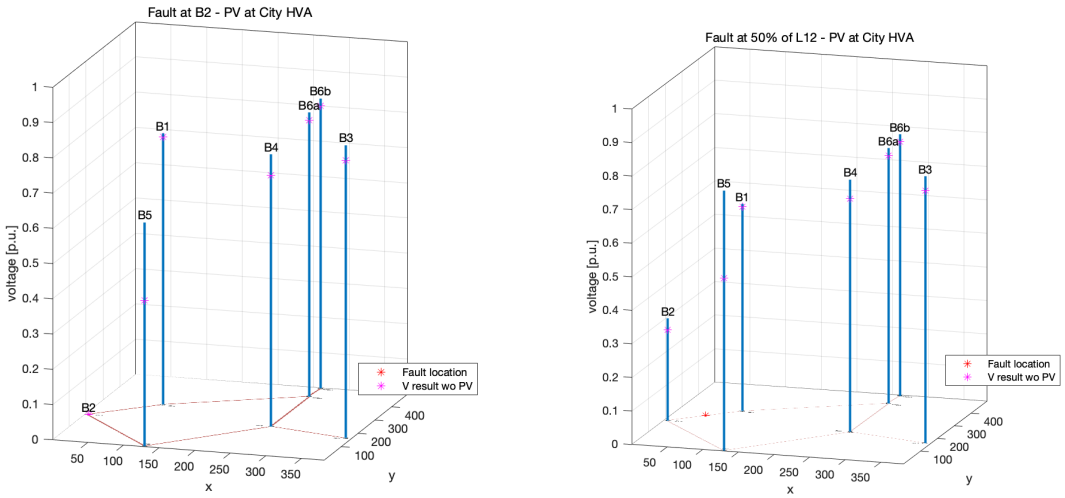

(a) Fault at B2 **(b)** Fault at L12

Figure 4.13: Fault two steps further away from B5/"South", in westerly direction, with 150 MW connected at SUB-grid underlying B5.

The results in figure 4.12a show that the PV-block in Case 5 has a considerable

impact on the voltage at B5 but is not affecting the voltages at the other busbars at this fault location. Figure 4.12b show that during fault in Line 25, the active power simulated in Case 5 have similar effect on the B5-voltage, in addition to a small impact on the voltages at B4 and B3.

Figure 4.13 above display a larger impact of the PV-block at B5 for these fault locations than in fig 4.12, and a slightly bigger impact on busbars further away aswell (B4 and B3 in particular).

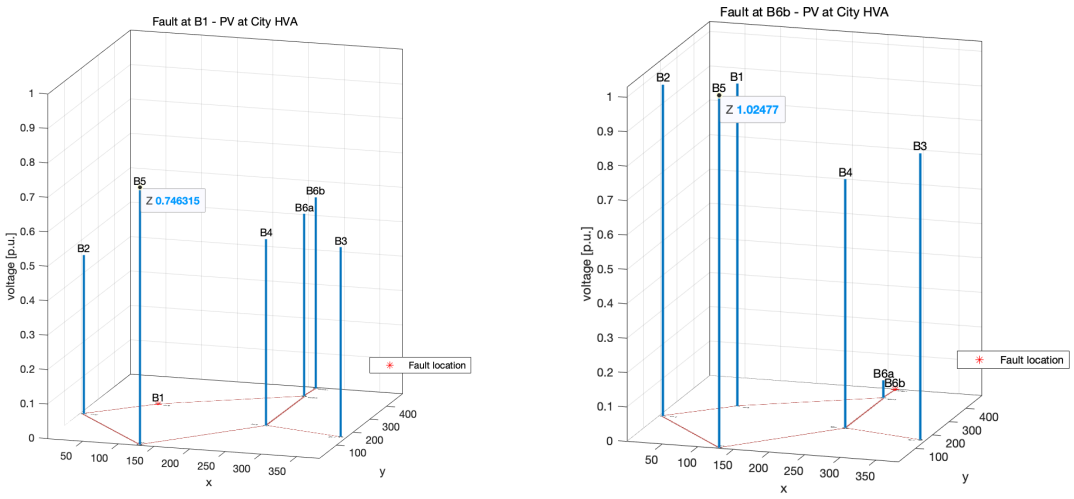

(a) Fault at B1 **(b)** Fault at B6b

Figure 4.14: Most outstanding faults for whole HV-grid.

The figure 4.14 above, show the most "extreme cases" of fault locations with PV-block. Figure 4.14b show that at a fault location furthest away from the focal point B5, the voltage is above 1 p.u. and almost at pre-fault levels, and the rest of busbars of the HV-network is almost unaffected (with exception of B6a which is a mere 10 km from B6b see fig 4.11). In stark contrast, figure 4.14a display the fault location that has the largest impact on all busbars in the network, with most voltages around 0.45-0.55 p.u., except the voltage at B5 which is upheld by the PV-block, to a voltage of roughly 0.75 p.u.

4.8 Impact of fault clearing time

Up till now in this thesis, the focus has been merely one-dimensional voltage dips in different points of the grid model at short circuit faults. However, in order to compare these results with the RfG-requirements on LVRT (specified by EIFS 2018:2), these voltage dips must be complemented with fault clearing times at the specified fault location, to mark the voltage at the busbars in question (with PV-generation) during the fault clearing time. These, now two-dimensional results is plotted in the LVRT-figure. As a sensitivity analysis, the fault clearing times will be presented both from normal fault clearing as well as from reserve/back up fault clearing which would represent a worst case scenario.

The different study cases examined in this thesis had two fault locations. Case 1-4 had a fault location at the SUB-part of the model, on an OHL called "L_AMV1", and case 5 had a fault location on the HV-part of the network model, at an OHL called "L25" feeding the key busbar B5. For visual presentation of the fault locations in SLD-diagram of the network model see figure 3.9 .

Ordinary fault clearing

The fault location in the subtransmission grid, OHL line "L_AMV1" would, in reality, have a protection scheme with instantaneous disconnection of faults from both directions of the line. This translates to a fault clearing time of only the switching time, normally between 40-70 ms, in this work set to 50 ms for simplicity. The protection assumed at this part of the grid is so a called communicative differential relay. For the fault placement in case 5, it is assumed that a protection system would consist of impedance relays situated at both ends of the OHL. Since these normally are set to reach 80-85% of the line (to enable co-ordination of relays), a fault situated at 50% of the line, as in case 5, would result in instantaneous disconnection from both line-ends. Thus the normal fault clearing time for case 5 is also the switching time, 50 ms.

However, if the fault was to be placed further towards one end of the OHL, the nearby relay would trip and disconnect instantaneously (50 ms) but the other end would have a time delay of 400 ms, due to selectivity and co-ordination reasons.

During this time delay the fault would still be present and be "fed" from this other direction. The voltage dip at the underlying PV/generating-busbar during this time delay would not be as severe as during the first 50 ms when the fault was fed through both lines. The impact is lowered since the selective disconnection of the fault from one line end renders the fault radially fed, and the short circuit power is then lower than in the initial meshed case. Thus, there are several more layers of complexity in fault clearing than what is presented here.

Reserve/Back up fault clearing

The backup fault clearing for a current differential protection, as presumed in cases 1-4, for short circuit faults is generally a distance relay with a typical time delay of 400 ms. Thus the total backup fault clearing time for the fault in cases 1-4 is 400+50 ms.

The backup fault clearing option for impedance relays, which was supposed in case 5, are usually relays from neighbouring stations/busbars located in zone 3 in a protection zone. Thus the fault clearing time would be further delayed to a total time of 1250 ms.

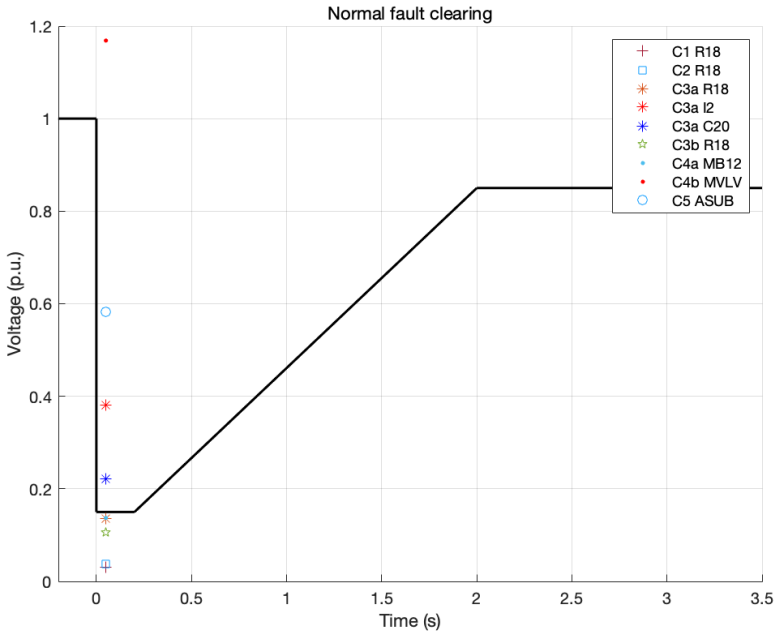

Figure 4.15: LVRT for B and C generator types, case results with PV plotted with normal fault clearing times

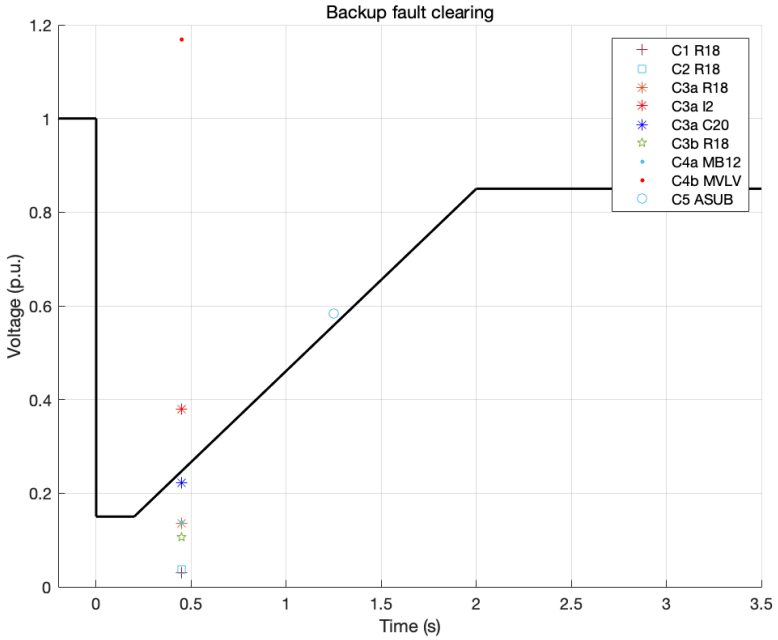

Figure 4.16: LVRT for B and C generator types, case results with PV plotted with backup fault clearing times

In the instance with ordinary fault clearing times shown in figure 4.15, there are two results above the LVRT-criteria from case 3a, a study case representing the solar-

production situation in the present, to some extent, with multiple micro-producers in the LV-grid. The most interesting observation being that the LV-node C20 is well above the requirements for fault ride through already in case 3, with only a few units of PV-microproduction placed on one feeder. This points toward that there is a possibility for accumulated solar production to contribute to voltage support during faults in LV-grids as of today already, for both small scale units as well as industrial sites.

In both figure 4.15 and 4.16, the C4-points are to be regarded as outliers, or as border-points within which the voltage for case 4 may be situated (for further details see section 4.6.2 above).

The result-points named "C3aR18" (Case 3a, node R18) and "C4aMB12" in the normal fault clearing scenario are situated just below the LVRT-boundary, as well as "C3aC20" in the backup-scenario; where "C5 ASUB" on the contrary is placed just above the limit. In relation to these results, it can be interesting to discuss and nuance the voltage. As mentioned earlier in the report, the simulations are based on load-flow calculations, where the voltages derived are based on generation, line impedances and loads, resulting in voltages which more closely corresponds to the physical reality in grids. Hence, it can be reasoned that at lower load or during other occasional circumstances in the grid, these first-mentioned points had also lied within the LVRT-requirements. Perhaps even more interesting is if the latter case were to be altered by changes in grid-circumstances where the resulting point of C5ASUB is just above the LVRT-limit.

This reasoning that real grid conditions may give different outcome than "flat/normed simulations" on models without load flow calculations is valid beyond this thesis, and it may be an idea for grid owners/operators to review their methods.

5 Fault registrations

As mentioned and described in sections 3.1.3 and 3.2.4 above, data from a PMU connected at the resident with the PV-unit in Bara were analysed in this study. In addition to this, disturbance recordings from the overlying stations were also analysed. Registrations from both disturbance-recorders are presented in this chapter, as well as a closer look at the previously introduced ramping response of the residential PV-unit. Observations from various fault types at different voltage levels (400, 130 and 20 kV) are presented giving an unique and valuable insight on how different faults are percieved at LV-connections.

5.1 PV-unit responses

Registrations made prior to this thesis, by Göran Runvik, captured different observations, e.g. on how this small-scale PV-unit acts during disconnection, and re-connection to the grid after disturbance. Thus, data on how fast the PV-unit in question ramps up in current were recorded and the corresponding ramp in active power output has from this been derived.

This response was recorded during a fault that occurred at 130 kV in 2021-07-15 where the PV-unit disconnected. The fault was deemed most likely a short circuit caused by lightning and it will not be further analysed in this section but merely brought up as an example of recordings of PV-responses. The recording can be seen in figure 5.1 below. The current depicted in the second subplot is the positive sequence current output from the unit, while the voltage in the first subplot is the line-ground voltage at the LV connection point of the PV inverter.

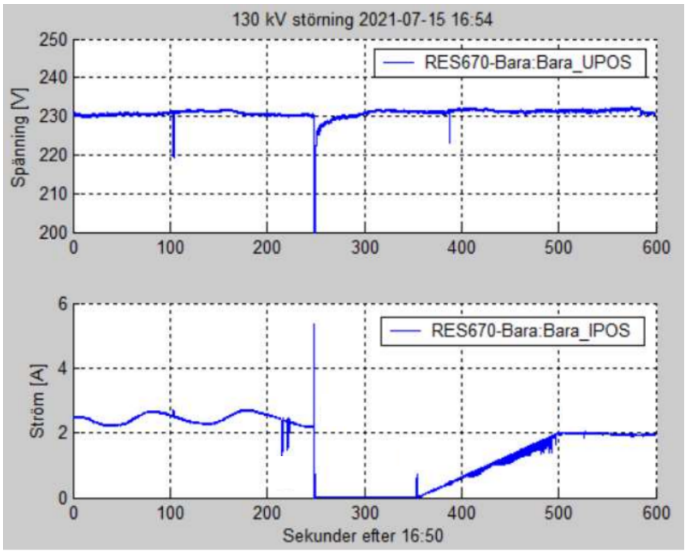

Figure 5.1: PV response from residential unit after a 130kV disturbance, voltage and current ramp during 250 s. The x-axis reads in English *Seconds after 16:50*, and the y-axises *Voltage [V]* and *Current [A]*.

Based on this recording, the speed of the increase in current output from the PV unit is determined to I_{ramp} 13.5 mA/s and the corresponding three phase active power ramping is P_{ramp} 9.41 W/s, thus a total up-ramping to the maximum output of 6 kW would take roughly 10 minutes assuming sufficient solar influx. (Runvik, 2022a and Hemmingsson, 2022)

A second observation made at the PV-unit during this 130 kV fault, is that for a short moment during part of the first 100 ms, as the voltage was declining the current increased. The PV-unit was feeding roughly 20% more than its rated current as maximum in fault current during these initial milliseconds.(Runvik, 2022a)

Additionally, at the end of this thesis work, another interesting registration was made at the PV-unit in Bara. Due to time constraints this fault will not be analysed either, but it will be shortly presented based on records of the registration and fault confirmation from the grid-owners at the location.

This time there was a 3ph SC fault that occurred and lasted for about 300 ms at 130 kV level in Helsingborg, which was registered in Bara. The unit in Bara stayed in operation throughout the fault despite a low grid-voltage; the voltage was around 200 V (-12%), so just above the limit for disconnection at 195 V. During 200-250 ms initially, before the fault was disconnected and the voltage restored, the power-

output from the PV-unit slightly increased. This is seen in figure 5.2 below, where the top graph depicts the voltage and the bottom graph the output AC-power(blue) as well as the DC-power(green).

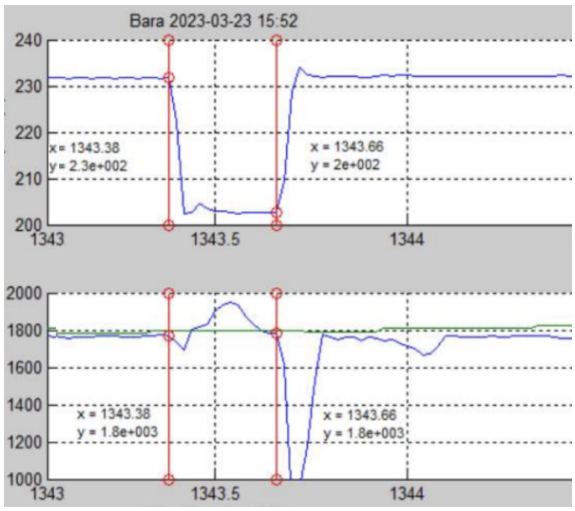

Figure 5.2: Voltage (V) and power (W) at PV-unit in Bara during 3ph SC at a remote location.

The insight that 3 ph SC faults, as opposed to unsymmetrical faults, occurring at high voltage levels have influence on large regions is hereby further supported. The fault occurred far from the unit in Bara but had a substantial effect. The margin to disconnection of this unit was very slim, had the pre-fault voltage been only 5 V (2.5%) lower, the unit had stopped. Likewise, had the fault time lasted slightly longer the unit had also been disconnected. It can be presumed that multiple inverters in the region was stopped at this disturbance and had delayed restarts minutes after the fault. (Clementson, 2023 and Runvik, 2023)

5.2 PMU-data

The recorded data from the PMU in Bara were complemented by a PMU in a lab in LTH as well as a unit in Tampere, Finland. The data from these are continuously stored in a central server and were analysed using a data-viewing program ”pmview” at IEA developed by Morten Hemmingsson. The data from the residential PMU in Bara are the main focal point and the data from the other locations are used as comparison and to determine the geographical extent of the fault-impact.

The unit at LTH is set up in one of IEA's laboratories, so the rather unusual voltage magnitude is due to settings in the lab.

5.2.1 400 kV disturbance 28/11-21

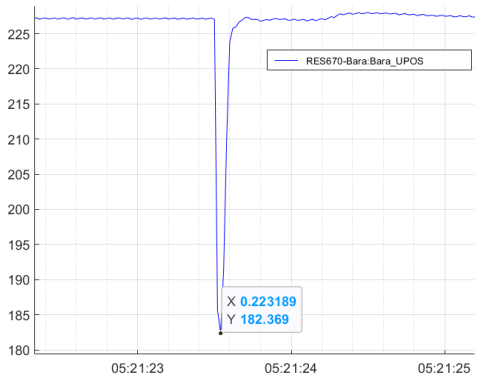

Figure 5.3: Voltage dip at point of connection of residential PV-unit, during fault the 28/11-21

This disturbance lead to a voltage dip of roughly 45 V (19%), with the lowest recorded voltage at 182.4 V; seen as y-coordinate/value of datapoint in figure 5.3 above.

This disturbance was also observed at one of the 'global' PMUs located in Tampere in Finland, although here the impact was barely visible with a voltage dip of just about 1 V (0.4%), viewed in the bottom graph in figure 5.4 below.

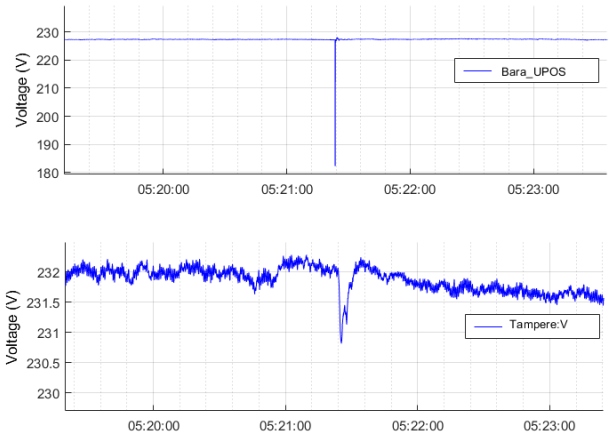

Figure 5.4: Voltage at Bara and in Tampere, Finland during 28/11-21 fault

5.2.2 130 kV disturbance 29/1-22

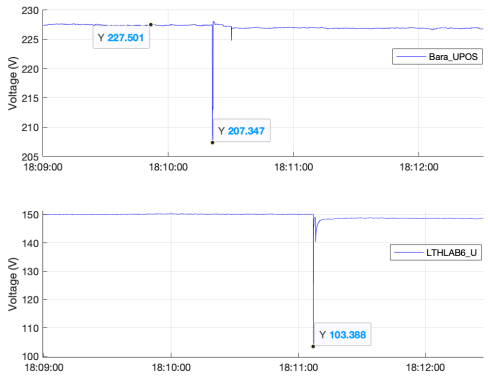

Figure 5.5: Voltage plot in Bara and LTH during 29/1-22 fault

At this occurance the disturbance was observed both in Bara and by the PMU at LTH, though the disturbance seemed to appear slightly later at LTH and be a bit deeper. The voltage dip in Bara was roughly 20 V (8%) from 227 to 207 V, and the impact at LTH was of around 50 V (33%) as seen in the top and bottom graph respectively in figure 5.5 above.

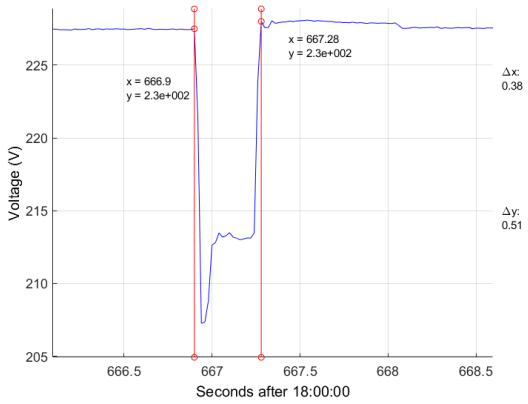

Figure 5.6: Detailed voltage plot in Bara during 29/1-22 fault, delta x is fault time

This disturbance lasted for about 0.4 s, shown in figure 5.6 above which is a more zoomed-in and detailed version of the previous figure.

5.2.3 20 kV disturbance 8/10-2021

This recorded disturbance was the most severe. The voltage dip were 140 V (60%) during the fault. Interestingly enough, the disturbance was barely noticeable at LTH, with a voltage dip of only 2-3 V (1.5%), see figure 5.7.

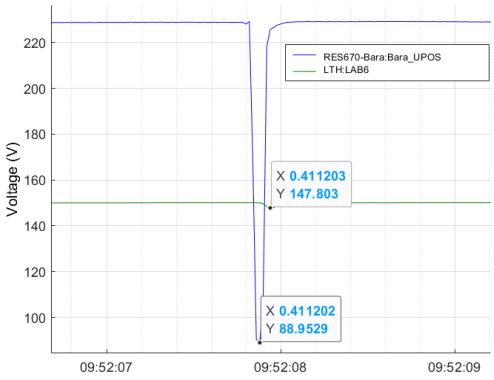

Figure 5.7: Voltage plot for signal in Bara (blue) and LTH (green) during 8/10-21 fault

In figure 5.8 below, the voltage dip is shown in normalized/normed units, with the prefault voltage value set as 1 p.u. Here the severity of the fault is more clear, since the voltage is as low as barely 0.4 p.u. as worst.

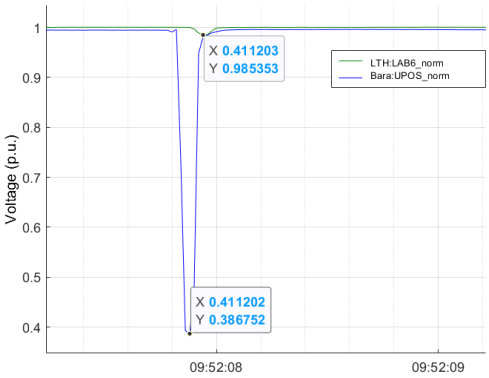

Figure 5.8: Normed voltage plot for Bara and LTH during 8/20-21 fault

5.2.4 20 kV disturbance 9/10-21

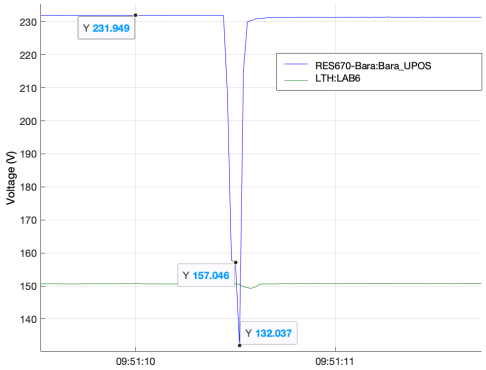

Figure 5.9: Voltage plot for signal in Bara (blue) and LTH (green) during 9/10-21 fault

This disturbance rendered a voltage dip of roughly 100 V (43%) at the low-voltage connection in Bara, see the blue line in figure 5.9. This voltage stated in per unit values show a lowest point at roughly 0.57 p.u (or 57% of nominal). Still, it barely had any impact at the voltage in LTH at all, similarly to the previous disturbance recording.

5.3 Fault recordings from overlying substation ”STM-”

In relation to the PMU-recordings at Bara the same disturbances were analysed on data collected by fault-recorders at E.ON from the overlying grid. The analysis carried out were made with methods from the Power System Analytics unit at E.ON and with help and support from co-workers and supervisor there.

The overlying grid has been roughly introduced in figure 3.7 with description, however, a closer look at the substation directly upstream to the PV-unit in Bara can be suitable. The station is called ”STM-” for anonymity purposes.

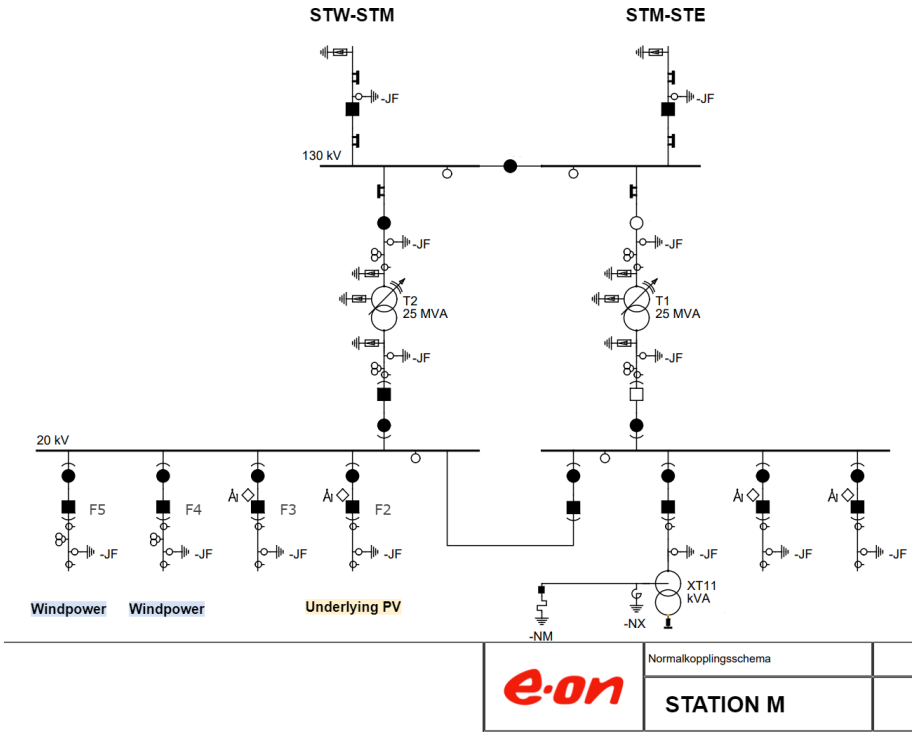

Figure 5.10: SLD of the overlying 130/20 kV station called ”STM-”

As is viewed in figure 5.10 above, the overlying station in question is a 130/20 kV

station with dual transformers of 25 MVA, for redundancy. The station is part of the meshed 130 kV network and OHLs goes on to a neighbouring station in easterly direction, called "STE-". To the west an OHL connects to "STW-", a 400 kV transmission-grid station which connects the 130 kV grid to the overlying transmission grid. This is one of many transmission-stations that feeds the 130 kV network, but since it is the closest it is the most significant.

5.3.1 400 kV disturbance 28/11-21

This disturbance was not recorded in the "STM" station but in the neighboring "STE" station(for grid topology, see fig 3.7). Although, this does not influence the method or outcome of the analysis since the disturbance was on the overlying 400 kV grid and affects a large area, thus the same fault pattern would have been observed in data from "STM" as from "STE".

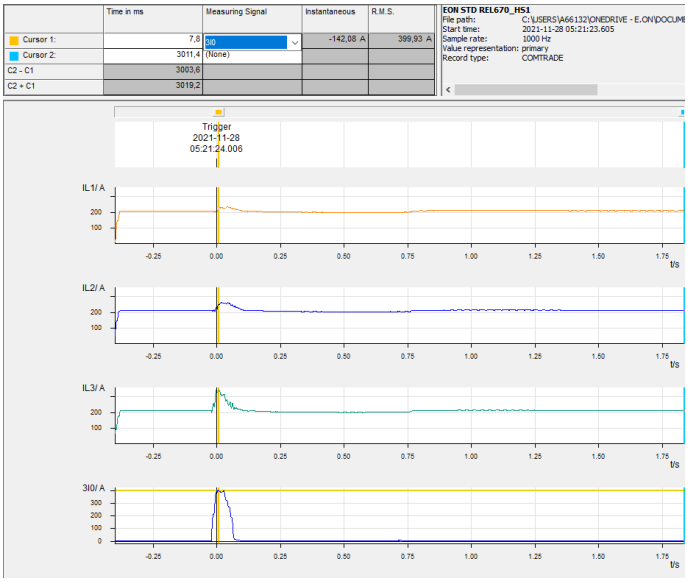

Figure 5.11: Phase currents recorded at 130 kV-level at E.ON during 28/11-21 fault

In figure 5.11 above, it is observed that there is a spike in the current in phase 3, IL3, as well as in residual current 3I0, which corresponds to the current in a neutral conductor. This indicates that the disturbance was a type of earth fault.

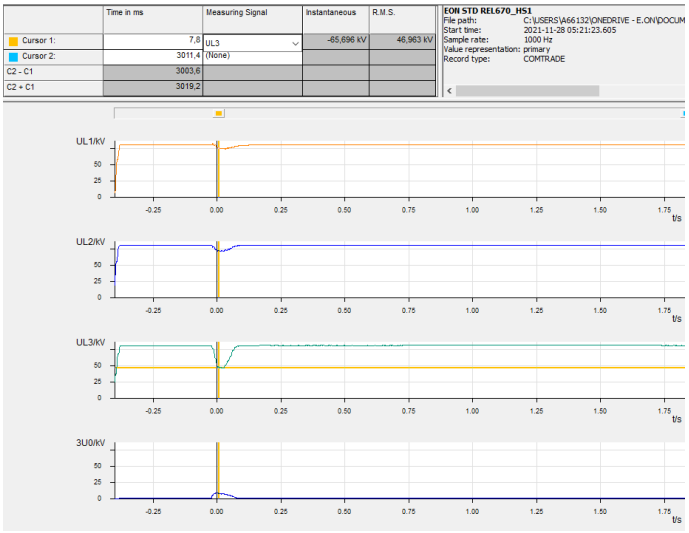

Figure 5.12: Phase voltages recorded at 130 kV-level at E.ON during 28/11-21 fault

Figure 5.12 depicts the phase voltages. Here it is seen that there is a sharp voltage drop in phase 3, UL3, suggesting that the conductor in phase 3 has a connection to ground since it is going towards ground potential. Small voltage dips are observed in the other phases, thus L1 and L2 is somewhat faulted as well. However, the disturbance seems to have been dominated by an earth fault in phase 3.

Data of the sequence currents in the network during this fault showed a clear registration of a zero sequence current (for detail see appendix C). A zero sequence current only develops during earth fault, further endorsing that this disturbance was an earth fault of some kind.

5.3.2 130 kV disturbance 29/1-22

This disturbance was an earth fault in phase 1, as seen in figure 5.13. This can be concluded since there was a peak in the current in phase 1, where the current rose to as high as 5kA at one point during the fault, as well as a drop in the voltage in the same phase. The fault occurred in the 130 kV meshed network, on an OHL out from the STW station. Additionally, in figure 5.14 it is also shown that a neutral point voltage, uE_N was recorded. The neutral point potential was thus displaced and further concluded the suspicion of an earth fault.

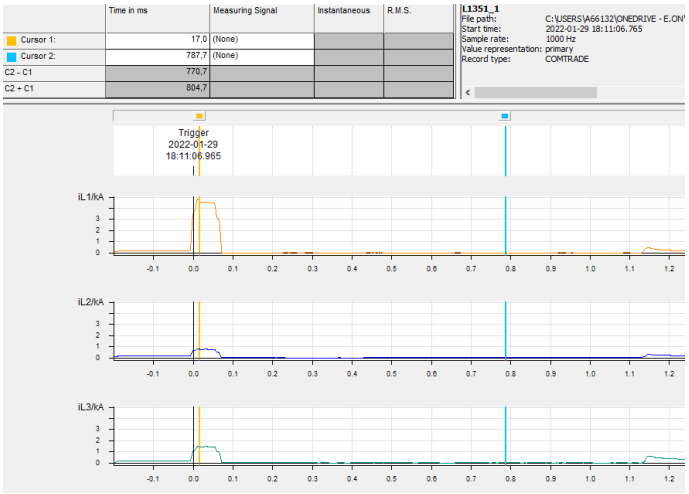

Figure 5.13: Phase currents recorded at 130 kV station at E.ON during 29/1-22 fault

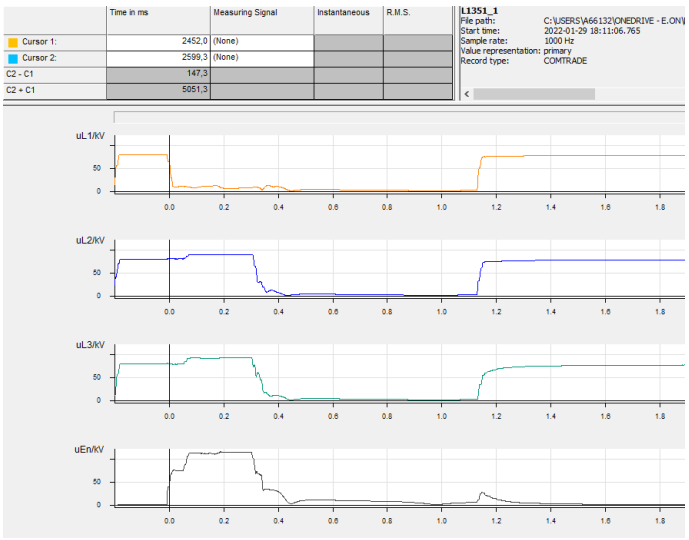

Figure 5.14: Phase voltages recorded at 130 kV station at E.ON during 29/1-22 fault

This disturbance file was also collected from the nearby station STE in the 130 kV network, but as in the previous case, the observations made in STE will show the same cause of fault as data from STM would. In fact, information from E.ON declared that the fault occurred at a location further to the west than STM, so that if anything, the fault output would be more clear in data at STM and the effect of the fault might be slightly more severe than in STE.

5.3.3 20 kV disturbance 8/10-21

This disturbance begun as an earth fault which developed into an almost completely balanced/symmetrical 3 phase short circuit. A so called residual voltage relay, which detects displacement voltage, in one of the bays connected to the wind power plant started recording, signaling that there was a raised voltage at the neutral point, originating somewhere in the power system. The voltages in the transformer-bay during the fault are shown in figure 5.15 below.

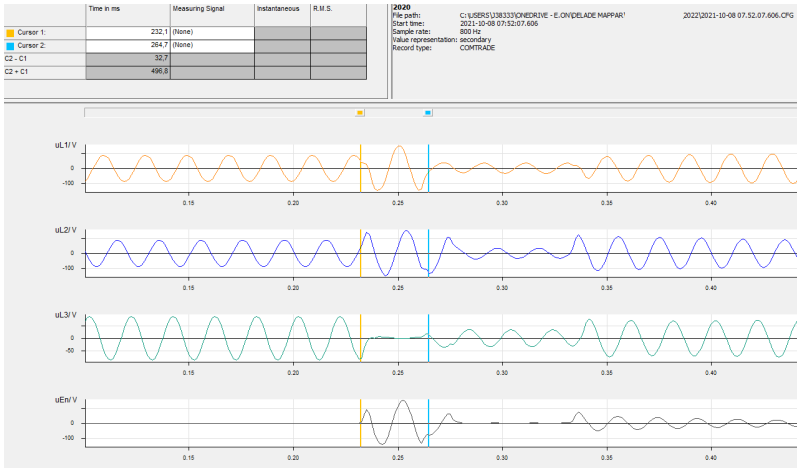

Figure 5.15: Phase voltages, viewed as instantaneous values, during the 8/10-21 fault, recorded in the transformer-bay in STM

Initially the voltage in phase 3 becomes zero and the voltages in the other phases are slightly raised (shown enclosed by the blue and yellow cursors in the figure above). At the same time there is a registration of displacement voltage *uEn*, witnessing of an earth fault in phase 3. Shortly after that, when *uEn* has ceased the voltages in all three phases are significantly lowered, which is when a 3ph short circuit occurred, shown below.

Figures 5.16 display the phase currents recorded at bay F3 as both RMS and Instantaneous values. The figures reveal spikes in all three phase currents which indicate a 3ph short circuit.

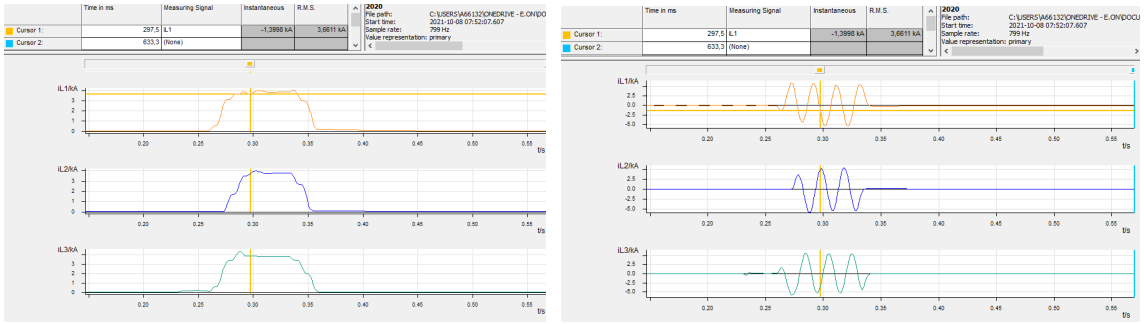

(a) RMS-values **(b)** Instantaneous values

Figure 5.16: Phase currents during 8/10-21 fault recorded at bay "F3" in STM

The instantaneous values of the phase currents in fig 5.16b, show that the phase currents are under balanced conditions suggesting a symmetrical 3ph fault.

When there is an ongoing earth fault in one phase, phase voltages in the unfaulted phases are raised which increases the risk of short circuit. This is most likely the turn of events during this fault.

The initial earth fault was for the analysis identified by searching after fault reports filed for that date and time in the nearby grid in dpPower, a documentation and mapping-system used by E.ON. The fault report revealed that there was a faulted disconnector in a secondary substation (20/0.4kV) further down in the 20 kV radial fed from bay F3. (Marstorp, 2022 and Clementson, 2022)

Furthermore, the suspicion of a balanced 3 phase short circuit is supported by looking at the phasor/vector representation of the phase currents and sequence currents respectively at 297.5 ms after fault recording, as depicted in figure 5.17. The phasors in the diagram to the left in the figure show that phase currents are almost exactly 120°apart, which is the case in a balanced system. The phasors in the right diagram depict the sequence currents, which reveal that almost all the current are of positive sequence. Since no zero sequence current are recorded at this point in the fault development one can draw the conclusion that there is no longer any earth fault present, and thus the fault is purely a short circuit fault at this point.

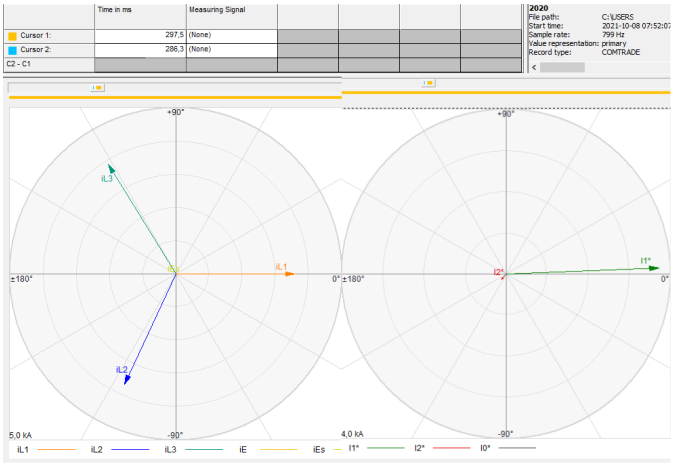

Figure 5.17: Vector plot of phase(left) and sequence(right) currents at one instant during the 8/10-21 fault, 297 ms after start of recording.

In summary, these fault records and the proceeding analysis concluded the 8/10-21 fault as an initial earth fault that developed into a 3 phase short circuit.

Logic signals - Fault clearing time

The figure 5.18 below shows the logic signals that were registered during the 8/10-21 fault. The cursors (blue and yellow vertical lines) enclose the switch time, i.e. the time it takes for the switch to open and clear the fault current. This time is recorded to be 44 ms, as is seen in the top left corner of the figure as the value of "C2-C1". Here the fault clearing time consists of only the switch time since the fault was so severe that momentary disconnection was triggered.

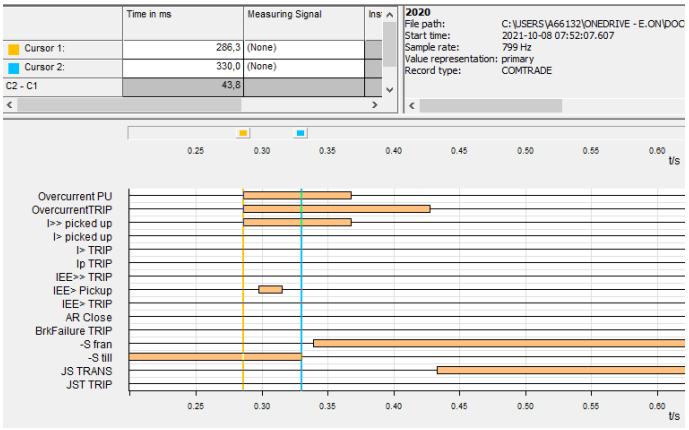

Figure 5.18: Logic signals registered at STM during 8/10-21 fault

Surrounding grid

Since this fault is of most interest for this thesis and has most similarities to the faults simulated (3ph bolted SC), some additional information was collected to get

an idea of how the surrounding grid behaved/was loaded during the fault time. All the information stated in this section was obtained from E.ON records. (Clementson, 2022)

Firstly, it was of interest to know if the nearby wind plants were producing during the fault, and if so, how much power that was being fed the "reversed direction" through the STM-station from the bays F4 and F5. Each wind-bay includes production from 3 wind turbines of 2 MW installed capacity, thus each bay has a maximum total power of 6 MW. Records showed that the registered hourly mean values for both wind-bays were 0 MW during the hour before, during and succeeding the fault. Thus none of the wind turbines produced any power during and around the time of the fault and the wind power plant were, most probably, offline at the time.

As for the usage and loading of the surrounding grid at and around the fault time, data recorded in the overlying station STM depicted that normal grid operation prevailed. Hourly mean data stated that the voltage were stable around 21 kV and the current fed through the transformer was about 150 A. The power fed through the transformer was around 4 MW active power and -3 Mvar reactive power respectively (where positive sign convention indicates power flow from regional- to distribution grid).

5.3.4 20 kV disturbance 9/10-21

This fault occurred less than a day after the previous disturbance, and was likewise recorded in the STM-station. In figure 5.19 below, the phase currents and iE (earth fault current) are shown. At the beginning of the fault, phases 1 and 3 display very high currents, of more than 3 kA, suggesting a 2 phase fault of some kind. However, towards the end of the fault, the current in phase 3 also rose, indicating that the 2 phase fault developed to a 3 phase fault.

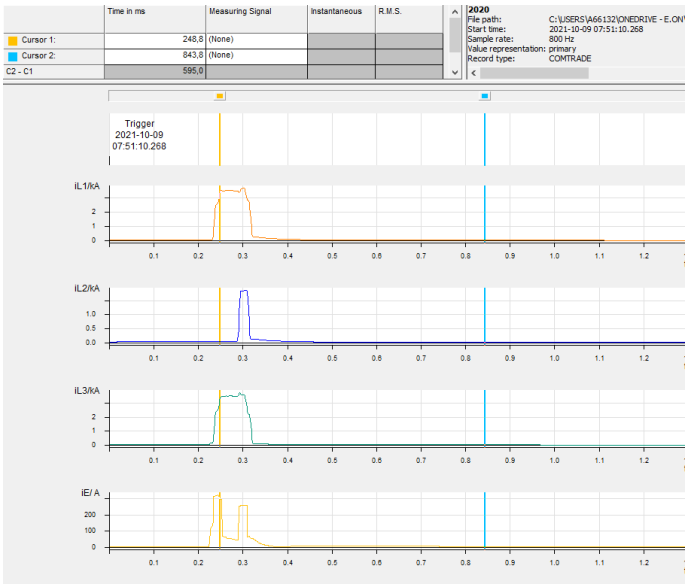

Figure 5.19: Phase currents during 9/10-21 fault recorded at bay "F3" in STM

As to the origin of this fault, no clear reason or location was found. It was known that there had been previous issues in a secondary substation (20/0.4 kV) and corona discharge had been observed there at the date of this fault (Marstorp, 2022), although the magnitude of the phase currents indicates a more severe disturbance than that.

The notion of an initial 2 phase fault that developed into an 3 phase fault is supported by the phase voltages recorded at the transformer-bay, as seen in figure 5.20 below. The voltages in the faulted phases decline while the voltage in the unfaulted phase increases, which is observed in the beginning of the fault. Towards the end of the fault (at 0.30 s) there is a small voltage-dip in phase 2 as well, which is when the fault shortly develops into a 3 phase fault and this phase also gets short circuited.

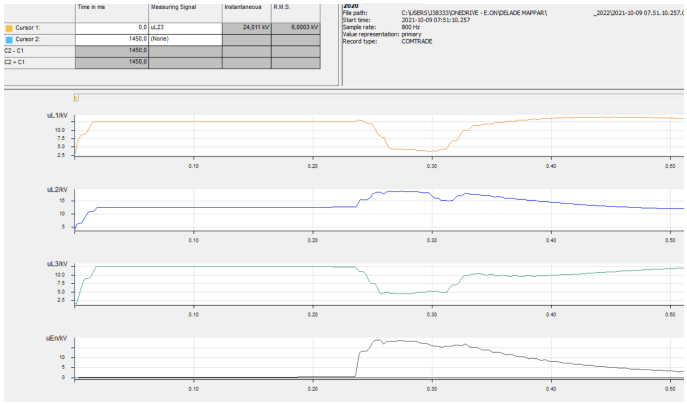

Figure 5.20: Phase voltages during the 9/10-21 fault, recorded in transformer-bay in STM

The recording in the faulted bay "F3" had signal-errors, displaying invalid phase voltages, which is why recordings from the transformer-bay was used instead. The measurement of phase voltage at each feeder-bay are normally collected from the transformer or incoming bay in use, thus these measurement shows the same output regarding voltage as a correct recording at bay "F3" would.

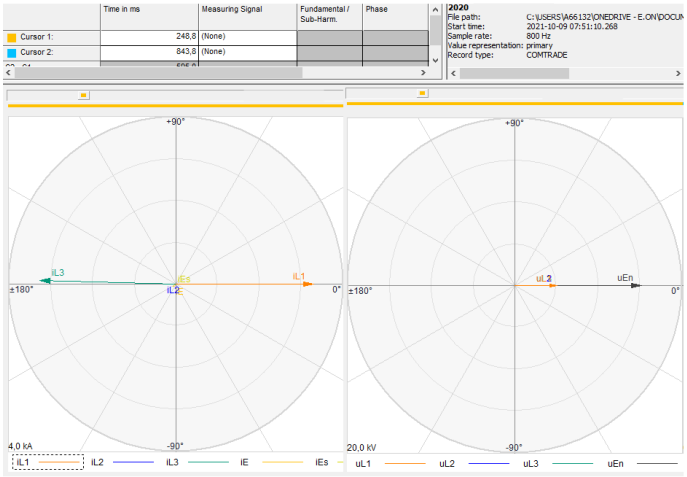

Figure 5.21: Vector plot of phase currents(left) and voltages(right) at one instant during the 9/10-21 fault

A closer look at the currents iL1 and iL3 in the beginning of the fault (249 ms after start of recording) is shown to the left in a vector diagram in figure 5.21 above. This diagram reveals that the phase currents are almost exactly 180° apart. Phase currents like these, that are equal and of opposite direction is the result of one phase current "directly feeding" the other, which verifies this as a phase-phase fault. However, the netural point potential *uEn* in the vector diagram to the right in the same figure (5.21) in addition to the earth fault current *iE* observed earlier

in figure 5.19, suggests that there was a connection to earth at this instant in the fault as well.

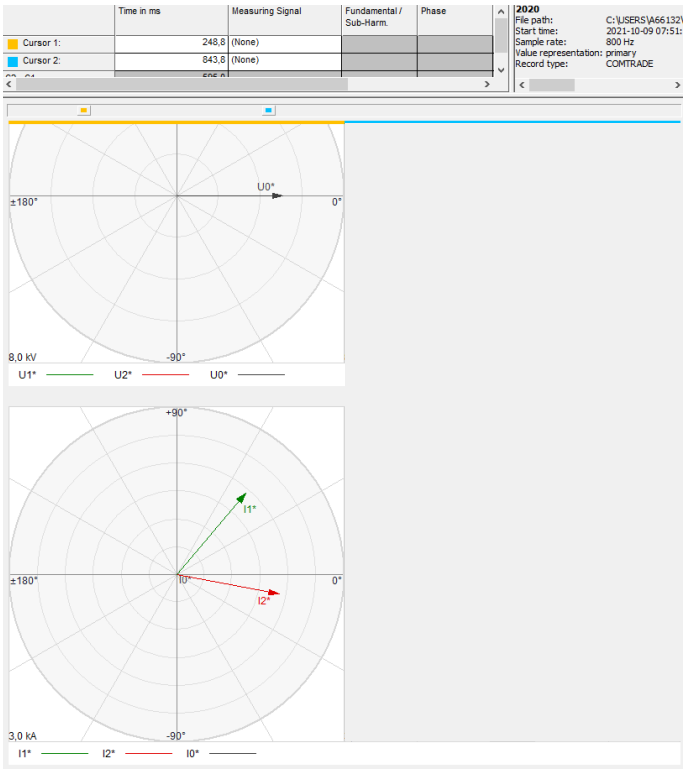

Figure 5.22: Vector diagram of sequence components at one instant during 9/10-21 fault

To further understand the fault, vector diagrams of the sequence voltage and currents were studied, see figure 5.22 above. They reveal that there is in fact zero sequence voltage, so there is a connection to ground from the two faulted phases. However, at the same instant the zero sequence current is barely noticeable, suggesting that there is almost no earth fault current at all. The most probable cause of this is that there is a connection to ground, but that the resistance in any possible return cable from ground (earthing points or petersen coils etc) are too high so that the majority of the current is instead going back in one of the two faulted phase-conductors.

Conclusively, this fault is interpreted as an initial phase-to-phase fault with connection to ground which developed into a 3 phase fault.

A side-note worth to mention is that fault current contribution was observed from one of the wind power-bays, even though they were not producing, suggesting that fault current addition from the wind power were that of idle generation or merely the capacitative earth fault contribution from the wind plant.

5.4 Summary of fault registrations

The former two disturbances (28/11-21 and 29/1-22) were both earth faults. This fault type does, in non direct earthed networks, typically not generate as high fault currents or low voltage dips as short circuits. However, they generally occur much more often and are sometimes hard to measure and particularly hard to handle selectively, leading to fault current being fed longer than usual (up to 5 s). Thus, if earth faults persist in grids for longer duration there are risks for other succeeding errors to arise with potentially more severe consequences.

These two faults occurred at medium and high-voltage level which entailed a more widespread impact. The 29/1-22 fault occurred in the meshed 130 kV grid and impacted the underlying grid, with a voltage dip of 20 V (8%) registered at 0.4 kV. However, earth fault occurring in the 130 kV grid should not affect the underlying grid due to the Y-D connection type of 130/20 kV transfomers all around the grid. Thus, the voltage dips registered at Bara and LTH are probably due to the selective disconnection of the faulted line in the overlying grid.

The 28/11-21 earth fault however, took place at the 400 kV grid, which gave a larger impact on the medium voltage levels as well. At the low voltage grid the PMU in Bara registered a dip of 45 V (19%) down to a voltage of roughly 0.8 p.u. The registration of a voltage dip of roughly 1V (0.4%) in Tampere, Finland might also be connected to this fault, which would indicate a more global impact even across the 400 kV grid.

The voltage dip during the 29/1-22 fault was slighlty deeper in LTH than in Bara, of 50 V (33%) compared to 20 V (8%) suggesting that the fault location and subsequently the disconnection of an OHL were closer to LTH than Bara.

There was also an unexplained time delay between the voltage dips in the recorded PMU signals from LTH and Bara. The time stamp of the trigger at E.ON was 18:11:06:955, which correspond to the voltage dip plotted from the PMU signal at LTH. However, in the second figure of the Bara signal (fig 5.6), the voltage dip started at 666.9ms after 18:00, which also match the time stamp of the trigger, thus the seemingly different disturbance times of the LTH and Bara-signals in figure 5.5 were merely a plotting error.

Of all disturbances presented in this thesis, the 8/10-21 fault had the most severe impact on the voltage recorded by the PMU in Bara. This is completely in line with expectations since the fault was a 3ph SC occurring at an adjacent bay in "STM-". Why there was barely any voltage impact at LTH, despite the grave disruption in Bara, is also explained by the fault location. This since the fault occurred at a 20 kV conductor underlying the "STM-"station and that there are two higher voltage levels in between the unit in Bara and LTH, where the disturbance impact does not translate "upward" in voltage levels.

This fault was of most interest to this thesis since it was a 3ph SC, which also is the simulated fault type, and resulted in a severe voltage dip down to 0.4 p.u. Generally, a voltage impact like this combined with a potentially slow up-ramping of power (as in the recording in figure 5.1) from microproduction units could give cause of concern in relation to the power balance. This also sheds light on the need to further study the settings of units and specifically the up-ramping from microproduction after different voltage dips.

Regarding the status in the surrounding grid at the 8/10-21 fault; the values of power, voltage and current during the fault were aligned with the values hours before and after the fault, indicating that the fault occurred during normal operating conditions. The nearby wind power plant was offline during the fault and thus the overlying station "STM-" had conventional direction of power, and not reversed.

The 9/10-21 disturbance was also a 20 kV fault, in this case it was a phase-phase fault with connection to ground, but barely any earth fault current. It rendered a voltage dip in Bara of 100 V (43%), to a lowest voltage of 0.57 p.u and hardly had any impact at the voltage signal from the PMU in LTH. This is as expected from a local fault at the specified voltage level, and the fact that it had such a large impact on the voltage at Bara could be both due to the proximity to the fault location as well as the phase-phase connection during the fault that also could contribute to the magnitude of the voltage impact.

6 Discussion

The network model used in this thesis differs from an actual grid model, and the results should be reviewed in that context. Yet the network model will not be discussed further here, since the scope of the thesis has been to present a satisfactory network model, not to discuss and alter it to produce the most fitting or advantageous model.

Faults placed at different parts of the grid and at different voltage levels gave, during simulations, voltage impacts of varied magnitude, as shown in 4.2.1 and 4.2.2. The largest impact were at high voltage levels and also where the network structure was vulnerable. The results in the latter section also displayed that proximity to fault location matters.

The fault registration and analysis carried out in chapter 4 also showed that faults at high voltage level have a large 'global impact' on voltages, while faults closer to the PV-unit/node in question gave a more severe voltage dip there. In addition it viewed that earth faults are common and the fact that the 8/10-21 registration was found to be almost a perfectly balanced 3ph SC fault suggests that, even though quite rare, this balanced 'text-book fault type' actually do occur in reality as well.

In the simulation of the study cases, case 1 and 2 had a rather modest impact on the voltages. Case 3 however, had a larger impact on the voltages at the LV-nodes, with the highest impact in Case 3a. There all loadpoints in the 'residential' and 'commersial' feeder were considered prosumers with 43.5 kW, and the 'industrial' feeder had a larger 'industrial sized' unit. There the difference ΔV at some nodes were between 0.2-0.35 p.u., where the industrial unit at node I2 had the largest impact but several other LV-nodes had voltages at or around 0.2 p.u. which is above the LVRT-limit for generator type B and C. This was a greater impact than in case 3b, where the biggest difference were around 0.1 p.u. (ΔV). Case 4a also had less impact than this, were the difference in voltage without or with solar production at nearly all nodes were 0.1 p.u. as well.

Regarding the 'future scenarios', case 4 and 5, the reasoning around micro-production became more conceptual since the results spring from simulations with

aggregated PV-power in a single block.

The grid-placement of the production is key, which became obvious in case 4, where there is a vast difference in voltage impact in subcase a and b. The fact that case 4a generated such a vast impact on the voltages at the LV-nodes is due to that there in this study case barely is any distance, and hence barely any impedance between the PV-block and the LV-nodes at all. That case 4b had a very low impact on the voltages is due to the same reason, the distance and thus impedance between solar production and LV-nodes were at a maximum in this subcase. The truth probably lies somewhere between these two extremes, as this case in reality should correspond to solar production of a total amount of 25 MW being distributed throughout the grid, wherever capacity is available and irrespective of unit-size. Thus voltage supporting active power from PV-units would be more evenly distributed throughout the grid, suggesting that the voltages at the inspected nodes would be somewhere between C4a and C4b voltages.

In general, it can be seen that the placements of the PV-units were of great importance in this model and work. A production of 25 MW that was placed far away from the LV-nodes had slightly less impact on the LV-voltages than only a few microproduction units placed on the LV-feeders in case 3 had.

The two future cases (C4 and C5) cannot be compared directly. However comparison between the voltage differences ΔV show that a total active power of 150 MW gave a reduction of the voltage dip by 0.3 p.u., while 25 MW had an impact of 0.1 p.u. to over 1 p.u. depending on placement.

At Case 5, the active power had a large impact on all underlying nodes, from LV-level to SUB-voltage level. The solar power gave a reduction of the voltage dip of around 0.3 p.u. at all nodes downstream the PV-block. This case can be reasoned to represent a scenario where a neighbouring grid is filled up with 150 MW of solar power, regardless of unit-size and connection point. This large mitigating impact on the voltage dip can conversely be regarded as a likely loss and further induced voltage dip by the disconnection of PV-units which could occur during SC-faults, if PV-units are of small scale and at LV-nodes were the voltage is severely reduced. Thus, one can argue that in grids with many small-scale PV units installed with an

large accumulated total power, disconnection of these during faults may worsen the situation. Based on this argument, it would be of interest to implement, or at least investigate LVRT criteria for smaller unit sizes as well.

This impact of possible loss of production could also be visualized in the plots presented in section 4.7.3, where the geographic voltage impact of PV-production is shown. Likewise here, a situation with a loss of an accumulated large amount PV-production would theoretically give a noticable increase of the voltage dip across considerable distances in the HV-grid, as seen most clearly in figure 4.13.

It is the TSOs responsibility to decide upon and implement LVRT requirements for generators/modules, today mandatory for units of category B or larger. Yet it might be a good idea for grid owners/operators to look into specifying fault ride through criteria for smaller units aswell (also mentioned in a Swedish standard, brought up in section 2.3.3). Considering that grid owners are required to connect all customers with distributed generation, and there is such an upswing in installations of PV-microproduction.

Nevertheless, there are several other factors that complicate the situation. If PV-microproduction is allowed to stay connected to grid during SC-faults to help uphold the voltage, the PV-system could be feeding current into the grid during earth faults as well which would be a fault current contribution, thus rendering fault clearing and relay settings more difficult.

Furthermore, if DERs keep increasing, there is a risk that some places would get a reversed power flow in feeder-bays in substations. Most substations are planned and built for uni-directional power flow, and some relay-settings are dependent on direction meaning that some ability to disconnect and clear certain faults could be lost when the power flow is reversed.

Ultimately, the grid owners and operators would have to know how grid-tied power electronics of small scale act during normal operation as well as during fault events, in order to be able to utilize auxiliary services, like fault ride through, from micro-production in a proper and secure way. Especially since there is such a large variety of inverters, with different specifications.

Grid operators might also need to revise their praxis on e.g. monitoring, fault analysis and network calculations. The work in this thesis has displayed that calculation and simulation with a loadflow-basis instead of an assumed normed voltage may render a more realistic representation of grids, especially in areas with a large amount of DERs. This since even small differences/margins may determine whether production is disconnected or not, which was seen (for three simulation results) and commented in section 4.8.

A further argument for revised method of operation by grid owners is supported by the recent event conveyed in 5.1 where a SC-fault in Helsingborg affected distant PV-units, and gave such a voltage dip there that the micro-production in Bara nearly disconnected. This event most likely impacted a large area and could surely have led to a more severe outcome had all micro-production in that area disconnected, which would have been a significant disturbance in the power balance. Thus, the fault clearing times might need to be further shortened if a normal fault clearing case, like in this instance, can lead to micro-production over large areas disconnect.

Furthermore, the grid owners/operators might need to take into account during preliminary investigation of DER-connections, not only the capacity availability in the grid necessary for the production/connection, but also if the loss of this added production, or all production under a 1.5 MW power limit in an area can be disconnected without causing disruption in the power balance. I.e. to study if there are hosting capacity enough for small scale production in the grid, but also if the grid can manage to satisfy loads if the accumulated micro-production is lost.

Consequently, it can be argued that it is no longer sufficient to have a "top-down" approach on monitoring, planning and fault analysis, but that there is a need for a larger focus on LV-level as well. In grids with large amount of micro-production it is especially called for, in order to get a suitable and comprehensive overview of the situation in the power grid.

7 Conclusions and Future work

7.1 Conclusions

This thesis simulated faults at different parts of a power network model to study the effect across the grid. Faults at high voltage levels were most severe and affected a majort part of the grid. Network structure also affected this matter, the model used in this thesis had a weak point/bottle neck at subtransmisson voltage level, which proved vulnerable. With micro production included during faults, the voltage dips were reduced. How much varied with total solar power simulated, as well as placement of the PV-units both in relation to voltage levels but also proximity to fault location.

Generally, active power from micro production of PV units was found to help uphold the voltage both at the connection point and at upstream voltage level during the faults simulated in this thesis. The capacity needed to uphold a voltage to a certain level could not be unanimously/universally stated, since it depends on severity and duration of fault (how deep the voltage dip is), network structure and proximity to fault location, and distance to production from the busbar in question. The large impact recorded in case 3b (36% voltage increase at one busbar I2) suggests that more attention should be set to these small to mid-sized PV-units, as they all together may have a large impact. Simulation with aggregation of many small units resulted in voltages during fault above the LVRT criteria for type B modules in RfG, in some cases. Which is rendering aggregated microproduction in the interest zone of utilization for fault ride through.

Furthermore, this thesis also investigated the geographic impact of faults and micro production. It was seen that the geographic impact of fault in transmission levels were wide. For nearly all fault locations in the HV-grid simulated in this thesis, all parts of the model were reduced in voltage. The impact of disconnection of micro-production were also sought out. Simulations on this showed that in a situation with the capacity of both local and regional parts of grids full of solar production, some mitigation of voltage dip during SC-faults were observed across the HV-grid. Thus conversely, disconnection of large amounts of PV-microproduction could render more severe voltage dips.

In this thesis it has been shown that active power input from PV-microproduction, similar to the present magnitude of installation capacity, can provide noticeable voltage support during faults. It has also been noted that PV systems can possibly contribute to fault currents. In both senses, input from PVs, whether harmful or desired, should not be neglected during faults.

In regards to other aspects or concerns connected to micro-production of PVs that could be beneficial for grid owners/operators to be aware of or further look into, this study has come across a few. Firstly, power balance disruptions might be caused if faults induce a voltage dip over a large area and consequently disconnect a large amount of microproduction with slow up-ramping of power output.

Secondly, loadflow-based simulation might be a way forward in fault analysis, which could take into account impacts of both loads and increasing DERs and render more realistic voltage-outcome as well as being a tool to predict voltage-issues. Plus, this increasingly complex grid situation, with inverter based generation filling up grid capacities, calls for more intricate grid planning with respect payed to possible loss of micro-production.

Lastly, if auxiliary services are wished to be utilized from micro-production, information and support from, or collaboration with inverter manufacturers may be necessary. In addition, a more comprehensive view of the power system by grid operators, with an increased focus on LV-grids and "bottom-up" approach could be beneficial to better determine potential outcomes of and/or handle increased micro production in grids, in both planning and analysis.

In conclusion, active power from micro-production can be used to support the grid during faults. In aggregated form, microproduction is theoretically able to meet LVRT requirements for type B generators. However, if grid owners/operators wish to implement these fault ride through requirements on units of smaller sizes, there ought to be a larger focus on LV-level and further investigations regarding inverter control systems and their restrictions.

7.2 Future work

In future work it would be optimal to do fault simulations, as those in this thesis, in a real model of the grid, in an actual network model. If that is not possible, the next best thing would be to expand the work with a generic network model as in this study, but to adjust the model and expand the PV units further. To model a more realistic placement of future expansion of microproduction. This thesis had to pursue a simplified version of future PV expansion. In future work, it is of great interest to examine the effects and possible synergies of multiple residential PV systems in proximity to one another and to PV-parks of larger sizes.

It would also be of interest to simulate faults from two different models with more realistic network configurations, one with a strong and the other with a weaker network for example.

It would also be beneficial, in future work, to model a more complex development of DERs and to include other inverter based renewable technology or storage systems (e.g. Battery Energy Storage Systems). In addition to this, it would be of interest to further elaborate the component models of the production systems (PVs, batteries, etc) to include reactive power exchange, and to more closely resemble the possibilities of modern inverters.

Furthermore, it would be interesting to develop the working method used in this thesis with load-flow as a basis for fault calculations, and to use real load-data from various time periods with different levels of stress or (over-)loading.

A natural expansion of this work, and thus next step in a future work would be to simulate more faults than explicitly 3ph bolted SC. If resources allow, it would also be of interest to make dynamic simulations and directly compare these to fault registrations made at PV units in LV-grids. Such simulations could also include circuit breakers with time delays as in relay schemes, in order to get results accurately representing grids comparable with fault registrations.

In future work it would also be of interest to study how an increase in grid-tied PV units (or all inverter based generation, batteries included) affect and contribute to fault currents in grids.

Two additional subjects that would be intriguing to continue to work with is the frequency-dependency or response of converter-based generation, in relation to RfG-requirements, and second the quality of electricity. Especially if or how vastly a larger penetration of PV systems in the power grid affects the quality of electricity and if PV production, on a bigger scale, causes flicker (as wind does).

It would also be of value to further investigate the control systems and fault-responses from different inverters. Specifically small scale units, since the possibility of central control of distributed inverter-based generation and the legislation around it will be an important issue for grid operators in the future.

References

Alaküla, Mats, Gertmar, Lars, and Samuelsson, Olof (2011). *Elenergiteknik*. KFS AB.

Alstom Grid (2011). *Network Protection & Automation Guide. Protective Relays, Measurement Control*.

Blaabjerg, Frede et al. (2015). "Power electronics - the key technology for renewable energy system integration". In: *2015 International Conference on Renewable Energy Research and Applications (ICRERA)*. DOI: 10.1109/ICRERA.2015.7418680.

Christensen, Peter et al. (2020). *High penetration of power electronic interfaced power sources and the potential contribution of grid forming converters*. European Network of Transmission System Operators for Electricity. URL: https://euagenda.eu/upload/publications/untitled-292051-ea.pdf.

CIGRÉ (2014). *Benchmark Systems for Network Integration of Renewable and Distributed Energy Resources*. ISBN: 978-285-873-270-8.

Clementson, Joel (2022). *Senior Power System Engineer at E.ON Power System Analytics*. Personal communication.

— (2023). *Senior Power System Engineer at E.ON Power System Analytics*. Personal communication.

Council of the European Union (2023). *Paris Agreement on climate change*. URL: https://www.consilium.europa.eu/en/policies/climate-change/paris-agreement/.

Dhaker, Abbes (2023). "Control of photovoltaic systems". In: *Encyclopedia of Electrical and Electronic Power Engineering*. Ed. by Jorge García. Oxford: Elsevier, pp. 502–514. ISBN: 978-0-12-823211-8. URL: https://www.sciencedirect.com/science/article/pii/B9780128212042001045.

DigSILENT Power Factory (2021). *Technical Reference Static Generator. ElmGenstat*.

DigSILENT Power Pactory (2021). *Power Factory 2021. User Manual*. DIgSILENT GmbH.

E.ON Energy Networks (2023). *Solar PV, a real "Hot Topic"*. E.ON Intranet, Connect.

EIFS (2018:2). *Energimarknadsinspektionens föreskrifter om fastställande av generellt tillämpliga krav för nätanslutning av generatorer*. Tech. rep. Energimarknadsinspektionen.

El Chaar, Lana (2011). "Chapter 3 - Photovoltaic System Conversion". In: *Alternative Energy in Power Electronics*. Ed. by Muhammad H. Rashid. Boston: Butterworth-Heinemann, pp. 155–175. ISBN: 978-0-12-416714-8. DOI: https://doi.org/10.1016/B978-0-12-416714-8.00003-2.

Energiföretagen (2018). *Anslutning av elproduktion till lågspänningsnätet - ALP*. Version 3.

Energimarknadsinspektionen (2023). *Solenergi och solceller*. URL: https://ei.se/konsument/el/solenergi-och-solceller.

Energimyndigheten (2022a). *Installerad effekt (MW) för solcellsanläggningar fördelat på effektkategori och år*. URL: https://www.energimyndigheten.se/statistik/den-officiella-statistiken/statistikprodukter/natanslutna-solcellsanlaggningar/.

— (2022b). *Kraftig ökning av installerade solcellsanläggningar*. URL: https://www.energimyndigheten.se/nyhetsarkiv/2022/kraftig-okning-av-installerade-solcellsanlaggningar/ (visited on 06/04/2023).

— (2022c). *Prognoser och scenarier*. URL: https://www.energimyndigheten.se/statistik/prognoser-och-scenarier/?currentTab=0.

— (2023a). *Kortsiktiga prognoser*. URL: https://www.energimyndigheten.se/statistik/prognoser-och-scenarier/kortsiktiga-prognoser.

— (2023b). *Scenarier över Sveriges energisystem 2023. Med fokus på elektrifieringen 2050*. ISBN: 978-91-7993-112-4.

ENTSO-E (2012). *Network Code For Requirements For Grid Connection Applicable To All Generators. Frequently asked questions*.

— (2023a). *Mission Statement*. URL: https://www.entsoe.eu/about/inside-entsoe/objectives/ (visited on 08/04/2023).

— (2023b). *Our Governance*. URL: https://www.entsoe.eu/about/inside-entsoe/governance/ (visited on 08/04/2023).

— (n.d.). *Network Codes*. URL: https://www.entsoe.eu/network_codes/ (visited on 09/04/2023).

European Commission (2016). "Commission Regulation (EU) 2016/631 of 14 April 2016, establishing a network code on requirements for grid connection of generators". In: *Official Journal of the European Union*. URL: https://eur-lex.europa.eu/legal-content/EN/TXT/?uri=OJ:JOL_2016_112_R_0001#d1e1572-1-1.

European Committee for Electrotechnical Standardization (2019). *SS-EN 50549-1: Requirements for generating plants to be connected in parallel with distribution networks. Part 1: Connection to a LV distribution network –Generating plants up to and including Type B*.

Glover, J Duncan, Overbye, Thomas, and Sarma, Mulukutla S (2016). *Power system analysis & design, Sixth edition, SI version*. Cengage Learning.

Hemmingsson, Morten (2022). *Ramping calculation*. Personal communication.

International Energy Agency (2021). *Photovoltaic Power Systems Programme Annual Report*. ISBN: 978-3-907281-29-1.

Johansson, Philip (2022). *Engineer at E.ON Regional Grid planning*. Personal communication.

Kenyon, Richard W. and Mather, Barry (2020). *Simulating Distributed Energy Resource Responses to Transmission System-Level Faults Considering IEEE 1547 Performance Categories on Three Major WECC Transmission Paths*. United States: National Renewable Energy Laboratory. DOI: 10.2172/1603268. URL: https://www.nrel.gov/docs/fy20osti/73071.pdf.

Kumar, L. Ashok, Albert Alexander, S., and Rajendran, Madhuvanthani (2020). *Power electronic converters for solar photovoltaic systems*. Academic Press. ISBN: 9780128227305. URL: https://ludwig.lub.lu.se/login?url=https://search.ebscohost.com/login.aspx?direct=true&AuthType=ip,uid&db=cat02271a&AN=atoz.ebs26985998e&site=eds-live&scope=site.

Marstorp, Caroline (2022). *Senior Engineer at E.ON Regional Network*. Personal communication.

National Renewable Energy Laboratory (n.d.). *Photovoltaic Research*. URL: https://www.nrel.gov/pv/cell-efficiency.html.

Patsalides, Minas et al. (2013). "Thevenin equivalent circuit for the study of high photovoltaic penetration in distribution grids". In: *IEEE PES ISGT Europe 2013*. DOI: 10.1109/ISGTEurope.2013.6695421.

Runvik, Göran (2022a). *Registration 2021-07-15*. Personal communication. Bara, Svedala.

— (2022b). *Report on Phasor Measurement Unit i Bara*. Personal communication.

— (2023). *130 kV kortslutning i ställverk – Mätningar i Bara*. Personal communication.

Runvik, Göran and Juntti, Åke (2022). *Förvaltning av solcellsanläggning i Bara år 2022*. Personal communication.

Samuelsson, Olof (2021a). *Introduction and power system components*. Course material, Electric Power Systems. IEA Lund University.

— (2021b). *Symmetrical fault and protection*. Course material, Electric Power Systems. IEA Lund University.

— (2021c). *Voltage*. Course material, Electric Power Systems. IEA Lund University.

Skatteverket (n.d.[a]). *Mikroproduktion av förnybar el – näringsfastighet*. URL: https://skatteverket.se/foretag/skatterochavdrag/fastighet/mikroproduktionavfornybarelnaringsfastighet.4.309a41aa1672ad0c837b4e8.html (visited on 04/03/2023).

— (n.d.[b]). *Mikroproduktion av förnybar el – privatbostad*. URL: https://www.skatteverket.se/privat/fastigheterochbostad/mikroproduktionavfornybarelprivatbostad.4.12815e4f14a62bc048f41a7.html (visited on 04/03/2023).

— (n.d.[c]). *Skatt på el*. URL: https://skatteverket.se/foretag/skatterochavdrag/punktskatter/energiskatter/skattpael.4.15532c7b1442f256bae5e4c.html (visited on 04/03/2023).

Sood, Vijay K. and Abdelgawad, Haytham (2019). "Chapter 14 - Power converter solutions and controls for green energy". In: *Distributed Energy Resources in Microgrids*. Ed. by Rajeev Kumar Chauhan and Kalpana Chauhan. Academic Press, pp. 357–387. ISBN: 978-0-12-817774-7.

Statistiska Central Byrån (2022). *Monthly electricity generation by type of production*. URL: https://www.scb.se/en/finding-statistics/statistics-by-subject-area/energy/energy-supply-and-use/monthly-electricity-statistics-including-switches-

of-electricity-supplier/pong/tables-and-graphs/monthly-electricity-generation-by-type-of-production/.

Stetz, Thomas, Marten, Frank, and Braun, Martin (2013). "Improved Low Voltage Grid-Integration of Photovoltaic Systems in Germany". In: *IEEE Transactions on Sustainable Energy* 4.2, pp. 534–542. DOI: 10.1109/TSTE.2012.2198925.

Svensk Solenergi (2023). *Anläggningar i Sverige*. URL: https://svensksolenergi.se/om-solenergi/anlaggningar/solcellsparker/.

Svenska Kraftnät (2019). *Systemdrifttillstånd*. URL: https://www.svk.se/contentassets/7dfa08444dab4d3aba1adbbc38456c2b/systemdrifttillstanden.pdf.

— (2021a). *Balansering av kraftsystemet*. URL: https://www.svk.se/om-kraftsystemet/om-systemansvaret/balansering-av-kraftsystemet/ (visited on 10/04/2023).

— (2021b). *Guide för anslutning av kraftproduktionsmodul till överföringssystemet*. URL: https://www.svk.se/siteassets/1.om-kraftsystemet/legalt-ramverk/eu-lagstiftning/anslutningskoder/guide-anslutning-av-kraftproduktionsmodul-till-overforingssystemet.pdf.

— (2021c). *Långsiktig marknadsanalys 2021*. URL: https://www.svk.se/siteassets/om-oss/rapporter/2021/langsiktig-marknadsanalys-2021.pdf.

— (2021d). *Leveranssäkerhet*. URL: https://www.svk.se/om-kraftsystemet/oversikt-av-kraftsystemet/leveranssakerhet/.

— (2022). *Sveriges Elnät*. URL: https://www.svk.se/om-kraftsystemet/oversikt-av-kraftsystemet/sveriges-elnat/ (visited on 04/09/2022).

United Nations (n.d.). *The Paris Agreement*. URL: https://unfccc.int/process-and-meetings/the-paris-agreement.

Wallnér, Erik (2022). *Utvecklingen kring solceller under 2023*. URL: https://www.solcellskollen.se/blogg/utvecklingen-kring-solceller-under-2023-ar-eran-av-prisminskningar-forbi.

A Appendix 1 - OHL and Cable data

OHLs

Name	V_{rated}	R'(AC,20°C)	X'	L'	R0'(AC)	X0'	L0'	Rn'(AC)	Xn'	Ln'	Rpn'(AC)	Xpn'	Lpn'
	kV	*Ohm/km*	*Ohm/km*	*mH/km*	*Ohm/km*	*Ohm/km*	*mH/km*	*Ohm/km*	*Ohm/km*	*mH/km*	*Ohm/km*	*Ohm/km*	*mH/km*
A1	20	0.51	0.366	1.16501	0.658	1.611	5.12797	0	0	0	0	0	0
A1 -110kV	110	0.819	0.345	1.09817	0.23	1.46	4.64733	0	0	0	0	0	0
Line 220kV -A1/S1A Cond.ID 1	220	0.06534	0.39785	1.26639	0.21344	1.31648	4.19049	0	0	0	0	0	0
Line 380kV EHV - A1/S1A Cond.ID 2	380	0.03278	0.3119	0.99282	0.18050	1.1552	3.67712	0	0	0	0	0	0
OHL C3C12	0.4	0.80013	0.1656	0.52712	0	0	0	0.8001	0.1656	0.52712	0	0	0
OHL C5C17	0.4	1.2883	0.25943	0.8258	0	0	0	1.2883	0.25943	0.8258	0	0	0
OHL1	0.4	0.491	0.272	0.8658	0.638	1.787	5.6882	0.491	0.272	0.8658	0.638	1.787	5.6882
OHL3	0.4	2.016	0.32	1.01859	2.163	1.835	5.84099	2.016	0.32	1.01859	2.163	1.835	5.84099

Cables

Name	V_{rated}	R'	X'	L'	R0'	X0'	L0'	Rn'	Xn'	Ln'	Rpn'	Xpn'	Lpn'
	kV	*Ohm/km*	*Ohm/km*	*mH/km*	*Ohm/km*	*Ohm/km*	*mH/km*	*Ohm/km*	*Ohm/km*	*mH/km*	*Ohm/km*	*Ohm/km*	*mH/km*
NA2XS2Y	20	0.501	0.716	2.2791	0.817	1.598	5.08659	0	0	0	0	0	0
UG1	0.4	0.162	0.074	0.23555	0.309	2.093	6.66223	0.162	0.074	0.23555	0.309	2.093	6.66223
UG2	0.4	0.265	0.075	0.23873	0.412	2.136	6.7991	0.265	0.075	0.23873	0.412	2.136	6.7991
UG3	0.4	0.822	0.078	0.24828	0.969	2.235	7.11423	0.822	0.078	0.24828	0.969	2.235	7.11423

B Appendix 2 - Component register and data

TRANSFORMERS HV-PART

ID	Type	**NAME**	*Tafo name in PF*	Connection	V2	V1	Xtr	Zgnd	Srated
					kV	kV	p.u.	Ohm	MVA
T1	TRT1	**TRT 1**	*YNyn0 380/220 1000 MVA*	3ph YNyn0	220	380	0.013	3	1000
T2	TRT1								
T3	TRT2	**TRT 2**	*YNd11 220/22 1000 MVA*	3ph YNd11	22	220	0.013	3	1000
T4	TRT2								
T5	TRT2								
T6	TRT3	**TRT 3**	*YNyn11 220/22 500 MVA*	3ph YNd11	22	220	0.026	3	500

GENERATORS				pu			s		pu			MVA	MW	pu
ID	Type	**NAME**	*Generator name in PF*	Xd	X'd	X"d	T'd0	T"d0	Xq	X"q	T"q0	Sr	Pout	Vout
G1	TG1	**TG1**	*Generator 1 - 700MVA*	1.25	0.333	0.292	5	0.002	1	0.292	0.002	700	500	1.03
G2	TG2	**TG2**	*Generator 2 - 500MVA*	1.667	0.25	0.233	6	0.002	1.125	0.225	0.002	700	500	1.03
G3	TG3	**TG3**	*Generator 3 - 500MVA*	1.25	0.333	0.292	5	0.002	1	0.292	0.002	500	300	1.03

LINES AND CABLES

OHL HV-PART

Line seg in PF	*Conductor ID in PF*
L12	Line 220kV -A1/S1A Cond.ID 1
L16	Line 220kV -A1/S1A Cond.ID 1
L25	Line 220kV -A1/S1A Cond.ID 1
L34a	Line 220kV -A1/S1A Cond.ID 1
L34b	Line 220kV -A1/S1A Cond.ID 1
L45	Line 220kV -A1/S1A Cond.ID 1
L46	Line 220kV -A1/S1A Cond.ID 1
L78	Line 380kV EHV - A1/S1A Cond.ID 2

OHL SUB HV

Line seg in PF	*Conductor ID in PF*
L_HV/A	Line 220kV -A1/S1A Cond.ID 1
L_A/MV	A1 -110kV

OHL "RURAL" MV-PART

Line segm.	*Conductor ID in PF*
Line1213	A1
Line1314	A1
LineMV/LV	A1

CABLES "CITY" MV-PART

Line segm.	*Conductor ID in PF*
Line12	NA2XS2Y
Line23	NA2XS2Y
Line34	NA2XS2Y
Line38	NA2XS2Y
Line45	NA2XS2Y
Line56	NA2XS2Y
Line89	NA2XS2Y
Line78	NA2XS2Y
Line910	NA2XS2Y
Line1011	NA2XS2Y
LineMV/LV	NA2XS2Y

LINES AND CABLES

OHL/CABLES LV-PART

Line segm.	*Conductor ID*	Line segm.	*Conductor ID*
LineR12	UG1	LineI12	UG2
LineR311	UG3		
LineR34	UG1	LineC13	OHL1
LineR412	UG3	LineC123	OHL C3C12
LineR46	UG1	LineC34	OHL 1
LineR616	UG3	LineC1617	OHL C5C17
LineR67	UG1	LineC56	OHL 1
LineR917	UG3	LineC819	OHL 3
LineR910	UG1	LineC89	OHL 1
LineR1018	UG3	LineC920	OHL 3

LOADS AND CAPACITANCES

HV LOADS

Name	P (MW)	Q (Mvar)
Load2	285	200
Load 3	325	244
Load4	326	244
Load6a	435	296

HV SHUNT

Name	C (Mvar)
ShuntC4	160
ShuntC5	80
ShuntC6a	180

LOADS AND CAPACITANCES

MV LOADS "RURAL"

At bus	Name	S (kVA)	*pf*
MB12	Res. Load 12	15300	0.98
MB12	Com.Ind. Load 12	5280	0.95
MB13	Com.Ind. Load 13	40	0.85
MB14	Res. Load 14	215	0.97
MB14	Com.Ind. Load 14	390	0.85

MV LOADS "CITY"

At bus	Name	S (kVA)	*pf*
MB1	Res. Load 1	15300	0.98
MB1	Com.Ind. Load 1	5100	0.95
MB3	Res. Load 3	285	0.97
MB3	Com.Ind. Load 3	265	0.85
MB4	Res. Load 4	445	0.97
MB5	Res. Load 5	750	0.97
MB6	Res. Load 6	565	0.97
MB7	Com.Ind. Load 7	90	0.85
MB8	Res. Load 8	605	0.97
MB9	Com.Ind. Load 9	675	0.85
MB10	Res. Load 10	490	0.97
MB10	Com.Ind. Load 10	80	0.85
MB11	Res. Load 11	340	0.97

LV LOADS

At bus	Name	S (kVA)	*pf*	At bus	Name	S (kVA)	*pf*
R1	LR1	200	0.95	C1	LC1	120	0.9
R11	LR11	15	0.95	C12	LC12	65	0.9
R15	LR15	52	0.95	C17	LC17	33	0.9
R16	LR16	55	0.95	C19	LC19	16	0.9
R17	LR17	35	0.95	C20	LC20	8	0.9
I2	LI2	100	0.85				

C Appendix 3 - Vector diagram 28/11-21 fault

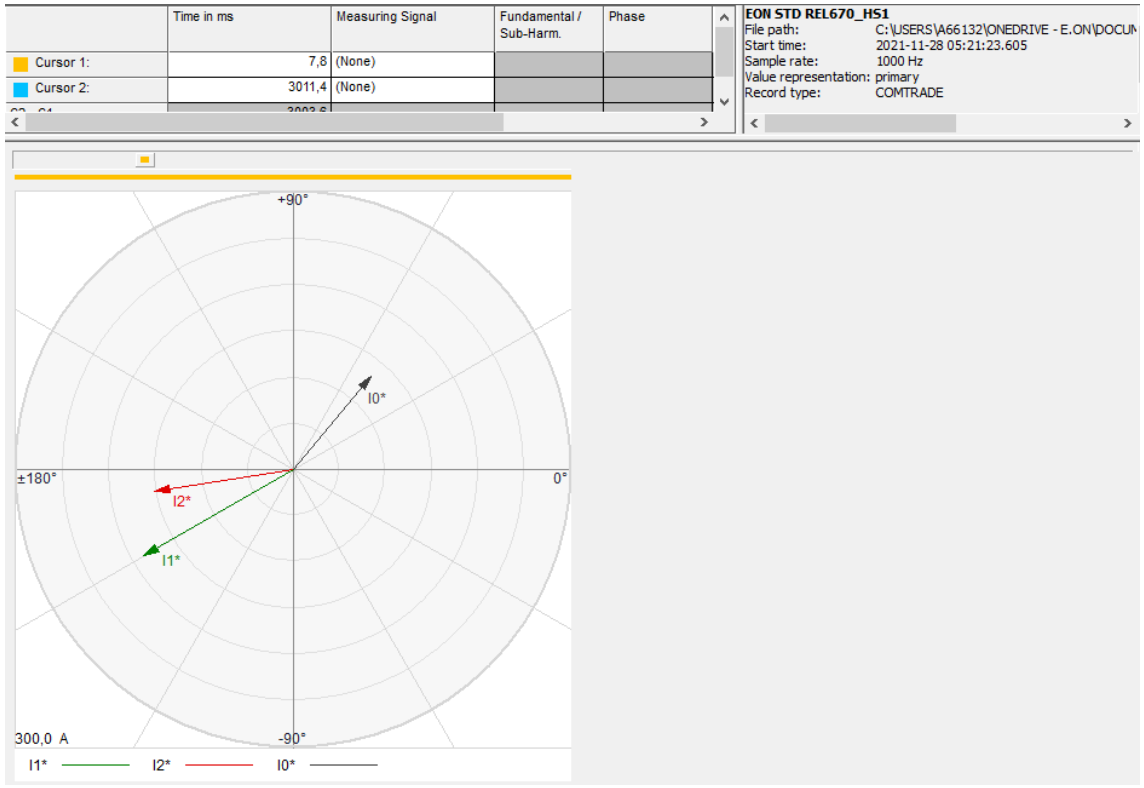

Figure C.1: Sequence currents of grid/network at one instant, 7.8 ms into fault recording, during 28/11-21 fault

Figure C.1 shows a clear detection of a zero sequence current, suggesting an earth fault of sorts. However, the positive and negative sequence currents are not typical for that of an earth fault in only one phase. Thus the exact fault type is unclear.